College of Engineering
Virginia Polytechnic Institute and State University
Blacksburg, Virginia 24061

VPI-E-76-1 January, 1976

Interlaminar Stresses in Composite Laminates -- A Perturbation Analysis

Peter W. Hsu [1]
Carl T. Herakovich [2]

Department of Engineering Science and Mechanics

Partially supported by NASA Grant NGR 47-004-090

1 Graduate Student
2 Associate Professor

INSTRUCTIONS FOR COMPLETING FORM NTIS-35 (Bibliographic Data Sheet based on COSATI Guidelines to Format Standards for Scientific and Technical Reports Prepared by or for the Federal Government, PB-180 600).

1. **Report Number.** Each individually bound report shall carry a unique alphanumeric designation selected by the performing organization or provided by the sponsoring organization. Use uppercase letters and Arabic numerals only. Examples FASEB-NS-73-87 and FAA-RD-73-09.

2. Leave blank.

3. **Recipient's Accession Number.** Reserved for use by each report recipient.

4. **Title and Subtitle.** Title should indicate clearly and briefly the subject coverage of the report, subordinate subtitle to the main title. When a report is prepared in more than one volume, repeat the primary title, add volume number and include subtitle for the specific volume.

5. **Report Date.** Each report shall carry a date indicating at least month and year. Indicate the basis on which it was selected (e.g., date of issue, date of approval, date of preparation, date published).

6. **Performing Organization Code.** Leave blank.

7. **Author(s).** Give name(s) in conventional order (e.g., John R. Doe, or J.Robert Doe). List author's affiliation if it differs from the performing organization.

8. **Performing Organization Report Number.** Insert if performing organization wishes to assign this number.

9. **Performing Organization Name and Mailing Address.** Give name, street, city, state, and zip code. List no more than two levels of an organizational hierarchy. Display the name of the organization exactly as it should appear in Government indexes such as Government Reports Index (GRI).

10. **Project/Task/Work Unit Number.** Use the project, task and work unit numbers under which the report was prepared.

11. **Contract/Grant Number.** Insert contract or grant number under which report was prepared.

12. **Sponsoring Agency Name and Mailing Address.** Include zip code. Cite main sponsors.

13. **Type of Report and Period Covered.** State interim, final, etc., and, if applicable, inclusive dates.

14. **Sponsoring Agency Code.** Leave blank.

15. **Supplementary Notes.** Enter information not included elsewhere but useful, such as: Prepared in cooperation with . . . Translation of . . . Presented at conference of . . . To be published in . . . Supersedes . . . Supplements . . . Cite availability of related parts, volumes, phases, etc. with report number.

16. **Abstract.** Include a brief (200 words or less) factual summary of the most significant information contained in the report. If the report contains a significant bibliography or literature survey, mention it here.

17. **Key Words and Document Analysis. (a). Descriptors.** Select from the Thesaurus of Engineering and Scientific Terms the proper authorized terms that identify the major concept of the research and are sufficiently specific and precise to be used as index entries for cataloging.
(b). **Identifiers and Open-Ended Terms.** Use identifiers for project names, code names, equipment designators, etc. Use open-ended terms written in descriptor form for those subjects for which no descriptor exists.
(c). **COSATI Field/Group.** Field and Group assignments are to be taken from the 1964 COSATI Subject Category List. Since the majority of documents are multidisciplinary in nature, the primary Field/Group assignment(s) will be the specific discipline, area of human endeavor, or type of physical object. The application(s) will be cross-referenced with secondary Field/Group assignments that will follow the primary posting(s).

18. **Distribution Statement.** Denote public releasability, for example "Release unlimited", or limitation for reasons other than security. Cite any availability to the public, other than NTIS, with address, order number and price, if known.

19 & 20. **Security Classification.** Do not submit classified reports to the National Technical Information Service.

21. **Number of Pages.** Insert the total number of pages, including introductory pages, but excluding distribution list, if any.

22. **NTIS Price.** Leave blank.

BIBLIOGRAPHIC DATA SHEET	1. Report No. VPI-E-76-1	2.	3. Recipient's Accession No.

4. Title and Subtitle

INTERLAMINAR STRESSES IN COMPOSITE LAMINATES -- A PERTURBATION ANALYSIS

5. Report Date: January, 1976

6.

7. Author(s): Peter W. Hsu and Carl T. Herakovich

8. Performing Organization Rept. No. VPI-E-76-1

9. Performing Organization Name and Address

Virginia Polytechnic Institute and State University
Engineering Science and Mechancis
Blacksburg, Virginia 24061

10. Project/Task/Work Unit No.

11. Contract/Grant No.: NGR 47-004-090

12. Sponsoring Organization Name and Address

National Aeronautics & Space Administration
Langley Research Center
Hampton, Virginia 23665

13. Type of Report & Period Covered

14.

15. Supplementary Notes

16. Abstracts

see page ii

17. Key Words and Document Analysis. 17a. Descriptors

Interlaminar Stresses
Edge Effects
Perturbation Analysis
Composites
Bi-directional Laminates
Angle-ply Laminates
Graphite/Epoxy
Singularity

17b. Identifiers/Open-Ended Terms

17c. COSATI Field/Group

18. Availability Statement	19. Security Class (This Report)	21. No. of Pages
Distribution unlimited	UNCLASSIFIED	97
	20. Security Class (This Page) UNCLASSIFIED	22. Price

TABLE OF CONTENTS

	Page
ACKNOWLEDGEMENTS	ii
LIST OF FIGURES	v
Chapter	
I. INTRODUCTION	1
1.1 REVIEW OF LITERATURE	1
1.2 THE FINITE DIFFERENCE SOLUTION	6
1.3 PERTURBATION METHOD	10
II. PROBLEM FORMULATION	16
2.1 GOVERNING FIELD EQUATIONS	16
2.2 EQUILIBRIUM CONSIDERATIONS	22
2.3 PERTURBATION SOLUTION	26
2.3.1 THE INTERIOR REGION	28
2.3.2 MODIFIED ZEROTH ORDER INTERIOR REGION SOLUTION	34
2.3.3 THE BOUNDARY LAYER REGION	39
III. SPECIAL LAMINATES	44
3.1 BIDIRECTIONAL LAMINATES WITH CONSTANT PLY THICKNESS	44
3.1.1 $[0/90]_S$ GRAPHITE-EPOXY LAMINATE	50
3.1.2 $[90/0]_S$ GRAPHITE-EPOXY LAMINATE	56
3.2 ANGLE-PLY LAMINATES WITH CONSTANT PLY THICKNESS	65
3.2.1 $[45/-45]_S$ GRAPHITE-EPOXY LAMINATE	68
3.2.2 $[-45/45]_S$ GRAPHITE-EPOXY LAMINATE	74
IV. RESULTS AND DISCUSSION	81
4.1 THE FOUR LAYER BIDIRECTIONAL LAMINATES	81

Page

4.2 THE FOUR LAYER ANGLE-PLY LAMINATES 83

4.3 ACCURACY AND LIMITATIONS 87

4.3.1 BIDIRECTION LAMINATES 87
4.3.2 ANGLE-PLY LAMINATES 89

4.4 GENERALITY AND APPLICABILITY 91

V. CONCLUSIONS 93

REFERENCES 95

VITA 98

LIST OF FIGURES

Figure		Page
1.	Laminate Geometry	2
2.	Free Body Diagram of Quarter YZ-Plane	23
3.	Partial Free Body Diagram of Quarter Section	24
4.	Limiting Free Body Diagram of the Interface $Z = Z_k$	27
5.	Free Body Diagram of First Quadrant of Typical Section	38
6.	Bidirectional and Angle-Ply Laminates	45
7.	Four-Ply Bidirectional Laminates	51
8.	Interlaminar Shear Stress τ_{yz} as a Function of ε for $[0/90]_s$ Gr/E	57
9.	Interlaminar Normal Stress σ_z as a Function of ε for $[0/90]_s$ Gr/E	58
10.	Present Theory and Finite Difference Results for τ_{yz} in $[0/90]_s$	59
11.	Present Theory and Finite Difference Results for σ_z in $[0/90]_s$	60
12.	Interlaminar Shear Stress τ_{yz} as a Function of ε for $[90/0]_s$ Gr/E	61
13.	Interlaminar Normal Stress σ_z as a Function of ε for $[90/0]_s$ Gr/E	62
14.	Present Theory and Finite Difference Results for τ_{yz} in $[90/0]_s$	63
15.	Present Theory and Finite Difference Results for σ_z in $[90/0]_s$	64
16.	Angle-Ply Laminate of 2m Layers	66
17.	Four-Layer Angle-Ply Laminates	69

Figure		Page
18.	Present Theory and Finite Difference Results for τ_{xz} in $[45/-45]_s$	75
19.	Present Theory and Finite Difference Results for τ_{yz} in $[45/-45]_s$	76
20.	Present Theory and Finite Difference Results for σ_z in $[45/-45]_s$	77
21.	Present Theory and Finite Difference Results for τ_{xz} in $[-45/45]_s$	78
22.	Present Theory and Finite Difference Results for τ_{yz} in $[-45/45]_s$	79
23.	Present Theory and Finite Difference Results for σ_z in $[-45/45]_s$	80

Chapter I

INTRODUCTION

Interlaminar stresses play an important role in the load transfer mechanism in composite laminates. Both numerical and experimental results have demonstrated that when a thin laminate is subjected to a uniaxial extension (Fig. 1), there exist highly localized stress concentration regions near the free edges, the so-called boundary layer regions. This phenomenon has been suggested to be the dominant factor initiating failure of some composite laminates.

The present thesis will analyze the boundary layer by "perturbing" the exact elasticity equations with a stretching transformation. Solutions to these transformed equations provide a higher order analysis than idealized lamination theory [1].* Hence better insight into the interlaminar stress behavior is obtained using the perturbation analysis [2].

1.1 REVIEW OF LITERATURE

Bogy [3] analyzed a bonded material containing two mutually dissimilar orthogonal wedges under arbitrary tractions. The stress fields were found to contain a mathematical singularity at the intersection of the interfacial plane and the loaded surface. Hein [4] studied the residual stresses in a two-material wedge and found similar behavior.

---

*Numbers in brackets refer to the references listed in the bibliography.

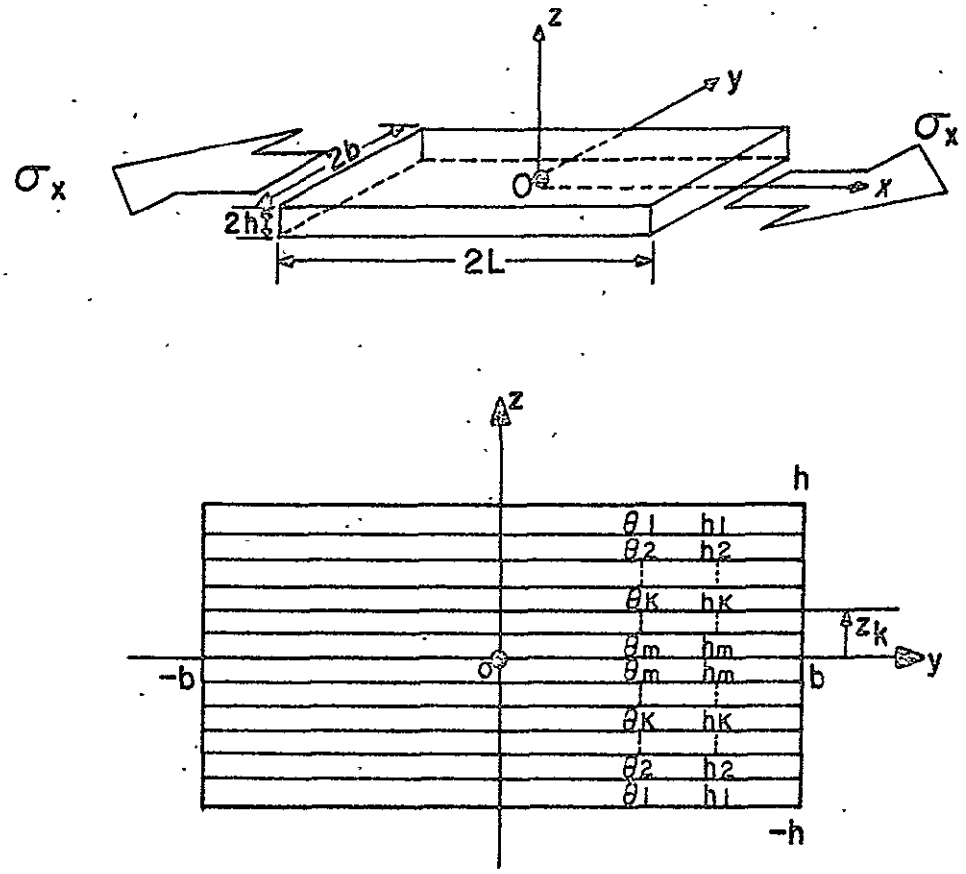

FIGURE 1. LAMINATE GEOMETRY

Hess [5] developed a plane elasticity solution for the end problem in a two-layer laminated strip and showed a mathematical singularity, defined to be a point where the convergence of an eigenfunction expansion could not be attained. Puppo and Evensen [6] modeled the finite-width symmetric laminate as a set of anisotropic layers separated by isotropic shear layers. Each anisotropic layer was assumed to be under generalized plane stress, i.e., the out-of-plane normal stress σ_z (Fig. 1) is zero and the in-plane stresses and displacements are the thickness averages of the actual values. Solutions to the corresponding equilibrium equations showed that while the interlaminar shear stresses vanish everywhere for a laminate of infinite width, they attained maximum finite values near the free edge of a finite width laminate. Furthermore, in regions far away from the free edge, the solution agreed well with the classical lamination theory [1]. A complete three dimensional analysis was carried out by Pipes and Pagano [7] using the finite difference technique to solve the exact elasticity equations. The results showed good agreements with those of Reference [6] except at the free edge where the interlaminar shear stress τ_{xz} seemed to grow without bound for some laminates. Due to the approximate nature of the finite difference analysis, however, no evidence was available to show the intensity of the suggested singularity. Isakson and Levy [8] used a finite element approach to analyze a model similar to that of Reference [6]. Based on the constant strain assumption within each element, the corresponding stresses were obtained from the constitutive equations. The total elastic strain energy was calculated and

minimized [9] to yield a set of simultaneous linear algebraic equations. Levy, et al. [10] used the same model and formulation as Reference [8] to further investigate the elastic and plastic interlaminar shear deformations in the laminate. The out-of-plane "peel stress" was not taken into account in both studies due to the modeling. Results from these solutions were quite similar to those of Reference [6] except at the free edge where the interlaminar shear stress τ_{xz} was 40% lower than that of Reference [6]. This presumably was due to the limitations of the finite element approximation. Improvements were made by Rybicki [11] who carried out a three-dimensional finite element analysis based on a complimentary energy formulation in terms of three Maxwell stress functions. These functions resulted in a set of simultaneous linear algebraic equations which were solved by Gauss reduction and the back substitution process. The "peel stress" was obtained in this investigation. The results showed excellent agreement with References [6] and [7] in regions removed from the free edges, while near the edges the interlaminar shear stress τ_{xz} agreed only with Reference [6]; the magnitude of τ_{xz} was much lower than the singular value of Reference [7]. The approximate nature of the finite element formulation for the laminated plate apparently leads to questionable and quite possibly poor results at the exact free edge. Pipes [12] used the finite difference procedure to carry out extensive parametric studies including laminate geometry, fiber orientations and stacking sequences. The program used in Reference [12] is capable of handling no more than an 8 layer symmetric laminate owing to the limited

computer capacity.

Several attempts have recently been made to verify experimentally the numerical predictions. Results by Pipes and Daniel [13], Herakovich [14], and Oplinger, et al. [15] have all showed significant stress concentration behavior near the free edges. Although stress intensities were not determined in these studies, there were strong evidences to support the numerical prediction of significant stress concentrations near the free edge.

Pipes and Pagano [16] more recently developed an analytical solution to the elasticity equations under the assumptions of zero interlaminar normal stress, σ_z, and zero transverse normal stress, σ_y, for the $[\pm 45]_s$ laminate. Pagano [17] obtained yet another approximate solution following the cylindrical bending theory of Whitney and Sun [18]. Good agreement with the elasticity solution of Reference [7] was found for the interlaminar normal stress, σ_z, (the "peel stress") on the midplane of a bidirectional $[0/90]_s$ laminate. However, the solution did not recognize the stress free boundary conditions $\tau_{yz}(\pm b,z) = 0$. In addition, no through thickness distribution of the stresses was available. An approximate approach was then considered by Tang [19] following the isotropic theory of Reiss and Locke [20]. The interior domain (regions removed from the free edges) was assumed to be in a state of plane stress, the axial displacement u was assumed to be a function of x only, and the displacement components, v and w, were both assumed to vanish identically. The boundary layer equilibrium equations coupled with the compatibility equations were split into

two problems. Namely, a modified torsion problem and a modified plane strain problem. The resulting fourth order differential equations were solved by asymptotic expansion in terms of the ply thickness h/2. The matching of the boundary layer solution with the interior domain solution was satisfied by the imposed boundary conditions for the two problems. The results for a $[\pm 45]_S$ graphite-epoxy laminate showed good agreement for the interior regions with References [6] and [7] while the interlaminar shear stress τ_{xz} at the free edge was found to be lower than the predicted singularity of Reference [7]. The through-thickness stress distributions showed nonzero shear stresses τ_{xz} and τ_{yz} on the free surfaces $z = \pm h$ as well as on the midplane $z = 0$. Also, the out-of-plane normal stress σ_z vanished on both the interfacial planes $z = \pm h/2$ and the midplane $z = 0$. This is unlike the results of Reference [7] which indicated maximum values of σ_z on the midplane of a $[0/90]_S$ laminate and on the interfacial planes of a $[\pm 45]_S$ laminate. Finally, it should be noted that the approximate nature of the formulation in Reference [19] did not satisfy the vanishing stress boundary conditions $\tau_{xy}(\pm b,z) = 0$ and $\sigma_y(\pm b,z) = 0$ for each layer.

1.2 THE FINITE DIFFERENCE SOLUTION

In view of the discussion in Section 1.1, the finite difference solution of Reference [7] seems to serve as the most dependable solution known to the researcher. This is due to the fact that the formulation was required to obtain the exact elasticity solution to the problem. However, there were inherent deficiencies in the finite

difference procedures as pointed out by Pagano and Pipes [21]. To this end, numerous tests were carried out by this author to examine the "exactness" of the solution in Reference [7] with emphasis on its behavior near the free edge. The following observations can be made.

(1) For bidirectional laminates (0° and 90° plies), all stress free boundary conditions were satisfied except at the four corners of the laminate where the out-of-plane normal stress did not vanish but took on a low value. Also, the sign of the outer layer σ_z at the exact free edge was found to be inconsistent with that of the inner layer. These results may be attributed to the dissatisfaction of the equilibrium equations on the free boundaries as can be seen in the work of Pipes [12].

(2) For angle-ply laminates $[\pm\theta]_s$, neither of the stress free boundary conditions, $\sigma_y(\pm b,z) = \tau_{xy}(\pm b,z) = 0$, was satisfied at the intersection of the interface and the free edge. Both σ_y and τ_{xy} at this suggested singularity were of an erroneously large order of magnitude--as high as the axial stress σ_x. As a result, the interlaminar shear stress τ_{xz} attained a maximum finite value rather than the possible infinity predicted by Pipes and Pagano [7]. Failure to satisfy the vanishing stress boundary conditions at the four corners, $\sigma_z(\pm b,\pm h) = \tau_{xz}(\pm b,\pm h) = 0$, was found again. Moreover, the sign reversal of stresses which was found for the bidirectional laminates as a result of change in the stacking sequence, was not observed for the angle-ply laminates. The above boundary violation may be due to errors inherent in the solution procedure for the angle-ply

laminates.

It may be concluded that despite the good agreement with the results of References [6], [11] and [19] in regions removed from the free edges, the finite difference solution yields poor results near the mathematical singularity. In order to determine the proper order of magnitude of stress intensity near the singular point, a more rigorous analytical solution to the field equations must be obtained. Such a solution was described by Pagano and Pipes [21] as a "mathematical nightmare."

The present thesis seeks a solution which predicts accurate interlaminar free edge stress intensities for laminates. Due to the above-mentioned mathematical complexities, it is certainly not an easy task. As described in the preceding section, all the previous investigations show a common result--the plane stress lamination theory is recovered near the central plane $y = 0$ provided the laminate is sufficiently wide ($b/h \gg 1$). This suggests that the boundary layer effect is directly related to the geometrical ratio b/h, and that the stress distribution throughout the laminate is the combination of the interior region solution and the boundary layer solution. The method of solution employed in the present thesis is the perturbation analyses [2, 22] developed in the 1940's to solve boundary value problems in fluid mechanics and extended to problems in solid mechanics in the 1950's. The isotropic theory of Reiss and Locke [20] and the anisotropic theory of Tang [19] were essentially based upon such analyses. The main differences between the present thesis and the

theory of Reference [19] are summarized as follows. (1) The present thesis is based upon the displacement formulation in which the compatibility equations are satisfied automatically. The resulting field equations are second order partial differential equations in terms of the displacement functions. Reference [19] was based upon the stress formulation in which satisfaction of the compatibility equations resulted in fourth order partial differential equations in terms of the stress functions. (2) For the interior regions, the present thesis determines the three dimensional solution to the reduced governing equations ($h/b \to 0$) while satisfying the symmetry and antisymmetry conditions, the displacement condition, the continuity conditions and the vanishing stress boundary conditions on the top and bottom surfaces. In reference [19] the displacement components v and w were both assumed to vanish identically for the interior regions and the axial displacement u was assumed to be a linear function of x alone for such regions. (3) For the boundary layer region, the present thesis removes mathematical complexities by considering the free body diagram of an infinitesimally thin slice containing the interfacial plane. Such a limiting analysis provides sufficiently accurate determination of the coefficients of the boundary layer solution for $h/b \ll 1$. The physical validity of the composite solution (interior and boundary layer solutions combined) is insured by the following requirements. The material immediately adjacent to the interfacial plane must satisfy the "stretched" governing differential equations, the matching principle of perturbation theory (Section 1.3),

the force and moment balance with the stress resultants on the central plane ($y = 0$), the self-equilibrating conditions of the out-of-plane normal stress resultant, and the free edge stress boundary conditions. Reference [19] considered two separate problems for the boundary layer region according to the even and odd nature of the stress components. A stress function following the isotropic torsion problem was assumed for the T° (modified torsion) problem. A similar function was then chosen as the particular solution to the fourth order equation of the P° (modified plane strain) problem. This particular solution along with the homogeneous solution (5^{th} order polynomial) constituted the solution to this problem. The combination of the T° problem and the P° problem failed to satisfy some of the stress boundary conditions at the free edge and on the free surfaces. And the approximate nature made the through-thickness stress distributions incapable of properly describing the force and moment equilibrium and the self equilibrating condition at any level of z.

1.3 PERTURBATION METHOD

Consider the differential equation

$$\varepsilon \cdot y'' - y' + y = 0 \quad , \quad 0 \leq x \leq 1 \tag{1.1}$$

$$y(0) = \alpha \quad , \quad y(1) = \beta \tag{1.2}$$

where $0 < \varepsilon << 1$.

Assuming the exact solution to the problem is not available, the following approximate steps must be taken:

As ϵ vanishes, Equation (1.1) reduces to

$$y' - y = 0 \tag{1.3}$$

which has a solution of the form

$$y^{\circ} = ae^{x} \tag{1.4}$$

where the superscript $^{\circ}$ denotes the solution corresponding to $\epsilon = 0$ and a is an unknown coefficient. Solution (1.4) can satisfy only one of the boundary conditions (1.2). For the other boundary condition to be satisfied, a stretching transformation is introduced in the form

$$\xi = |B - x|/\epsilon^{\lambda} \tag{1.5}$$

where $\lambda > 0$ and B is the boundary limit of the stretched end (0 or 1 in the present problem). It will be shown that this transformation magnifies a small region called the boundary layer in which y changes rapidly in order to retrieve the dropped boundary condition at the end $x = B$. Solution to the boundary layer equation must match the solution of the reduced equation (1.3) according to Prandtl's matching principle [2],

$$\underset{B}{m}\, y^{\circ} = \lim_{\xi \to \infty} y^{BL} \tag{1.6}$$

where y^{BL} is the boundary layer solution.

It may be shown [2] for the present problem that the boundary layer exists near the end $x = 1$ and the value of λ in Equation (1.5) is found to be 1. Hence

$$y^{\circ} = \alpha e^{x} \tag{1.7}$$

since it must satisfy the first of Equations (1.2). Also, the stretching transformation (1.5) becomes

$$\xi = \frac{1 - x}{\varepsilon} \tag{1.8}$$

Equation (1.8) is now introduced to transform the original Equation (1.1) into

$$\frac{d^2y}{d\xi^2} + \frac{dy}{d\xi} = 0 \tag{1.9}$$

for $\varepsilon << 1$.

Equation (1.9) has the solution

$$y^{BL} = c + de^{-\xi} \tag{1.10}$$

which should satisfy the second of Equation (1.2). Hence,

$$c + d = \beta \tag{1.11}$$

The matching principle (1.6) is now applied as

$$\lim_{x \to 1} y^{\circ} = \lim_{\xi \to \infty} y^{BL} \tag{1.12}$$

or,

$$c = \alpha e \tag{1.13}$$

Hence from Equation (1.11),

$$d = \beta - \alpha e \tag{1.14}$$

which yields

$$y^{BL} = \alpha e + (\beta - \alpha e)e^{-\xi} \tag{1.15}$$

Finally a uniformly valid solution is formed according to the equation

$$y_c = y^\circ + y^{BL} - (y^\circ)^{BL} \tag{1.16}$$

where y_c is the composite solution and $(y^\circ)^{BL}$ represents the common part contained in both solutions.

It is clear that in the present problem

$$(y^\circ)^{BL} = \lim_{\xi \to \infty} y^{BL} = \lim_{x \to 1} y^\circ = \alpha e \ , \tag{1.17}$$

hence the composite solution to the original equation is

$$y_c = \alpha e^x + (\beta - \alpha e)e^{-\xi} \tag{1.18}$$

The above derivation was required for the zeroth order problem of Equation (1.1). For a very small ε, the zeroth order composite solution (1.18) provides sufficient accuracy. For a relatively larger ε, solution to higher orders must be carried out to achieve better accuracy. This is shown in the following steps.

The solution to the original equation (1.1) may be expressed as an asymptotic expansion of the form

$$y = \sum_{n=0}^{\infty} \varepsilon^n y_n(x) \quad , \quad \varepsilon << 1 \tag{1.19}$$

Substituting (1.19) into Equation (1.1) results in

$$\sum_{n=0}^{\infty} (\varepsilon^{n+1} y''_n - \varepsilon^n y'_n + \varepsilon^n y_n) = 0 \tag{1.20}$$

Since this is an identity equation in the nonzero parameter ε, the coefficients corresponding to each n must vanish for all x in the domain specified by (1.1). Hence,

$$y'_0 - y_0 = 0 \tag{1.21}$$

$$y'_n - y_n = y''_{n-1} \qquad n \geq 1 \tag{1.22}$$

Also, substituting (1.19) into the boundary condition (1.2) leads to

$$y_0(0) = \alpha \tag{1.23}$$

$$y_0(1) = \beta \tag{1.24}$$

$$y_n(0) = y_n(1) = 0 \qquad n \geq 0 \tag{1.25}$$

It is clear that the zeroth order problem is defined by Equations (1.21), (1.23) and (1.24). The composite solution to this problem can be shown to be identical to (1.18). Also, it is seen that at any level of approximation n, y_{n-1} is known, hence y_n for any n is given by the first-order equation (1.22). Therefore, the stretching transformation (1.8) should be continually introduced near the end x = 1 where the boundary condition is dropped. If the asymptotic expansion

$$y = \sum_{n=0}^{\infty} \varepsilon^n y_n(\xi) \quad , \quad \varepsilon << 1 \tag{1.26}$$

is assumed, the transformed equations are

$$\frac{d^2y_0}{d\xi^2} - \frac{dy_0}{d\xi} = 0 \tag{1.27}$$

$$\frac{d^2y_n}{d\xi^2} - \frac{dy_n}{d\xi} = -y_{n-1} \qquad n \geq 1 \tag{1.28}$$

And the boundary condition at $x = 1$ becomes

$$y_0(\xi = 0) = \beta \tag{1.29}$$

$$y_n(\xi = 0) = 0 \qquad n \geq 1 \tag{1.30}$$

At this point it must be noted that Prandtl's matching principle (1.6) fails to match expansions containing higher-order solutions. Instead, Van Dyke's matching principle [2, 22] should be employed to obtain a composite solution. For simplicity in the present thesis, only the zeroth order problem will be considered, hence no elaboration will be given. Nevertheless, it may well be an intriguing topic of future study.

Chapter II

PROBLEM FORMULATION

Figure 1 shows a balanced symmetric laminate of 2m plies of homogeneous orthotropic lamina oriented at angles $[\theta_1/\theta_2/\theta_3/..../\theta_m]_s$ with the x axis. The laminate thickness is small compared to other dimensions, i.e., the length dimensions are of the order $L > b >> h$. One of the orthotropic axes of the laminate coincides with the z axis. The laminate is subjected to a constant inplane axial strain ε_x. Assuming elastic response exists everywhere throughout the laminate, the field equations can be derived as indicated in the following section.

2.1 GOVERNING FIELD EQUATIONS

Introducing a rotational transformation (Reference [1]) to the layerwise orthotropic material leads to the following constitutive equations with respect to the reference coordinate axes xyz

$$\begin{bmatrix} \sigma_x \\ \sigma_y \\ \sigma_z \\ \tau_{yz} \\ \tau_{xz} \\ \tau_{xy} \end{bmatrix}^{(k)} = \begin{bmatrix} C_{11} & C_{12} & C_{13} & 0 & 0 & C_{16} \\ C_{12} & C_{22} & C_{23} & 0 & 0 & C_{26} \\ C_{13} & C_{23} & C_{33} & 0 & 0 & C_{36} \\ 0 & 0 & 0 & C_{44} & C_{45} & 0 \\ 0 & 0 & 0 & C_{45} & C_{55} & 0 \\ C_{16} & C_{26} & C_{36} & 0 & 0 & C_{66} \end{bmatrix}^{(k)} \begin{bmatrix} \varepsilon_x \\ \varepsilon_y \\ \varepsilon_z \\ \gamma_{yz} \\ \gamma_{xz} \\ \gamma_{xy} \end{bmatrix}^{(k)} \tag{2.1}$$

where the superscript k denotes the k^{th} layer in the laminate. The strain-displacement relations in each layer are

$$
\begin{aligned}
\varepsilon_x &= u,x \\
\varepsilon_y &= v,y \\
\varepsilon_z &= w,z \\
\gamma_{yz} &= w,y + v,z \\
\gamma_{xz} &= w,x + u,z \\
\gamma_{xy} &= v,x + u,y
\end{aligned}
\tag{2.2}
$$

where a comma denotes partial differentiation.

Since the long laminate is loaded only at its ends $x = \pm L$. Saint Venant's principle [23] can be invoked such that the stresses in regions far away from the ends are independent of x. Thus, the equilibrium equations in such regions reduce to

$$
\begin{aligned}
\frac{\partial \tau_{xy}}{\partial y} + \frac{\partial \tau_{xz}}{\partial z} &= 0 \\
\frac{\partial \sigma_y}{\partial y} + \frac{\partial \tau_{yz}}{\partial z} &= 0 \\
\frac{\partial \tau_{yz}}{\partial y} + \frac{\partial \sigma_z}{\partial z} &= 0
\end{aligned}
\tag{2.3}
$$

Combining equations (2.1) and (2.2), and integrating the resulting stress-displacement relations (independent of x) results in the following displacement fields for each layer.

$$
\begin{aligned}
u &= (C_1 y + C_2 z + C_3)x + U(y,z) \\
v &= (C_4 z + C_5)x - C_1 \frac{x^2}{2} + V(y,z) \\
w &= -C_4 xy + C_6 x - C_2 \frac{x^2}{2} + W(y,z)
\end{aligned}
\tag{2.4}
$$

where C_1 through C_6 are unknown constants and U, V and W are unknown

functions of y and z only.

The following symmetry and antisymmetry conditions must be imposed:

$$\begin{aligned} u(x,y,z) &= u(x,y,-z) \\ v(x,y,z) &= v(x,y,-z) \\ w(x,y,z) &= -w(x,y,-z) \\ v(x,y,z) &= -v(x,-y,z) \\ w(x,y,z) &= w(x,-y,z) \end{aligned} \tag{2.5}$$

and the experimentally verified [13] condition

$$u(0,y,h) = -u(0,-y,h) \tag{2.6}$$

is imposed.

Equation (2.6) leads to a more general antisymmetry condition

$$u(0,y,z) = -u(0,-y,z) \tag{2.7}$$

for continuity consideration.

At this point, the even and odd nature of the displacements u, v, w in relation to y and z can readily be seen. Substitution of Equations (2.4) into Equations (2.5) and (2.7) results in

$$C_1 = C_2 = C_4 = C_5 = C_6 = 0 \tag{2.8}$$

and

$$\begin{aligned} &U(y,z) = U(y,-z),\ V(y,z) = V(y,-z),\ W(y,z) = -W(y,-z) \\ &U(y,z) = -U(-y,z),\ V(y,z) = -V(-y,z),\ W(y,z) = W(-y,z) \end{aligned} \tag{2.9}$$

This greatly reduces the layerwise displacement field functions (2.4) to

$$\begin{aligned} u &= C_3 x + U(y,z) \\ v &= V(y,z) \\ w &= W(y,z) \end{aligned} \tag{2.10}$$

As defined in the beginning of the present chapter, the laminate is subjected to a uniform axial strain. Hence the constant C_3 in Equations (2.10) is nothing but the applied strain ε_x.

Combining Equations (2.1), (2.2), (2.3) and (2.10) results in the following set of simultaneous partial differential equations within each layer.

$$\begin{aligned} &C_{66}U,yy + C_{55}U,zz + C_{26}V,yy + C_{45}V,zz + (C_{36} + C_{45})W,yz = 0 \\ &C_{26}U,yy + C_{45}U,zz + C_{22}V,yy + C_{44}V,zz + (C_{23} + C_{44})W,yz = 0 \\ &(C_{45} + C_{36})U,yz + (C_{44} + C_{23})V,yz + C_{44}W,yy + C_{33}W,zz = 0 \end{aligned} \tag{2.11}$$

The appropriate traction-free boundary conditions are (Fig. 1):

$$\begin{aligned} \sigma_y(\pm b,z) &= 0 \\ \tau_{xy}(\pm b,z) &= 0 \\ \tau_{yz}(\pm b,z) &= 0 \end{aligned} \tag{2.12}$$

along the free edges, and

$$\begin{aligned} \sigma_z(y,\pm h) &= 0 \\ \tau_{xz}(y,\pm h) &= 0 \\ \tau_{yz}(y,\pm h) &= 0 \end{aligned} \tag{2.13}$$

on the top and bottom surfaces of the laminate.

Equations (2.12) and (2.13) may be expressed in terms of the unknown functions U, V, W in the form

$$\begin{aligned}
&\{C_{12}\varepsilon_x + C_{22}V,y(\pm b,z) + C_{23}W,z(\pm b,z) + C_{26}U,y(\pm b,z)\}^{(k)} = 0\\
&\{C_{16}\varepsilon_x + C_{26}V,y(\pm b,z) + C_{36}W,z(\pm b,z) + C_{66}U,y(\pm b,z)\}^{(k)} = 0\\
&\{C_{44}V,z(\pm b,z) + C_{44}W,y(\pm b,z) + C_{45}U,z(\pm b,z)\}^{(k)} = 0
\end{aligned} \tag{2.12}$$

$$\begin{aligned}
&\{C_{13}\varepsilon_x + C_{23}V,y(y,\pm h) + C_{33}W,z(y,\pm h) + C_{36}U,y(y,\pm h)\}^{(1)} = 0\\
&\{C_{44}V,z(y,\pm h) + C_{44}W,y(y,\pm h) + C_{45}U,z(y,\pm h)\}^{(1)} = 0\\
&\{C_{45}V,z(y,\pm h) + C_{45}W,y(y,\pm h) + C_{55}U,z(y,\pm h)\}^{(1)} = 0
\end{aligned} \tag{2.13}$$

where the superscripts k and 1 denote the k^{th} layer and the outermost layer (Fig. 1), respectively. Equations (2.9) also yield the following restrictions on the displacement fields

$$\begin{aligned}
&\{U,z(y,0)\}^{(m)} = 0\\
&\{V,z(y,0)\}^{(m)} = 0\\
&\{W(y,0)\}^{(m)} = 0
\end{aligned} \tag{2.14}$$

along the midplane and

$$\begin{aligned}
&\{U(0,z)\}^{(k)} = 0\\
&\{V(0,z)\}^{(k)} = 0\\
&\{W,y(0,z)\}^{(k)} = 0
\end{aligned} \tag{2.15}$$

along the central plane and the superscript m denotes the layer

adjacent to the midplane (Fig. 1).

Equations (2.11) along with Equations (2.12) - (2.15) represent a well defined boundary value problem. Also, it is important to note that these field equations were derived for individual layers. Hence continuity in displacements and tractions across the interfaces must be enforced to insure completeness of the solution.

Equations (2.11) - (2.15) can be put in the dimensionless forms

$$\begin{aligned}
&\{Q_{66}(h/b)^2U,_{YY} + Q_{55}U,_{ZZ} + Q_{26}(h/b)^2V,_{YY} + Q_{45}V,_{ZZ} \\
&\qquad + (Q_{36} + Q_{45})(h/b)W,_{YZ}\}^{(k)} = 0 \\
&\{Q_{26}(h/b)^2U,_{YY} + Q_{45}U,_{ZZ} + Q_{22}(h/b)^2V,_{YY} + Q_{44}V,_{ZZ} \\
&\qquad + (Q_{23} + Q_{44})(h/b)W,_{YZ})\}^{(k)} = 0 \\
&\{(Q_{45} + Q_{36})(h/b)U,_{YZ} + (Q_{44} + Q_{23})(h/b)V,_{YZ} \\
&\qquad + Q_{44}(h/b)^2W,_{YY} + Q_{33}W,_{ZZ}\}^{(k)} = 0
\end{aligned} \tag{2.16}$$

$$\begin{aligned}
&\{Q_{12}\varepsilon_x + \frac{Q_{22}}{b}V,_{Y}(\pm 1,Z) + \frac{Q_{23}}{h}W,_{Z}(\pm 1,Z) + \frac{Q_{26}}{b}U,_{Y}(\pm 1,Z)\}^{(k)} = 0 \\
&\{Q_{16}\varepsilon_x + \frac{Q_{26}}{b}V,_{Y}(\pm 1,Z) + \frac{Q_{36}}{h}W,_{Z}(\pm 1,Z) + \frac{Q_{66}}{b}U,_{Y}(\pm 1,Z)\}^{(k)} = 0 \\
&\left\{\frac{Q_{44}}{h}V,_{Z}(\pm 1,Z) + \frac{Q_{44}}{b}W,_{Y}(\pm 1,Z) + \frac{Q_{45}}{h}U,_{Z}(\pm 1,Z)\right\}^{(k)} = 0
\end{aligned} \tag{2.17}$$

$$\begin{aligned}
&\{Q_{13}\varepsilon_x + \frac{Q_{23}}{b}V,_{Y}(Y,\pm 1) + \frac{Q_{33}}{h}W,_{Z}(Y,\pm 1) + \frac{Q_{36}}{b}U,_{Y}(Y,\pm 1)\}^{(1)} = 0 \\
&\left\{\frac{Q_{44}}{h}V,_{Z}(Y,\pm 1) + \frac{Q_{44}}{b}W,_{Y}(Y,\pm 1) + \frac{Q_{45}}{h}U,_{Z}(Y,\pm 1)\right\}^{(1)} = 0 \\
&\left\{\frac{Q_{45}}{h}V,_{Z}(Y,\pm 1) + \frac{Q_{45}}{b}W,_{Y}(Y,\pm 1) + \frac{Q_{55}}{h}U,_{Z}(Y,\pm 1)\right\}^{(1)} = 0
\end{aligned} \tag{2.18}$$

$$\{U,Z(Y,0)\}^{(m)} = 0$$
$$\{V,Z(Y,0)\}^{(m)} = 0 \qquad (2.19)$$
$$\{W(Y,0)\}^{(m)} = 0$$

$$\{U(0,Z)\}^{(k)} = 0$$
$$\{V(0,Z)\}^{(k)} = 0 \qquad (2.20)$$
$$\{W,Y(0,Z)\}^{(k)} = 0$$

where $Q_{ij}^{(k)} = C_{ij}^{(k)}/C_{max}^{(k)}$ with $C_{max}^{(k)}$ being the largest stiffness coefficient of the k^{th} layer, $Y = \frac{y}{b}$ and $Z = \frac{z}{h}$, the dimensionless coordinates, and U, V, W and their partial derivatives being dimensionless quantities.

2.2 EQUILIBRIUM CONSIDERATIONS

Before developing the solution procedures, it will be shown that a close examination of the force and moment equilibrium of a section of the laminate will lead to significant reduction in the mathematical complexity. Consider the free body diagram in Fig. 2. Let

$$t_k = \frac{h_k}{h}, \quad k = 1,2,\ldots,m \qquad (2.21)$$

hence,

$$\sum_{j=1}^{m} t_j = 1 . \qquad (2.22)$$

The force and moment equilibrium per unit length require

$$\Sigma F_y = 0$$

NOTE : τ_{xy} , τ_{xz} (NOT SHOWN)

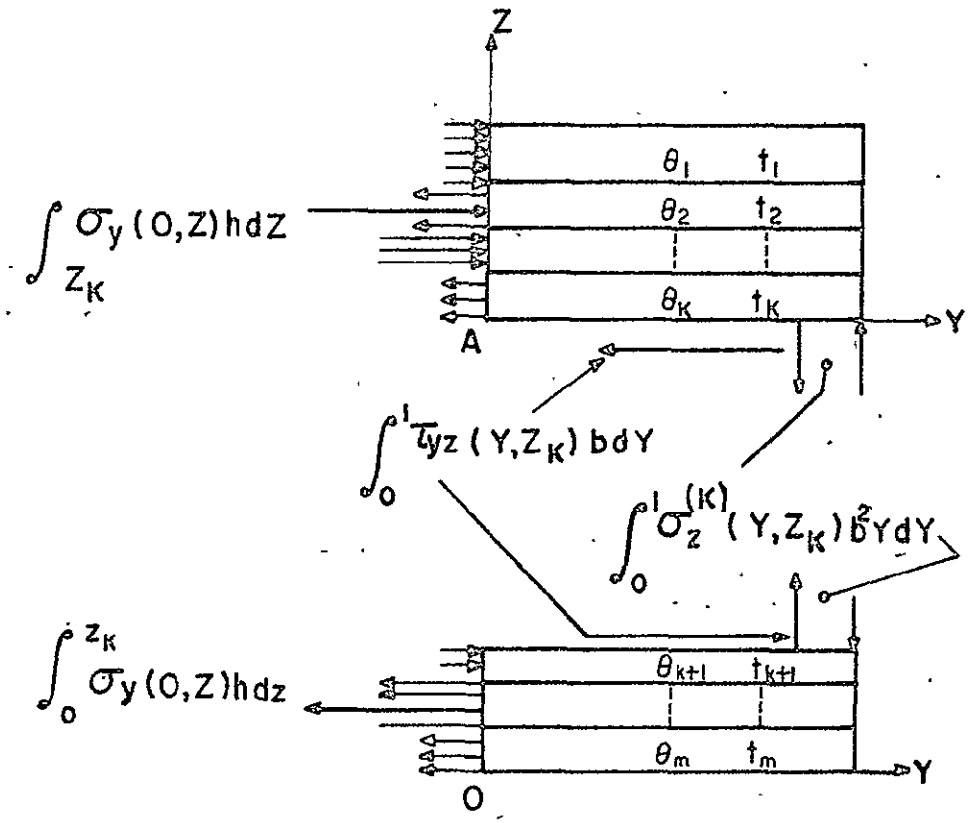

FIGURE 2 FREE BODY DIAGRAM OF QUARTER YZ-PLANE

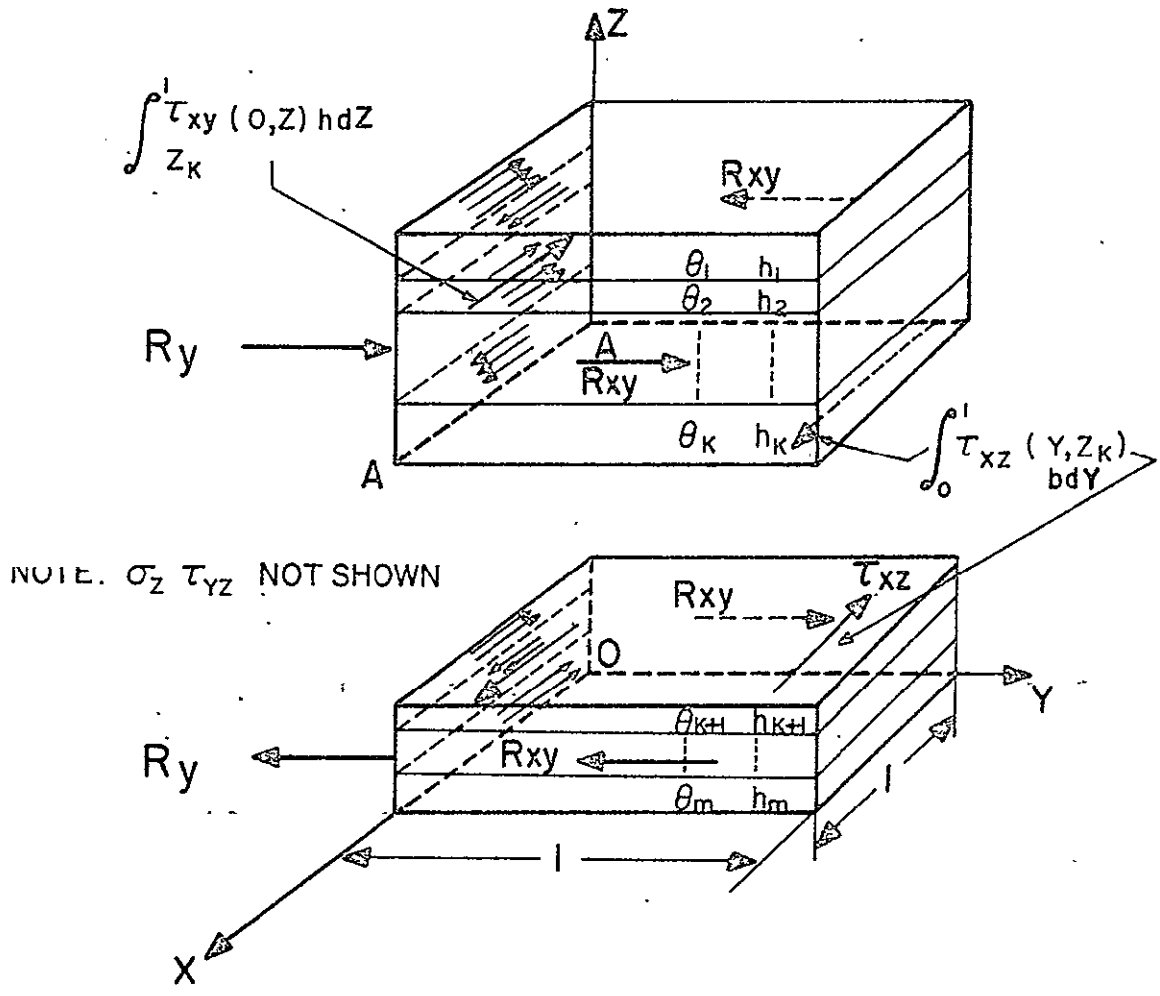

FIGURE 3. PARTIAL FREE BODY DIAGRAM OF QUARTER SECTION.

which gives

$$\int_{Z_k}^{1} \sigma_y(0,Z)hdZ = \int_0^1 \tau_{yz}^{(k)}(Y,Z_k)bdY \tag{2.23}$$

and $\Sigma M_A = 0$ which gives

$$\int_{Z_k}^{1} \sigma_y(0,Z)h^2(Z - Z_k)dZ = \int_0^1 \sigma_z^{(k)}(Y,Z_k)b^2YdY \tag{2.24}$$

where $Z_k = 1 - \sum_{j=1}^{k} t_j$ is the elevation of the k^{th} interface in the first quadrant.

On the other hand, the force equilibrium per unit length requires

$$\Sigma F_x = 0$$

which yields

$$\int_{Z_k}^{1} \tau_{xy}(0,Z)hdZ = \int_0^1 \tau_{xz}(Y,Z_k)bdY \tag{2.25}$$

At this point, an important premise must be recognized in the solution method of the present thesis. It has been numerically observed in [24] and examined in the present study that the central plane stresses $\sigma_y^{(k)}(0,Z)$ and $\tau_{xy}^{(k)}(0,Z)$ are essentially constant in each layer for $h/b << 1$ (Figs. 2, 3). Hence it may be expressed mathematically that

$$\Sigma F_y = \sum_{k=1}^{m} \sigma_y^{(k)}(0,Z)\, t_k = 0 \tag{2.26}$$

and

$$\Sigma F_x = \sum_{k=1}^{m} \tau_{xy}^{(k)}(0,Z)\, t_k = 0 \tag{2.27}$$

for equilibrium considerations.

Equations (2.23) through (2.27) together serve as an important tool to reduce the mathematical complexities in the present thesis. Since the material on either side of the k^{th} interface $Z = Z_k$ must satisfy the governing equations (2.16) and the boundary conditions (2.17) and (2.20), and since the interlaminar stress distributions are of primary interests, the boundary layer equations will be solved by considering only the infinitesimally thin free body diagram about this interface (Fig. 4). By doing so, the boundary value problem is replaced by the free body force and moment system of Fig. 4. Thus, the stress boundary conditions on the top and bottom surfaces, (2.18), can be safely ignored. This will be elaborated upon in Subsection 2.3.2.

2.3 PERTURBATION SOLUTION

As described in Section 1.3, two regions will be considered separately. Namely, the interior region where the solution to the reduced equations ($\varepsilon \to 0$) satisfies boundary conditions at one end, and the boundary-layer region where solution to the "stretched" equations satisfies the boundary condition at the other end. Matching of these two solutions must be enforced to insure uniformity of the resulting

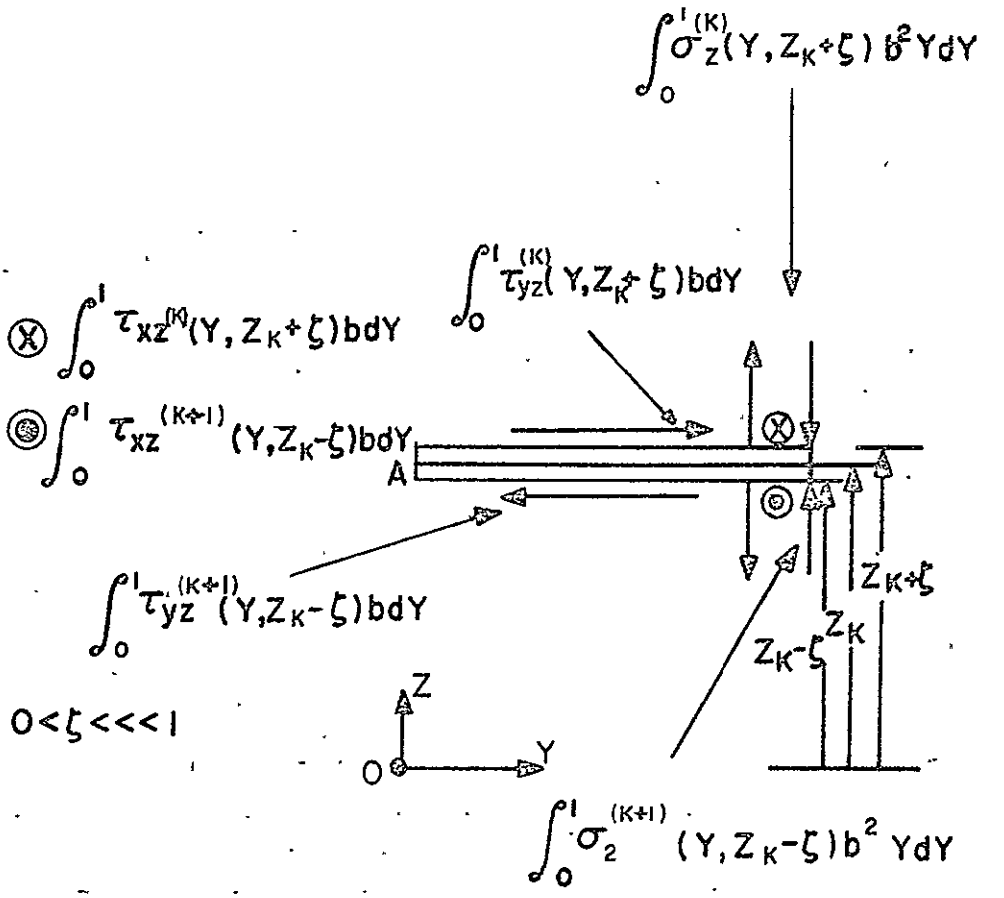

FIGURE 4. LIMITING FREE BODY DIAGRAM OF THE INTERFACE $Z = Z_K$

composite solution.

2.3.1 THE INTERIOR REGION

To seek a straightforward expansion, let

$$U^{(k)} = \sum_{n=0}^{\infty} \varepsilon^n U_n^{(k)}(Y,Z)$$

$$V^{(k)} = \sum_{n=0}^{\infty} \varepsilon^n V_n^{(k)}(Y,Z) \tag{2.28}$$

$$W^{(k)} = \sum_{n=0}^{\infty} \varepsilon^n W_n^{(k)}(Y,Z) \qquad \varepsilon << 1, \quad k = 1,2,3,\ldots,m$$

where the small parameter ε represents the geometrical ratio h/b.

Substituting these expansions into Equations (2.16) and equating coefficients of equal powers of ε to zero result in the following sets of equations:

$$\varepsilon^0 : \begin{aligned} \left\{Q_{55}U_{0,ZZ} + Q_{45}V_{0,ZZ}\right\}^{(k)} &= 0 \\ \left\{Q_{45}U_{0,ZZ} + Q_{44}V_{0,ZZ}\right\}^{(k)} &= 0 \\ \left\{Q_{33}W_{0,ZZ}\right\}^{(k)} &= 0 \end{aligned} \tag{2.29}$$

$$\varepsilon^1 : \begin{aligned} &\left\{Q_{55}U_{1,ZZ} + Q_{45}V_{1,ZZ} + (Q_{36} + Q_{45})W_{0,YZ}\right\}^{(k)} = 0 \\ &\left\{Q_{45}U_{1,ZZ} + Q_{44}V_{1,ZZ} + (Q_{23} + Q_{44})W_{0,YZ}\right\}^{(k)} = 0 \\ &\left\{(Q_{45} + Q_{36})U_{0,YZ} + (Q_{44} + Q_{23})V_{0,YZ} + Q_{33}W_{1,ZZ}\right\}^{(k)} = 0 \end{aligned} \tag{2.30}$$

$$\varepsilon^r : \left\{Q_{66}U_{r-2,YY} + Q_{55}U_{r,ZZ} + Q_{26}V_{r-2,YY} + Q_{45}V_{r,ZZ} + (Q_{36} + Q_{45})W_{r-1,YZ}\right\}^{(k)} = 0$$

$$\left\{Q_{26}U_{r-2,YY} + Q_{45}U_{r,ZZ} + Q_{22}V_{r-2,YY} + Q_{44}V_{r,ZZ} + (Q_{23} + Q_{44})W_{r-1,YZ}\right\}^{(k)} = 0 \qquad (2.31)$$

$$\left\{(Q_{45} + Q_{36})U_{r-1,YZ} + (Q_{44} + Q_{23})V_{r-1,YZ} + Q_{44}W_{r-2,YY} + Q_{33}W_{r,ZZ}\right\}^{(k)} = 0 \qquad r \geq 2$$

Now the displacement conditions (2.19) and (2.20) give

$$\begin{aligned} U_{n,Z}^{(m)}(Y,0) &= 0 \\ V_{n,Z}^{(m)}(Y,0) &= 0 \\ W_n^{(m)}(Y,0) &= 0 \qquad n = 0,1,2,\ldots. \end{aligned} \qquad (2.32)$$

and

$$\begin{aligned} U_n^{(k)}(0,Z) &= 0 \\ V_n^{(k)}(0,Z) &= 0 \\ W_{n,Y}^{(k)}(0,Z) &= 0 \qquad n = 0,,2,\ldots. \\ & \qquad\quad k = 1,2,\ldots,m \end{aligned} \qquad (2.33)$$

Recognizing that the boundary layer regions exist near $Y = \pm 1$, the stress free boundary conditions (2.17) are dropped for this interior region.

The stress boundary conditions on the top and bottom surfaces, Equations (2.18), yield

$$\left\{Q_{13}\varepsilon_x + \frac{Q_{23}}{b} V_{n,Y}(Y,\pm 1) + \frac{Q_{33}}{h} W_{n,Z}(Y,\pm 1) + \frac{Q_{36}}{b} U_{n,Y}(Y,\pm 1)\right\}^{(1)} = 0$$

$$\left\{\frac{Q_{44}}{h} V_{n,Z}(Y,\pm 1) + \frac{Q_{44}}{b} W_{n,Y}(Y,\pm 1) + \frac{Q_{45}}{h} U_{n,Z}(Y,\pm 1)\right\}^{(1)} = 0 \qquad (2.34)$$

$$\left\{\frac{Q_{45}}{h} V_{n,Z}(Y,\pm 1) + \frac{Q_{45}}{b} W_{n,Y}(Y,\pm 1) + \frac{Q_{55}}{h} U_{n,Z}(Y,\pm 1)\right\}^{(1)} = 0$$

$$n = 0,1,2,\ldots.$$

For the lamination theory, $\sigma_z^{(k)} = \tau_{xz}^{(k)} = \tau_{yz}^{(k)} = 0$ $(k = 2,3,4,\ldots,m)$ must also hold for the interior region. Hence Equations (2.34) may be generalized to

$$\left\{Q_{13}\varepsilon_x + \frac{Q_{23}}{b} V_{n,Y}(Y,\pm 1) + \frac{Q_{33}}{h} W_{n,Z}(Y,\pm 1) + \frac{Q_{36}}{b} U_{n,Y}(Y,\pm 1)\right\}^{(k)} = 0$$

$$\left\{\frac{Q_{44}}{h} V_{n,Z}(Y,\pm 1) + \frac{Q_{44}}{b} W_{n,Y}(Y,\pm 1) + \frac{Q_{45}}{h} U_{n,Z}(Y,\pm 1)\right\}^{(k)} = 0 \qquad (2.35)$$

$$\left\{\frac{Q_{45}}{h} V_{n,Z}(Y,\pm 1) + \frac{Q_{45}}{b} W_{n,Y}(Y,\pm 1) + \frac{Q_{55}}{h} U_{n,Z}(Y,\pm 1)\right\}^{(k)} = 0$$

$$n = 0,1,2,\ldots.$$

$$k = 1,2,\ldots,m$$

The derived symmetry and antisymmetry conditions (2.9) lead to

$$\begin{aligned}
U_n^{(k)}(Y,Z) &= U_n^{(k)}(Y,-Z)\\
V_n^{(k)}(Y,Z) &= V_n^{(k)}(Y,-Z)\\
W_n^{(k)}(Y,Z) &= -W_n^{(k)}(Y,-Z)\\
U_n^{(k)}(Y,Z) &= -U_n^{(k)}(-Y,Z)\\
V_n^{(k)}(Y,Z) &= -V_n^{(k)}(-Y,Z)\\
W_n^{(k)}(Y,Z) &= W_n^{(k)}(-Y,Z)
\end{aligned} \qquad (2.36)$$

$$n = 0,1,2,\ldots.$$

$$k = 1,2,\ldots,m$$

Equations (2.35) may be put in the following form with respect to the order of ε, similar to Equations (2.29) through (2.31).

$$\begin{aligned}
\varepsilon^0 : \; & Q_{13}^{(k)}\,\varepsilon_{xh} + Q_{33}^{(k)} W_{o,Z}^{(k)}(Y,\pm 1) = 0 \\
& Q_{44}^{(k)} V_{o,Z}(Y,\pm 1) + Q_{45}^{(k)} U_{o,Z}(Y,\pm 1) = 0 \\
& Q_{45}^{(k)} V_{o,Z}(Y,\pm 1) + Q_{55}^{(k)} U_{o,Z}(Y,\pm 1) = 0
\end{aligned} \tag{2.37}$$

$$\begin{aligned}
\varepsilon^r : \; & Q_{23}^{(k)} V_{r-1,Y}^{(k)}(Y,\pm 1) + Q_{33}^{(k)} W_{r,Z}^{(k)}(Y,\pm 1) \\
& + Q_{36}^{(k)} U_{r-1,Y}^{(k)}(Y,\pm 1) = 0 \\
& Q_{44}^{(k)} V_{r,Z}^{(k)}(Y,\pm 1) + Q_{45}^{(k)} U_{r,Z}^{(k)}(Y,\pm 1) \\
& + Q_{44}^{(k)} W_{r-1,Y}^{(k)}(Y,\pm 1) = 0 \\
& Q_{45}^{(k)} V_{r,Z}^{(k)}(Y,\pm 1) + Q_{55}^{(k)} U_{r,Z}^{(k)}(Y,\pm 1) \\
& + Q_{45}^{(k)} W_{r-1,Y}^{(k)}(Y,\pm 1) = 0 \qquad r \geq 1
\end{aligned} \tag{2.38}$$

Thus, the interior region problem is redefined by the infinite sets of equations with respect to the order of ε.

The Zeroth Order Problem:

Equations (2.29), (2.32), (2.33), (2.36) and (2.37), (n = 0) constitute the zeroth order problem for the interior region.

The solutions to Equations (2.29) have the form

$$\begin{aligned}
U_o^{(k)} &= A_o^{(k)}(Y)Z + B_o^{(k)}(Y) \\
V_o^{(k)} &= C_o^{(k)}(Y)Z + D_o^{(k)}(Y) \\
W_o^{(k)} &= E_o^{(k)}(Y)Z + F_o^{(k)}(Y)
\end{aligned} \tag{2.39}$$

$$k = 1,2,\ldots,m$$

where $A_o^{(k)}(Y)$ through $F_o^{(k)}(Y)$ are unknown functions. It may be

noted that the form of Solution (2.39) is similar to Pagano's approximate solution of Reference [17].

From Equations (2.36) with n = 0, it may be shown that

$$A_o^{(k)}(Y) = C_o^{(k)}(Y) = F_o^{(k)}(Y) = 0 \tag{2.40}$$

The first of Equation (2.37) then leads to

$$E_o^{(k)}(Y) = - \frac{Q_{13}^{(k)} \varepsilon_x h}{Q_{33}^{(k)}}$$

hence

$$W_o^{(k)} = - \frac{Q_{13}^{(k)} \varepsilon_x h}{Q_{33}^{(k)}} Z = - \frac{C_{13}^{(k)} \varepsilon_x h}{C_{33}^{(k)}} Z \tag{2.41}$$

The last two of Equations (2.37) are identically satisfied.

From Equations (2.32) with n = 0

$$B_o^{(k)}(0) = D_o^{(k)} = 0 \qquad k = 1,2,\ldots,m \tag{2.42}$$

Also, from Equations (2.36) with n = 0

$$\begin{aligned} B_o^{(k)}(-Y) &= - B_o^{(k)}(Y) \\ D_o^{(k)}(-Y) &= - D_o^{(k)}(Y) \qquad k = 1,2,\ldots,m \end{aligned} \tag{2.43}$$

Equations (2.26) and (2.27) may now be expressed in the form

$$\sum_{k=1}^{m} \left[\left(C_{12} - \frac{C_{23} C_{13}}{C_{33}} \right)^{(k)} \right] h_k \varepsilon_x b + \sum_{k=1}^{m} C_{22}^{(k)} h_k D_o'^{(k)}(Y) + \sum_{k=1}^{m} C_{26}^{(k)} h_k B_o'^{(k)}(Y) = 0 \tag{2.44}$$

$$\sum_{k=1}^{m}\left[\left(C_{16} - \frac{C_{26}C_{13}}{C_{33}}\right)^{(k)}\right]h_k\epsilon_x b + \sum_{k=1}^{m} C_{26}{}^{(k)}h_k D_o{}'^{(k)}(Y)$$

$$+ \sum_{k=1}^{m} C_{66}{}^{(k)}h_k B_o{}'^{(k)}(Y) = 0 \qquad (2.45)$$

where $B_o{}'^{(k)}(Y)$ and $D_o{}'^{(k)}(Y)$ are the first derivatives of the corresponding functions. Note that the higher order terms were neglected in these equations.

Equation (2.41) implies that continuity in the displacement $W(Y,Z)$ can be insured only when higher order terms are included since $Q_{ij}{}^{(k)}$ $(k = 1,2,\ldots,m)$ are different in general.

Enforcing displacement continuity in $U(Y,Z)$ and $V(Y,Z)$ results in

$$B_o{}^{(1)}(Y) = B_o{}^{(2)}(Y) = \ldots\ldots = B_o{}^{(m)}(Y) \qquad (2.46)$$

$$D_o{}^{(1)}(Y) = D_o{}^{(2)}(Y) = \ldots\ldots = D_o{}^{(m)}(Y) \qquad (2.47)$$

Integrating Equations (2.44) and (2.45), making use of Equations (2.42) and combining the resulting Equations with Equations (2.46) and (2.47) lead to

$$B_o{}^{(k)}(Y) = -\frac{(q_1q_3 - q_2q_4)}{(q_2q_5 - q_3q_3)}\epsilon_x bY$$

$$k = 1,2,\ldots,m \qquad (2.48)$$

$$D_o{}^{(k)}(Y) = -\frac{(q_1q_5 - q_3q_4)}{(q_2q_5 - q_3q_3)}\epsilon_x bY$$

where

$$
\begin{aligned}
q_1 &= \sum_{k=1}^{m} \left[C_{12} - \frac{C_{23}C_{13}}{C_{33}} \right]^{(k)} h_k \\
q_2 &= \sum_{k=1}^{m} C_{22}^{(k)} h_k \\
q_3 &= \sum_{k=1}^{m} C_{26}^{(k)} h_k \\
q_4 &= \sum_{k=1}^{m} \left[C_{16} - \frac{C_{26}C_{13}}{C_{33}} \right]^{(k)} h_k \\
q_5 &= \sum_{k=1}^{m} C_{66}^{(k)} h_k
\end{aligned}
\tag{2.49}
$$

As mentioned in the preceding section, higher-order approximations are not pursued in this thesis for simplicity. Hence, the interior region solutions are found to be

$$
\begin{aligned}
U^{(k)} &= B_0^{(k)}(Y) + O(\varepsilon) \\
V^{(k)} &= D_0^{(k)}(Y) + O(\varepsilon) \\
W^{(k)} &= -\frac{C_{13}^{(k)} \varepsilon_x h}{C_{33}^{(k)}} Z + O(\varepsilon) \qquad k = 1,2,\ldots,m
\end{aligned}
\tag{2.50}
$$

where $B_0^{(k)}(Y)$ and $D_0^{(k)}(Y)$ are given by Equations (2.48), and $O(\varepsilon)$ represents the highest order term truncated in the asymptotic expansion.

2.3.2 MODIFIED ZEROTH ORDER INTERIOR REGION SOLUTION

Solution (2.50) does not completely satisfy the vanishing stress condition (2.35) to the proper order of ε. This can be seen from Equation (2.38) where the zeroth order displacements $U_0^{(k)}(Y,Z)$

and $V_0^{(k)}(Y,Z)$ were related to the undetermined first order displacement $W_1^{(k)}(Y,Z)$. It has been described (Section 1.3) that solving higher order problems requires more complex mathematical procedures such as Van Dyke's matching principle. Also in Section 2.2, it was shown that the uniform stress distribution on the central xz - plane (Y = 0), a numerical result, is utilized as an important tool to reduce mathematical complexity for the boundary layer region. Therefore, an improved zeroth order interior region solution to evaluate better stress intensity near the central plane is certainly quite demanding.

To seek such an improvement, Equation (2.39) along with Equation (2.40) are now required to satisfy the stress conditions (2.35) exactly. Equations (2.32), (2.33) and (2.36) remain satisfied. The following equations are obtained.

$$W_0^{(k)} = E_0^{(k)} Z \tag{2.51}$$

$$U_0^{(k)} = B_0^{(k)}(Y) \tag{2.52}$$

$$V_0^{(k)} = D_0^{(k)}(Y) \tag{2.53}$$

$$\{Q_{13}\varepsilon_x + \frac{Q_{23}}{b} D_0'(Y) + \frac{Q_{33}}{h} E_0 + \frac{Q_{36}}{b} B_0'(Y)\}^{(k)} = 0 \tag{2.54}$$

where $E_0^{(k)}$ now becomes an unknown constant for the k^{th} layer.

Again enforcing continuity in displacements $U_0^{(k)}(Y,Z)$ and $V_0^{(k)}(Y,Z)$, respectively, yields

$$B_0^{(1)}(Y) = B_0^{(2)}(Y) = \ldots = B_0^{(k)}(Y) = \overline{B}_0(Y) \tag{2.55}$$

and $$D_o^{(1)}(Y) = D_o^{(2)}(Y) = \ldots = D_o^{(k)}(Y) = \overline{D}_o(Y) \tag{2.56}$$

Hence, Equation (2.54) may be written as

$$C_{13}^{(k)}\varepsilon_x + \frac{C_{23}^{(k)}}{b}\overline{D}_o'(Y) + \frac{C_{33}^{(k)}}{h}E_o^{(k)} + \frac{C_{36}^{(k)}}{b}\overline{B}_o'(Y) = 0 \tag{2.57}$$

Continuity in the displacement $W_o^{(k)}(Y,Z)$, as developed in Subsection 2.3.1 (Equation (2.41)), will be insured only by higher order considerations, hence it is not imposed as a physical requirement in the present modification.

Finally, recalling Equations (2.26) and (2.27) gives

$$\left[\sum_{k=1}^{m}\left(C_{12} + \frac{C_{23}}{h}E_o\right)^{(k)}h_k\right]\varepsilon_x + \left[\sum_{k=1}^{m}\frac{C_{22}^{(k)}h_k}{b}\right]\overline{D}_o'(Y)$$

$$+ \left[\sum_{k=1}^{m}\frac{C_{26}^{(k)}h_k}{b}\right]\overline{B}_o'(Y) = 0 \tag{2.58}$$

and

$$\left[\sum_{k=1}^{m}\left(C_{16} + \frac{C_{36}}{h}E_o\right)^{(k)}h_k\right]\varepsilon_x + \left[\sum_{k=1}^{m}\frac{C_{26}^{(k)}h_k}{b}\right]\overline{D}_o'(Y)$$

$$+ \left[\sum_{k=1}^{m}\frac{C_{66}^{(k)}h_k}{b}\right]\overline{B}_o'(Y) = 0 \tag{2.59}$$

Since there are m + 2 simultaneous equations ((2.57) - (2.59)) for the m + 2 unknowns $\overline{B}_o'(Y)$, $\overline{D}_o'(Y)$, and $E_o^{(k)}$; the modified zeroth order interior solution can be readily determined.

To show the improvement made in the present modified interior region solution, two numerical examples are given in Tables 1 and 2.

TABLE 1*

$[0/90]_s$ ($\epsilon = 0.133$)

Displacement	Finite Difference	ZIR** Solution	Modified ZIR Solution
$U^{(k)}/(\epsilon_x bY)$	0	0	0
$V^{(k)}/(\epsilon_x bY)$	-0.0397	-0.0391	-0.0396
$W^{(1)}/(\epsilon_x hZ)$	-0.2467	-0.2534	-0.2448
$W^{(2)}/(\epsilon_x hZ)$	-0.2055	-0.2172	-0.2072

* Material: graphite-epoxy laminate with constant ply thickness.

** Zeroth order interior region.

TABLE 2

$[45/-45]_s$ ($\epsilon = 0.133$)

Displacement	Finite Difference	ZIR Solution	Modified ZIR Solution
$U^{(k)}/(\epsilon_x bY)$	0	0	0
$V^{(k)}/(\epsilon_x bY)$	-0.7409	-0.7298	-0.7433
$W^{(1)}/(\epsilon_x hZ)$	-0.0607	-0.2354	-0.0604
$W^{(2)}/(\epsilon_x hZ)$	-0.0613	-0.2354	-0.0604

As expected, the Modified ZIR solution yields more reliable results than the ZIR solution.

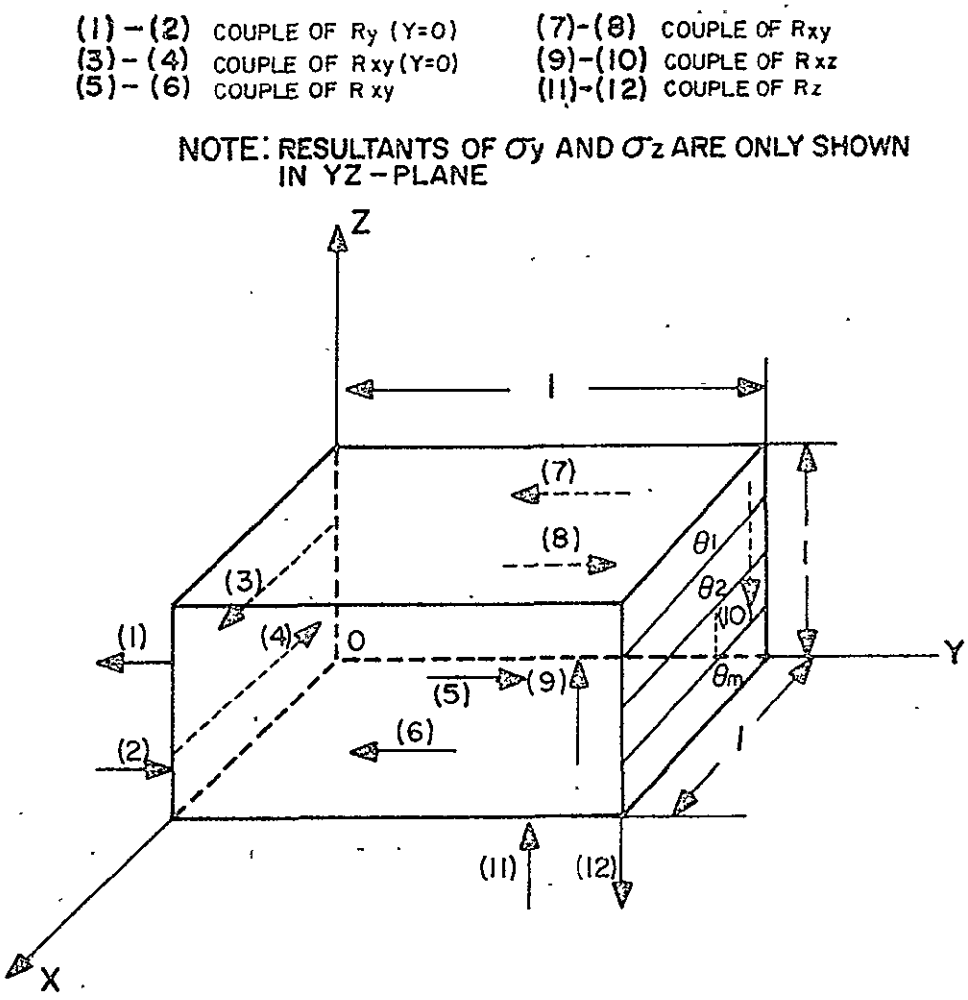

FIGURE 5. FREE BODY DIAGRAM OF FIRST QUADRANT OF TYPICAL SECTION

Hence the former will be employed throughout the present thesis to evaluate the central plane stress intensity for the determination of the unknown coefficients in the boundary layer region solution.

2.3.3 THE BOUNDARY LAYER REGION

Consider the first quadrant of the yz - plane as shown in Figure 5. Introducing the stretching transformation

$$\eta = \frac{(1 - Y)}{\varepsilon} \tag{2.60}$$

near the free edge Y = 1 to the governing equations (2.16) results in the following equations for this quarter plane of the laminate.

$$\begin{aligned}
&\{Q_{66}U_{,\eta\eta} + Q_{55}U_{,ZZ} + Q_{26}V_{,\eta\eta} + Q_{45}V_{,ZZ} - (Q_{36} + Q_{45})W_{,\eta Z}\}^{(k)} = 0\\
&\{Q_{26}U_{,\eta\eta} + Q_{45}U_{,ZZ} + Q_{22}V_{,\eta\eta} + Q_{44}V_{,ZZ} - (Q_{23} + Q_{44})W_{,\eta Z}\}^{(k)} = 0\\
&\{-(Q_{45} + Q_{36})U_{,\eta Z} - (Q_{44} + Q_{23})V_{,\eta Z} + Q_{44}W_{,\eta\eta} + Q_{33}W_{,ZZ}\}^{(k)} = 0
\end{aligned} \tag{2.61}$$

To satisfy Prandtl's matching principle (Section 1.3), assume the following composite expansions

$$\begin{aligned}
U^{(k)} &= [B_0(Y) + P_0 e^{\lambda_0 \eta} \cos \alpha_0 Z]^{(k)} + O(\varepsilon)\\
V^{(k)} &= [D_0(Y) + R_0 e^{\lambda_0 \eta} \cos \alpha_0 Z]^{(k)} + O(\varepsilon) \qquad k = 1,2,\ldots,m\\
W^{(k)} &= [E_0 Z + S_0 e^{\lambda_0 \eta} \sin \alpha_0 Z]^{(k)} + O(\varepsilon)
\end{aligned} \tag{2.62}$$

where $B_0^{(k)}(Y)$, $D_0^{(k)}(Y)$ and $E_0^{(k)}$ are the Modified ZIR solution given by Equations (2.57) - (2.59), $P_0^{(k)}$, $R_0^{(k)}$ and $S_0^{(k)}$ are undetermined coefficients, and $\alpha_0^{(k)}$ are undetermined positive quantities

in radians. The subscript o implies the zeroth order solution for the boundary layer region.

Substituting Equations (2.62) into Equations (2.61) and neglecting the $O(\varepsilon)$ terms results in the following set of three simultaneous algebraic equations corresponding to the ε^0 order:

$$\{(Q_{66}\lambda_o^2 - Q_{55}\alpha_o^2)P_o + (Q_{26}\lambda_o^2 - Q_{45}\alpha_o^2)R_o - (Q_{36} + Q_{45})\lambda_o\alpha_o S_o\}^{(k)} = 0$$

$$\{(Q_{26}\lambda_o^2 - Q_{45}\alpha_o^2)P_o + (Q_{22}\lambda_o^2 - Q_{44}\alpha_o^2)R_o - (Q_{23} + Q_{44})\lambda_o\alpha_o S_o\}^{(k)} = 0$$

$$\{(Q_{45} + Q_{36})\lambda_o\alpha_o P_o + (Q_{44} + Q_{23})\lambda_o\alpha_o R_o + (Q_{44}\lambda_o^2 - Q_{33}\alpha_o^2)S_o\}^{(k)} = 0$$

$$k = 1,2,\ldots,m \qquad (2.63)$$

For each nontrivial term of Solution (2.62) to exist the determinants of these algebraic equations must vanish individually. Thus,

$$\begin{vmatrix} Q_{66}\lambda_o^2 - Q_{55}\alpha_o^2 & Q_{26}\lambda_o^2 - Q_{45}\alpha_o^2 & -(Q_{36} + Q_{45})\lambda_o\alpha_o \\ Q_{26}\lambda_o^2 - Q_{45}\alpha_o^2 & Q_{22}\lambda_o^2 - Q_{44}\alpha_o^2 & -(Q_{23} + Q_{44})\lambda_o\alpha_o \\ (Q_{45} + Q_{36})\lambda_o\alpha_o & (Q_{44} + Q_{23})\lambda_o\alpha_o & Q_{44}\lambda_o^2 - Q_{33}\alpha_o^2 \end{vmatrix}^{(k)} = 0 \qquad (2.64)$$

$$k = 1,2,\ldots,m$$

These sixth order equations may be regarded as third-order equations by the classical treatment [25] and the method of complex variables [26].

The six roots are found to be in the form

$$\{\lambda_o(1,2) = \pm \bar{a}\,\alpha_o\}^{(k)}$$

$$\{\lambda_o(3,4) = \pm \bar{b}\,\alpha_o\}^{(k)} \qquad (2.65)$$

$$\{\lambda_o(5,6) = \pm \bar{c}\,\alpha_o\}^{(k)}$$

where $\bar{a}^{(k)}$, $\bar{b}^{(k)}$, $\bar{c}^{(k)}$ are three positive constants in terms of material constants of the k^{th} layer (see Section 3.2). For matching consideration, however, the positive roots must be dropped since they lead to exponential growths of the displacements for large η (or small Y).

Upon determining the characteristic roots from Equations (2.65), Solution (2.62) takes the following general form.

$$U^{(k)} = \{B_0(Y) + (P_1 e^{-\bar{a}\alpha_0\eta} + P_2 e^{-\bar{b}\alpha_0\eta} + P_3 e^{-\bar{c}\alpha_0\eta}) \cos \alpha_0 Z\}^{(k)} + O(\varepsilon)$$

$$V^{(k)} = \{D_0(Y) + (R_1 e^{-\bar{a}\alpha_0\eta} + R_2 e^{-\bar{b}\alpha_0\eta} + R_3 e^{-\bar{c}\alpha_0\eta}) \cos \alpha_0 Z\}^{(k)} + O(\varepsilon)$$

$$W^{(k)} = \{E_0 Z + (S_1 e^{-\bar{a}\alpha_0\eta} + S_2 e^{-\bar{b}\alpha_0\eta} + S_3 e^{-\bar{c}\alpha_0\eta}) \sin \alpha_0 Z\}^{(k)} + O(\varepsilon) \quad (2.66)$$

where $P_0^{(k)}$, are replaced by $P_1^{(k)}$, $P_2^{(k)}$, $P_3^{(k)}$, etc.

With the above solution, the stress boundary conditions (2.17a), (2.17b) and (2.17c) transform to

$$\{[Q_{26}(\bar{a}P_1 + \bar{b}P_2 + \bar{c}P_3) + Q_{22}(\bar{a}R_1 + \bar{b}P_2 + \bar{c}R_3) + Q_{23}(S_1 + S_2 + S_3)]\alpha_0 \cos(\alpha_0 Z_k) = -[(Q_{12} + \frac{Q_{23}}{h} E_0)\varepsilon_x + \frac{Q_{22}}{b} D_0'(\pm 1) + \frac{Q_{26}}{b} B_0'(\pm 1)]h\}^{(k)} \quad (2.67)$$

$$\{[Q_{66}(\bar{a}P_1 + \bar{b}P_2 + \bar{c}P_3) + Q_{26}(\bar{a}R_1 + \bar{b}R_2 + \bar{c}R_3) + Q_{36}(S_1 + S_2 + S_3)]\alpha_0 \cos(\alpha_0 Z_k) = -[(Q_{16} + \frac{Q_{36}}{h} E_0)\varepsilon_x + \frac{Q_{26}}{b} D_0'(\pm 1) + \frac{Q_{66}}{b} B_0'(\pm 1)h\}^{(k)} \quad (2.68)$$

$$\{Q_{44}[(R_1 + R_2 + R_3) - (S_1\bar{a} + S_2\bar{b} + S_3\bar{c})] + Q_{45}(P_1 + P_2 + P_3)\}^{(k)} = 0$$
$$k = 1,2,\ldots,m \qquad (2.69)$$

Note that the right hand sides of Equations (2.67) and (2.68) are all known quantities from the interior problem. Since there are ten unknown coefficients in the k^{th} layer, solving simultaneously three equations from the boundary conditions (2.67) through (2.69), and six equations from Equations (2.63) leads to the determination of the nine unknown coefficients in terms of α_0. The accuracy of the coefficients thus obtained can be readily checked by the self-equilibrating condition of the stress resultant,

$$\Sigma F_z = \int_0^b \sigma_z^{(k)} dY = 0 \qquad (2.70)$$

for any level of Z (Fig. 2).

Finally, imposing the moment equilibrium conditions (2.24) and the force equilibrium conditions (2.23) and (2.25) determines the values of $\alpha_0^{(k)}$ and $\tan(\alpha_0^{(k)} Z_k)$ to their orders of accuracy.

In summary, the zeroth order interior solution (ZIR) was obtained by letting h/b go to zero. The Modified ZIR solution improved the ZIR solution by satisfying the vanishing stress boundary conditions (2.35) exactly. The zeroth order boundary layer solution was obtained by transforming the governing equations and the boundary conditions (2.17) at the free edge. The matching principle was satisfied by the composite solution, and the self-equilibrating condition of the interlaminar normal stress resultant was employed to check the accuracy of the calculated coefficients. The continuity conditions

in both displacements and tractions were imposed. And the force and moment equilibrium of the composite solution with the central plane stress resultants were satisfied for the k^{th} interfacial plane $Z = Z_K$ (Figs. 3, 4).

Chapter III

SPECIAL LAMINATES

The solution method developed in the preceding chapter applies to balanced, symmetric laminates with variable-thickness plies. For certain special cases the field equations are greatly simplified by the vanishing of some elements in the stiffness matrix. Among the various laminates studied in the literature (Section 1.1) are the bi-directional laminates $[0/90]_s$ and $[90/0]_s$, and the angle-ply laminates $[\theta/-\theta]_s$ and $[-\theta/\theta]_s$. These two laminates will be considered in this chapter.

3.1 BIDIRECTIONAL LAMINATES WITH CONSTANT PLY THICKNESS

When the orientation of the fibrous layer is either 0° or 90° with respect to the x axis, the constitutive equation reduces to

$$\begin{bmatrix}\sigma_x\\ \sigma_y\\ \sigma_z\\ \tau_{yz}\\ \tau_{xz}\\ \tau_{xy}\end{bmatrix}^{(k)} = \begin{bmatrix}C_{11} & C_{12} & C_{13} & 0 & 0 & 0\\ C_{12} & C_{22} & C_{23} & 0 & 0 & 0\\ C_{13} & C_{23} & C_{33} & 0 & 0 & 0\\ 0 & 0 & 0 & C_{44} & 0 & 0\\ 0 & 0 & 0 & 0 & C_{55} & 0\\ 0 & 0 & 0 & 0 & 0 & C_{66}\end{bmatrix}^{(k)} \begin{bmatrix}\varepsilon_x\\ \varepsilon_y\\ \varepsilon_z\\ \gamma_{yz}\\ \gamma_{xz}\\ \gamma_{xy}\end{bmatrix}^{(k)} \qquad (3.1)$$

$$k = 1,2,\ldots,m.$$

Consider the laminate consisting of 2m layers with the stacking sequence $[0/90/0/90/0/90\ldots]_s$ as shown in Fig. 6a.

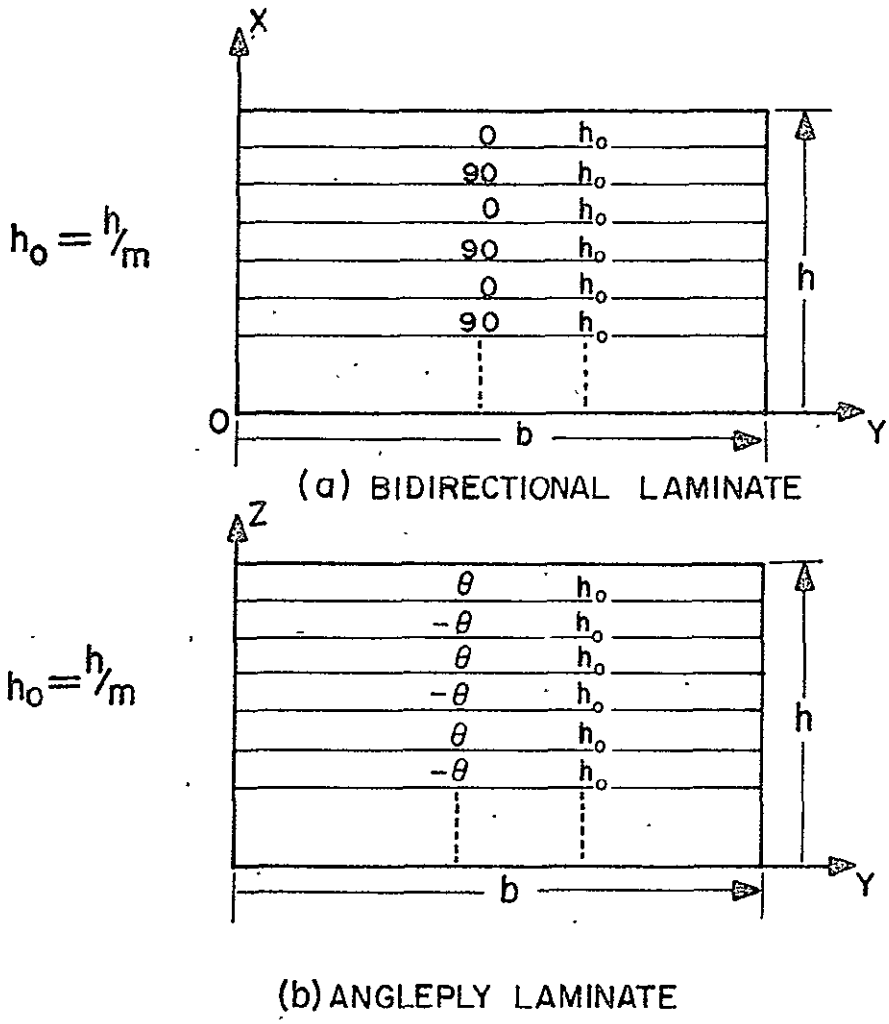

FIGURE 6. BIDIRECTIONAL AND ANGLE-PLY LAMINATES

Equations (2.16) reduce to

$$\{Q_{66}\left(\frac{h}{b}\right)^2 U_{,YY} + Q_{55}\, U_{,ZZ}\}^{(k)} = 0$$

$$\{Q_{22}\left(\frac{h}{b}\right)^2 V_{,YY} + Q_{44}\, V_{,ZZ} + (Q_{23} + Q_{44})\left(\frac{h}{b}\right) W_{,YZ}\}^{(k)} = 0 \qquad (3.2)$$

$$\{(Q_{44} + Q_{23})\left(\frac{h}{b}\right) V_{,YZ} + Q_{44}\left(\frac{h}{b}\right)^2 W_{,YY} + Q_{33}\, W_{,ZZ}\}^{(k)} = 0$$

Note that the first equation is an independent equation whose complete solution may be assumed in the form

$$U^{(k)} = \left\{\sum_{n=0}^{\infty} a_n\, e^{\lambda_n Y} \cos \alpha_n Z\right\}^{(k)} \qquad (3.3)$$

where $a_n^{(k)}$ $(n = 0,1,2,....)$ are unknown coefficients.

Substituting Equation (3.3) into the first of Equations (3.2) yield

$$\lambda_{n_{(1,2)}}^{(k)} = \left\{\pm\sqrt{\frac{Q_{55}}{Q_{66}}}\,\frac{b}{h}\,\alpha_n\right\}^{(k)} \qquad n = 0,1,2,.... \qquad (3.4)$$

Hence

$$U^{(k)} = \left\{\sum_{n=0}^{\infty} a_n \sinh\left(\sqrt{\frac{Q_{55}}{Q_{66}}}\,\frac{b}{h}\,\alpha_n\, Y\right) \cos \alpha_n Z\right\}^{(k)} \qquad (3.5)$$

Solution (3.5) automatically satisfies the first of the displacement symmetry conditions (2.19) and (2.20). The second equation of the free edge stress boundary conditions (2.17) reduces to

$$\left\{\frac{Q_{66}}{b}\, U_{,Y}\,(\pm 1,Z)\right\}^{(k)} = 0 \qquad (3.6)$$

Substituting Solution (3.5) into Equation (3.6) results in

$$a_n^{(k)} = 0 \qquad n = 0,1,2,.... \tag{3.7}$$

hence,

$$U^{(k)} = 0 \tag{3.8}$$

everywhere in this laminate.

This leads to the vanishing of the shear stresses $\tau_{xy}^{(k)}$ and $\tau_{xz}^{(k)}$ throughout the bidirectional laminate as may be physically expected.

The modified ZIR solution (Subsection 2.3.2) for $V^{(k)}$ and $W^{(k)}$ may be determined by solving Equations (2.57) - (2.59) simultaneously with $\bar{B}_o'(Y)$ vanishing identically. For the simplest case of the four layer symmetric $[0/90]_s$ laminate, the displacements are found to be

$$\begin{aligned} V^{(k)} &= D_o^{(k)}(Y) \\ W^{(1)} &= E_o^{(1)} Z \\ W^{(2)} &= E_o^{(2)} Z \end{aligned} \tag{3.9}$$

where

$$E_o^{(1)} = \frac{\{C_{23}^{(2)}(C_{23}^{(2)}C_{13}^{(1)}-C_{23}^{(1)}C_{13}^{(2)})+C_{33}^{(2)}[C_{13}^{(1)}(C_{22}^{(1)}+C_{22}^{(2)})-C_{23}^{(1)}(C_{12}^{(1)}+C_{12}^{(2)})]\}\varepsilon_x h}{(C_{23}^{(2)}C_{23}^{(1)}C_{33}^{(1)}+C_{23}^{(1)}C_{23}^{(2)}C_{33}^{(1)})-C_{33}^{(1)}C_{33}^{(2)}(C_{22}^{(1)}+C_{22}^{(2)})} \tag{3.10}$$

$$E_o^{(2)} = \frac{C_{23}^{(2)} C_{33}^{(1)}}{C_{23}^{(1)} C_{33}^{(2)}} E_o^{(1)} + \left[- \frac{C_{13}^{(2)}}{C_{33}^{(2)}} + \frac{C_{13}^{(1)} C_{23}^{(2)}}{C_{23}^{(1)} C_{33}^{(2)}} \right] \varepsilon_x h \tag{3.11}$$

$$D_o^{(k)}(Y) = -\left[\frac{C_{33}^{(1)} b}{C_{23}^{(1)} h} E_o^{(1)} + \frac{C_{13}^{(1)} \varepsilon_x b}{C_{23}^{(1)}} \right] Y \tag{3.12}$$

Introducing the stretching transformation

$$\eta = \frac{(1 - Y)}{\left(\frac{h}{b}\right)} \tag{3.13}$$

into the remaining coupled equations of (3.2) results in the boundary layer equation in the form

$$\begin{aligned} &\{Q_{22}\, V_{,\eta\eta} + Q_{44}\, V_{,ZZ} - (Q_{23} + Q_{44})\, W_{,\eta Z}\}^{(k)} = 0 \\ &\{-(Q_{44} + Q_{23})\, V_{,\eta Z} + Q_{44}\, W_{,\eta\eta} + Q_{33}\, W_{,ZZ}\}^{(k)} = 0 \end{aligned} \tag{3.14}$$

Following Subsection 2.3.3, the displacements are assumed to be

$$\begin{aligned} V^{(k)} &= D_0{}^{(k)}(Y) + [R_0 e^{\lambda_0 \eta} \cos \alpha_0 Z]^{(k)} + O(\varepsilon) \\ W^{(k)} &= E_0{}^{(k)} Z + [S_0\, e^{\lambda_0 \eta} \sin \alpha_0 Z]^{(k)} + O(\varepsilon) \end{aligned} \tag{3.15}$$

where $D_0{}^{(k)}(Y)$, $E_0{}^{(k)}$ are known quantities from the modified ZIR solution. For the four ply $[0/90]_S$ laminate, they are given by Equations (3.10) - (3.12). $R_0{}^{(k)}$ and $S_0{}^{(k)}$ are unknown coefficients.

Substituting Equations (3.15) into Equations (3.14) results in the algebraic equations for the zeroth order boundary layer problem as follows.

$$\begin{aligned} &\{(Q_{22}\, \lambda_0{}^2 - Q_{44}\, \alpha_0{}^2) R_0 - (Q_{23} + Q_{44}) \lambda_0\, \alpha_0\, S_0\}^{(k)} = 0 \\ &\{(Q_{44} + Q_{23}) \lambda_0\, \alpha_0\, R_0 + (Q_{44}\, \lambda_0{}^2 - Q_{33}\, \alpha_0{}^2) S_0\}^{(k)} = 0 \end{aligned} \tag{3.16}$$

For a nontrivial solution, the determinant of these equations must vanish. Thus,

$$\begin{vmatrix} Q_{22}\, \lambda_0{}^2 - Q_{44}\, \alpha_0{}^2 & -(Q_{23} + Q_{44}) \lambda_0\, \alpha_0 \\ (Q_{44} + Q_{23}) \lambda_0\, \alpha_0 & Q_{44}\, \lambda_0{}^2 - Q_{33}\, \alpha_0{}^2 \end{vmatrix}^{(k)} = 0 \tag{3.17}$$

whence

$$\lambda_0^{(k)} = \pm \left\{ \frac{\rho \pm \left[\rho^2 - 4\frac{Q_{33}}{Q_{22}}\right]^{1/2}}{2} \right\}^{(k)} \alpha_0^{(k)} \tag{3.18}$$

$$\rho^{(k)} = \left[\frac{Q_{33}}{Q_{44}} - \frac{Q_{23}Q_{23} + 2Q_{23}Q_{44}}{Q_{22}Q_{44}}\right]^{(k)} \tag{3.19}$$

Note that the 2 x 2 determinant is only a principal minor of the determinant in Equations (2.64). For conventional composites, such as graphite-epoxy and boron-epoxy laminates,

$$\left[\rho^2 - 4\frac{Q_{33}}{Q_{22}}\right]^{(k)} > 0 \tag{3.20}$$

Hence Equation (3.18) yields two pairs of real roots. For matching considerations, the positive roots are dropped, and the zeroth order composite solution (Section 1.3) takes the following form

$$\begin{aligned} V_c^{(k)} &= D_0^{(k)}(Y) + \{(R_1 e^{-\beta_1 \alpha_0 n} + R_2 e^{-\beta_2 \alpha_0 n})\cos \alpha_0 Z\}^{(k)} \\ W_c^{(k)} &= E_0^{(k)} Z + \{(S_1 e^{-\beta_1 \alpha_0 n} + S_2 e^{-\beta_2 \alpha_0 n})\sin \alpha_0 Z\}^{(k)} \end{aligned} \tag{3.21}$$

where

$$\begin{aligned} \beta_1^{(k)} &= \sqrt{\frac{\rho + \left[\rho^2 - 4\frac{Q_{33}}{Q_{22}}\right]^{1/2}}{2}}^{(k)} \\ \beta_2^{(k)} &= \sqrt{\frac{\rho - \left[\rho^2 - 4\frac{Q_{33}}{Q_{22}}\right]^{1/2}}{2}}^{(k)} \end{aligned} \tag{3.22}$$

and Prandtl's matching principle (Section 1.3) is satisfied.

The first and third of boundary conditions (2.17) lead to

$$\{[Q_{22}(\beta_1 R_1 + \beta_2 R_2) + Q_{23}(S_1 S_2]\alpha_o \cos(\alpha_o Z_k) = -\epsilon_x h(Q_{12} + Q_{22} D_o'(Y) + Q_{23} E_o)\}^{(k)} \qquad (3.23)$$

$$\{Q_{44}(R_1 + R_2 - S_1\beta_1 - S_2\beta_2)\}^{(k)} = 0$$

From Equations (3.16), additional relations between R_1 and S_1 R_2 and S_2, are obtained as follows

$$[(Q_{22}\beta_1^2 - Q_{44})R_1 - (Q_{23} + Q_{44})\beta_1 S_1]^{(k)} = 0 \qquad (3.24)$$

$$[(Q_{22}\beta_2^2 - Q_{44})R_2 - (Q_{23} + Q_{44})\beta_2 S_2]^{(k)} = 0 \qquad (3.25)$$

Solving Equations (3.23) - (3.25) simultaneously results in $R_1^{(k)}$, $R_2^{(k)}$, $S_1^{(k)}$ and $S_2^{(k)}$ in terms of $h\epsilon_x/(\alpha_o \cos \alpha_o(Z_k \pm \zeta))$ where $0 < \zeta <<< 1$ and Z_k is defined in Equation (2.24) and (2.25).

Equations (2.23) and (2.24) then lead to the determination of $\alpha_o^{(k)}$ and $\tan(\alpha_o^{(k)} Z_k - \zeta)$ to their orders of accuracy.

Thus the complete solution for the zeroth order displacement function $U^{(k)}$, $V^{(k)}$, $W^{(k)}$ are obtained and the interlaminar stresses between the k^{th} layer and the $(k+1)^{th}$ layer, $Z_k = 1 - \sum_{r=1}^{k} t_r$, may be readily calculated from the strain-displacement equations (2.2) and the constitutive equations (3.1).

3.1.1 $[0/90]_s$ GRAPHITE-EPOXY LAMINATE

As a numerical example, the four-ply $[0/90]_s$ graphite-epoxy laminate with constant ply thicknesses (Fig. 7a) is considered. The stiffness coefficients (after transformation) are listed below.

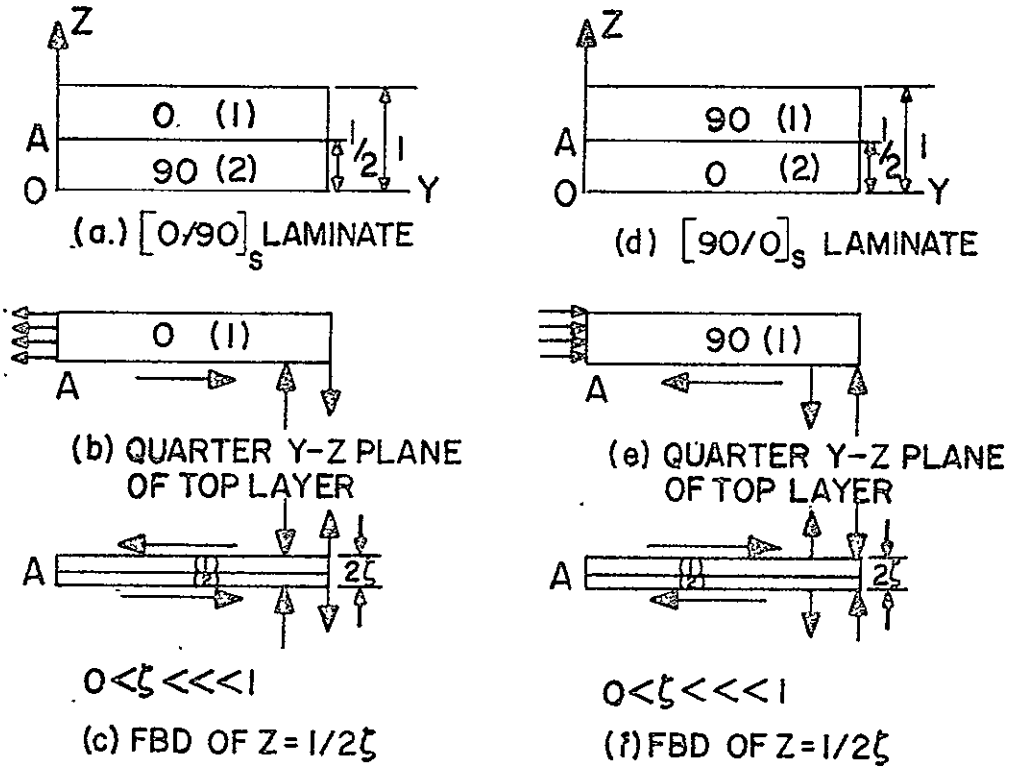

FIGURE 7. FOUR PLY BIDIRECTIONAL LAMINATES

0 (x 10^{-6} psi)	90 (x 10^{-6} psi)
$C_{11}^{(1)} = 20.2$	$C_{11}^{(2)} = 2.21$
$C_{12}^{(1)} = 0.56$	$C_{12}^{(2)} = 0.56$
$C_{22}^{(1)} = 2.21$	$C_{22}^{(2)} = 20.2$
$C_{13}^{(1)} = 0.56$	$C_{13}^{(2)} = 0.48$
$C_{23}^{(1)} = 0.48$	$C_{23}^{(2)} = 0.56$
$C_{33}^{(1)} = 2.21$	$C_{33}^{(2)} = 2.21$
$C_{44}^{(1)} = 0.85$	$C_{44}^{(2)} = 0.85$
$C_{55}^{(1)} = 0.85$	$C_{55}^{(2)} = 0.85$
$C_{66}^{(1)} = 0.85$	$C_{66}^{(2)} = 0.85$

(3.26)

From Equation (3.8), the axial displacement function U vanishes everywhere in the laminate.

The interior region solutions (3.9) are found to be

$$V_o^{(1)} = V_o^{(2)} = -0.0396\ \varepsilon_x bY \tag{3.27}$$

$$W_o^{(1)} = -0.2448\ \varepsilon_x hZ \tag{3.28}$$

$$W_o^{(2)} = -0.2072\ \varepsilon_x hZ \tag{3.29}$$

From Equations (2.2), (3.1), and (3.27) - (3.29), the central plane (Y = 0) stresses are found to be

$$\sigma_y^{(1)}(0,Z) = 0.3552\ \varepsilon_x(10^6\ \text{psi}) \tag{3.30}$$

$$\sigma_y^{(2)}(0,Z) = -0.3552\ \varepsilon_x(10^6\ \text{psi}) \tag{3.31}$$

$$\tau_{xy}^{(1)}(0,Z) = \tau_{xy}^{(2)}(0,Z) = 0$$

Equation (3.22) gives

$$\begin{aligned} \beta_1^{(1)} &= 1.10899 \\ \beta_2^{(1)} &= 0.90172 \\ \beta_1^{(2)} &= 1.57550 \\ \beta_2^{(2)} &= 0.20994 \end{aligned} \tag{3.32}$$

Considering continuity of Equations (3.28) and (3.29) at the interfaces $Z = \pm \frac{1}{2}$ and the exponents given by Equations (3.32), it may be postulated that the boundary layer effect in the 90°-ply (Layer 2) penetrates deeper into the interior of the laminate than that in the 0°-ply (Layer 1).

Hence the zeroth order composite solution (3.21) is in the form

$$\begin{aligned} V_c^{(1)} &= -0.0396\ \varepsilon_x bY + [(R_1 e^{-\beta_1\alpha_0\eta} + R_2 e^{-\beta_2\alpha_0\eta})\cos\alpha_0 Z]^{(1)} \\ W_c^{(1)} &= -0.2448\ \varepsilon_x hZ + [(S_1 e^{-\beta_1\alpha_0\eta} + S_2 e^{-\beta_2\alpha_0\eta})\sin\alpha_0 Z]^{(1)} \\ V_c^{(2)} &= -0.0396\ \varepsilon_x bY + [(R_1 e^{-\beta_1\alpha_0\eta} + R_2 e^{-\beta_2\alpha_0\eta})\cos\alpha_0 Z]^{(2)} \\ W_c^{(2)} &= -0.2072\ \varepsilon_x hZ + [(S_1 e^{-\beta_1\alpha_0\eta} + S_2 e^{-\beta_2\alpha_0\eta})\sin\alpha_0 Z]^{(2)} \end{aligned} \tag{3.33}$$

The unknown coefficients are found (setting $Z = \frac{1}{2}$) to be

$$
\begin{aligned}
R_1^{(1)} &= 0.8385\ \phi_1 & R_1^{(2)} &= -0.0028\ \phi_2 \\
R_2^{(1)} &= -1.1776\ \phi_1 & R_2^{(2)} &= 0.0984\ \phi_2 \\
S_1^{(1)} &= -1.0619\ \phi_1 & S_1^{(2)} &= 0.0625\ \phi_2 \\
S_2^{(1)} &= 0.9298\ \phi_1 & S_2^{(2)} &= -0.0134\ \phi_2
\end{aligned}
\tag{3.34}
$$

where

$$\phi_1 = \frac{\varepsilon_x h}{\alpha_0^{(1)} \cos\left(\alpha_0^{(1)}\left(\frac{1}{2} + \zeta\right)\right)} \tag{3.35}$$

$$\phi_2 = \frac{\varepsilon_x h}{\alpha_0^{(2)} \cos\left(\alpha_0^{(2)}\left(\frac{1}{2} - \zeta\right)\right)} \tag{3.36}$$

$$0 < \zeta <<< 1$$

The self-equilibrating condition $\Sigma F_z = 0$, Equation (2.70), can be written in the form

$$-\int_{\infty}^{0} \sigma_z^{(k)}\left(\eta, \frac{1}{2} \pm \zeta\right) h d\eta = 0 \qquad 0 < \zeta <<< 1 \tag{3.37}$$

Substituting the coefficients of Equations (3.34) into Equations (3.21) and the constitutive equation (3.1) determines the stresses on either side of the interface $Z = \frac{1}{2}$. It may be shown that Equation (3.37) is satisfied identically. This further confirms the correctness of the calculated coefficients of Equations (3.34).

Equations (2.23) and (2.24) now become

$$\int_{\infty}^{0} -\tau_{yz}^{(1)}\left(\eta, \frac{1}{2} + \zeta\right) h d\eta = -\frac{0.3552}{2} h\varepsilon_x (10^6) \tag{3.38}$$

$$\int_{\infty}^{0} -\tau_{yz}^{(2)}\left(\eta, \frac{1}{2} - \zeta\right) h d\eta = -\frac{0.3552}{2} h\varepsilon_x (10^6) \tag{3.39}$$

$$\int_{\infty}^{0} - \sigma_z^{(1)}(\eta, \frac{1}{2} + \zeta)bh(1 - \varepsilon\eta)d\eta = - \frac{0.3552}{2} h\varepsilon_x(10^6)\frac{h}{4} \qquad (3.40)$$

$$\int_{\infty}^{0} - \sigma_z^{(2)}(\eta, \frac{1}{2} - \zeta)bh(1 - \varepsilon\eta)d\eta = \frac{0.3552}{2} h\varepsilon_x(10^6)\frac{h}{4} \qquad (3.41)$$

$$0 < \zeta <<< 1$$

where $\frac{h}{4}$ is the approximate distance of the resultants $R_y^{(1)}$, $R_y^{(2)}$ from the interfacial plane.

To compare with the numerical results of Pipes and Pagano [7], the interlaminar stresses are calculated based on the 90° ply (the lower layer). Equation (3.39) leads to

$$\frac{\tan\left[\frac{\alpha_o^{(2)}}{2} - \alpha_o^{(2)}\,\zeta\right]}{\alpha_o^{(2)}} = 0.5 \qquad 0 < \zeta <<< 1 \qquad (3.42)$$

whence $\alpha_o^{(2)} = 0.180,\ 8.9868,\ 15.4505,\ \ldots.$ (3.43)

Equation (3.41) gives

$$\alpha_o^{(2)} = 2.8284 \qquad (3.44)$$

From Equations (3.38) - (3.41), it is clear that the stress resultant is of order $O(h\varepsilon_x 10^5)$ while the couple moment is of order $O(h^2\varepsilon_x 10^5)$. Hence, requiring exact satisfaction of Equation (3.39) and approximate satisfaction of Equation (3.41) fixes the value of $\alpha_o^{(2)}$ at

$$\alpha_o^{(2)} = 8.9868 \qquad (3.45)$$

While τ_{xy} and τ_{xz} vanish throughout the laminate, the other stress components are obtained in the following zeroth order form

$$\sigma_x^{(2)}(\eta, \frac{1}{2} - \zeta) = [2.08837 + (0.0275\, e^{-1.8868\eta} + 0.0051\, e^{-14.158\eta})]\varepsilon_x(10^6 \text{ psi}). \qquad (3.46)$$

$$\sigma_y^{(2)}(\eta,\tfrac{1}{2}-\zeta) = -(0.3552 + 0.0546\, e^{-14.158\eta} - 0.4098\, e^{-1.887\eta})\varepsilon_x(10^6 \text{ psi}) \quad (3.47)$$

$$\tau_{yz}^{(2)}(\eta,\tfrac{1}{2}-\zeta) = 0.3865(e^{-1.887\eta} - e^{-14.158\eta})\varepsilon_x(10^6 \text{ psi}) \quad (3.48)$$

$$\sigma_z^{(2)}(\eta,\tfrac{1}{2}-\zeta) = (0.1356\, e^{-14.158\eta} - 0.0185\, e^{-1.887\eta})\varepsilon_x(10^6 \text{ psi}) \quad (3.49)$$

where $0 < \zeta <<< 1$

The last two components of stress, the interlaminar stresses, are plotted and compared with numerical results in Figs. 8 - 11.

If the stacking sequence of the laminate is reversed to $[90/0]_s$, (Fig. 7d), the derivation of these interlaminar stresses is as indicated in the following subsection.

3.1.2 $[90/0]_s$ GRAPHITE-EPOXY LAMINATE

While $U^{(k)}$ vanishes everywhere in the laminates, the modified ZIR solution for $V^{(k)}$ and $W^{(k)}$ can be obtained by interchanging the superscripts in Equations (3.27) through (3.41).

To compare with the numerical results [7], the 0° ply is now used as the reference layer for the interlaminar stresses.

The stress components in zeroth order forms are obtained as

$$\sigma_x^{(2)}(\eta,\tfrac{1}{2}-\zeta) = [20.04 - 0.074(e^{-9.966\eta} + e^{-8.104\eta})]\varepsilon_x(10^6 \text{ psi}) \quad (3.50)$$

$$\sigma_y^{(2)}(\eta,\tfrac{1}{2}-\zeta) = (0.3552 + 1.5452\, e^{-9.966\eta} - 1.9004\, e^{-8.104\eta})\varepsilon_x(10^6 \text{ psi}) \quad (3.51)$$

$$\tau_{yz}^{(2)}(\eta,\tfrac{1}{2}-\zeta) = 7.6996(e^{-9.966\eta} - e^{-8.104\eta})\varepsilon_x(10^6 \text{ psi}) \quad (3.52)$$

$$\sigma_z^{(2)}(\eta,\tfrac{1}{2}-\zeta) = (-1.9004\, e^{-9.966\eta} + 1.5452\, e^{-8.104\eta})\varepsilon_x(10^6 \text{ psi}) \quad (3.53)$$

$0 < \zeta <<< 1$

where the last two are the interlaminar stresses.

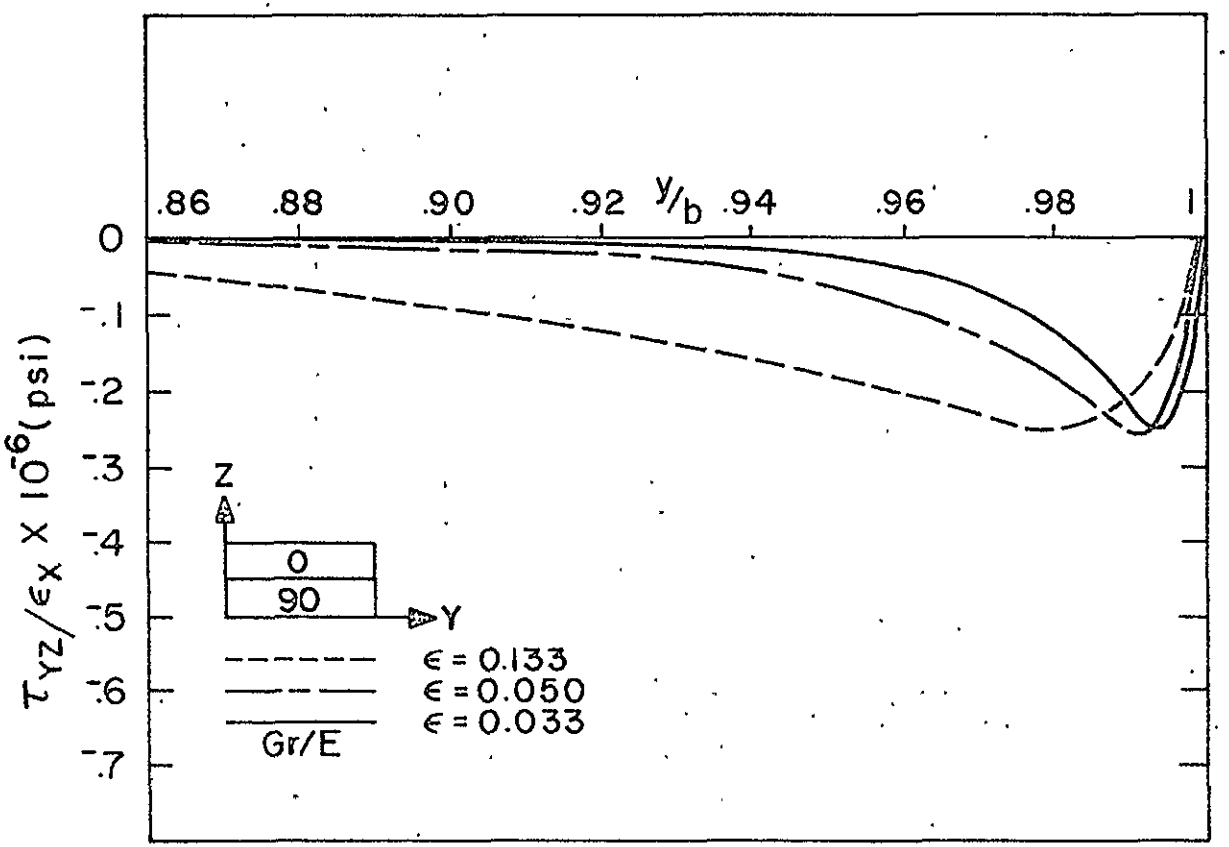

FIGURE 8. INTERLAMINAR SHEAR STRESS τ_{yz} AS A FUNCTION OF ϵ FOR $[0/90]_S$

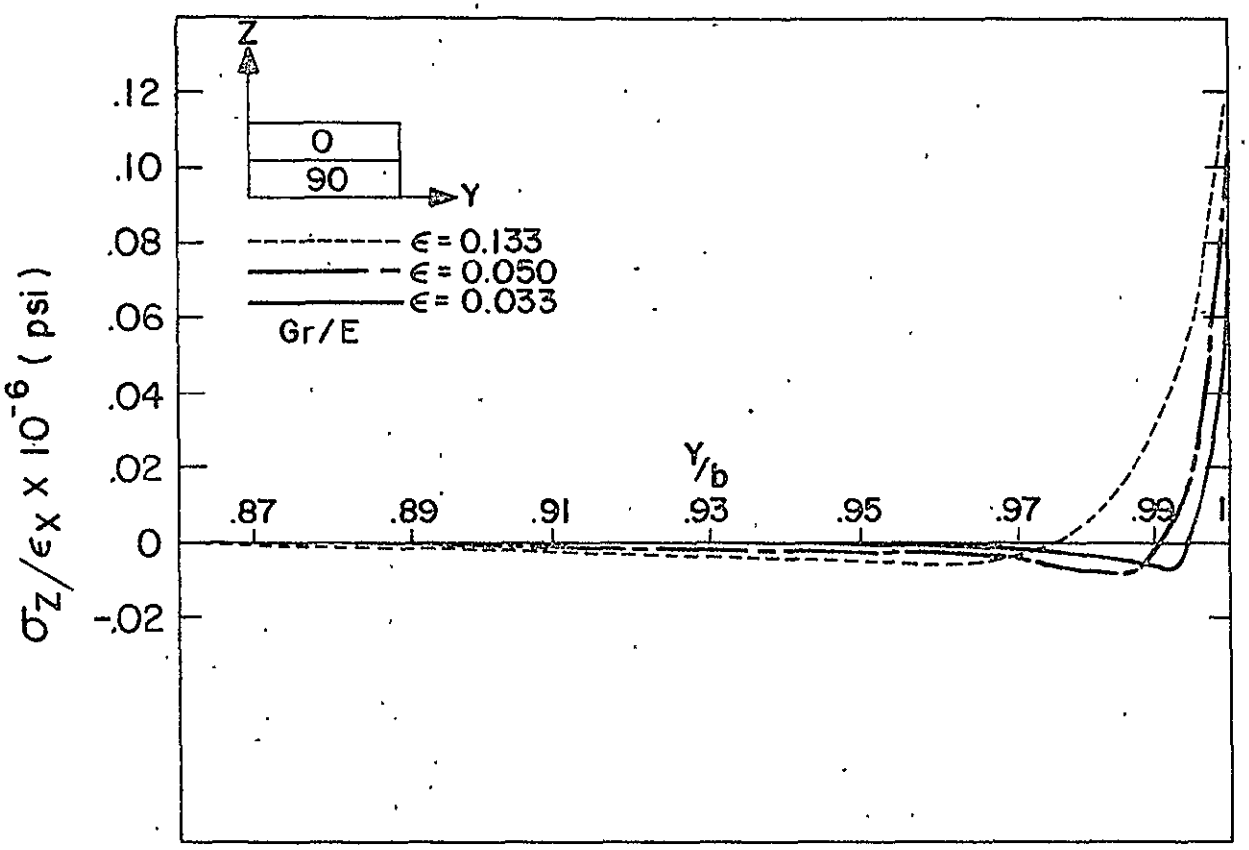

FIGURE 9. INTERLAMINAR NORMAL STRESS σ_z AS A FUNCTION OF ϵ FOR $[0/90]_s$

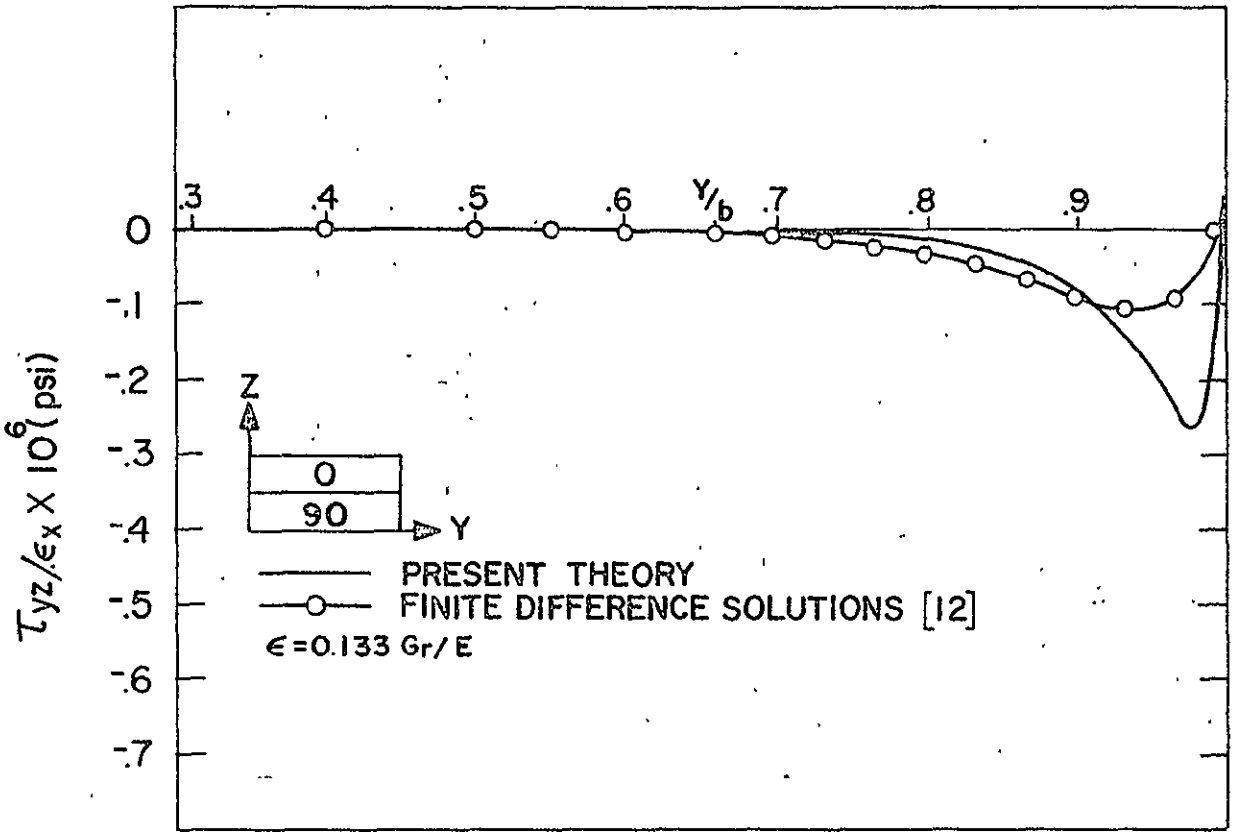

FIGURE 10. PRESENT THEORY AND FINITE DIFFERENCE RESULTS FOR τ_{yz} IN $[0/90]_S$

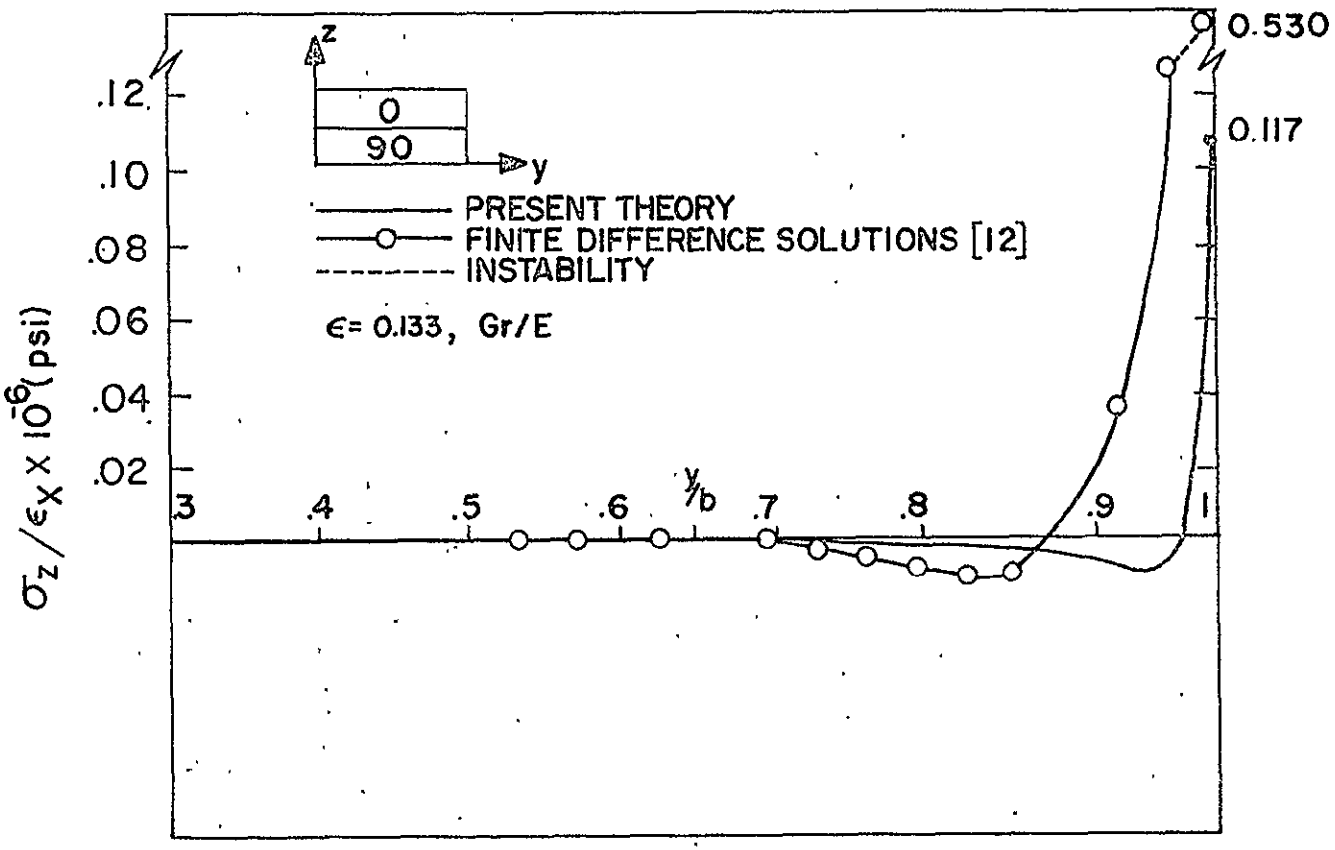

FIGURE 11. PRESENT THEORY AND FINITE DIFFERENCE RESULTS FOR σ_z IN $[0/90]_s$

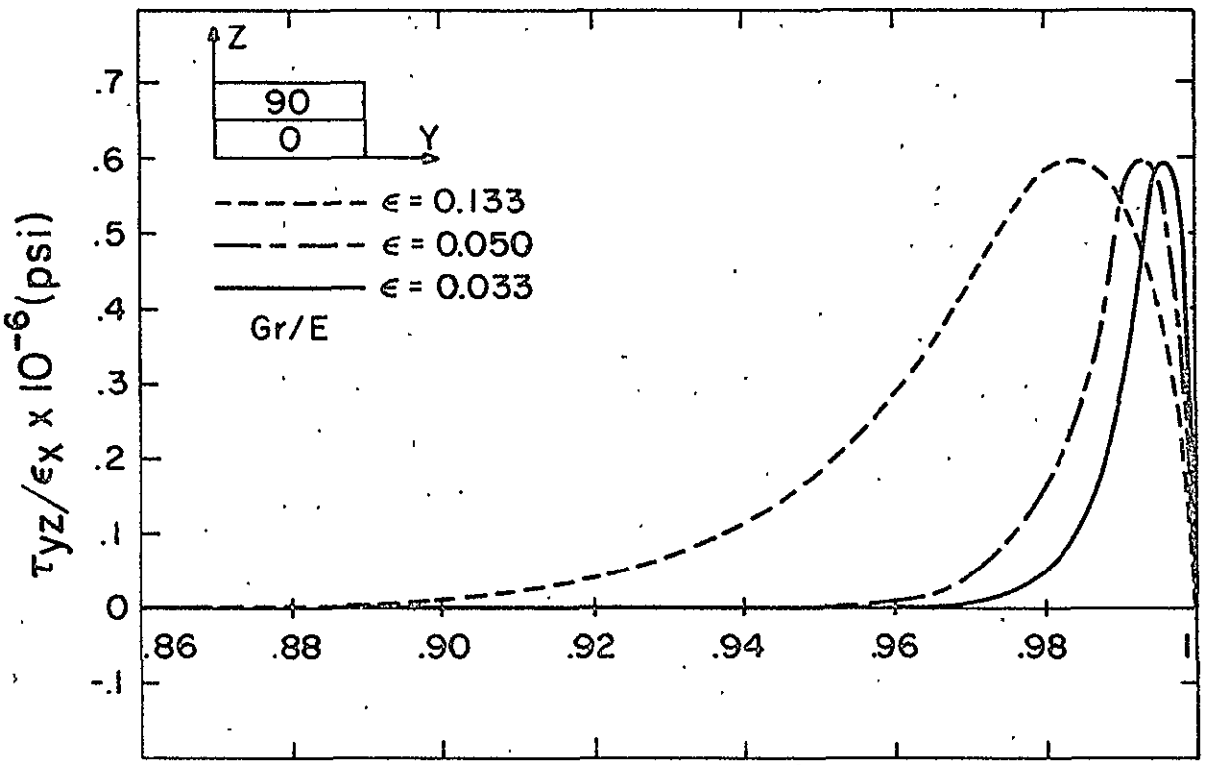

FIGURE 12. INTERLAMINAR SHEAR STRESS τ_{yz} AS A FUNCTION OF ϵ FOR $[90/0]_s$.

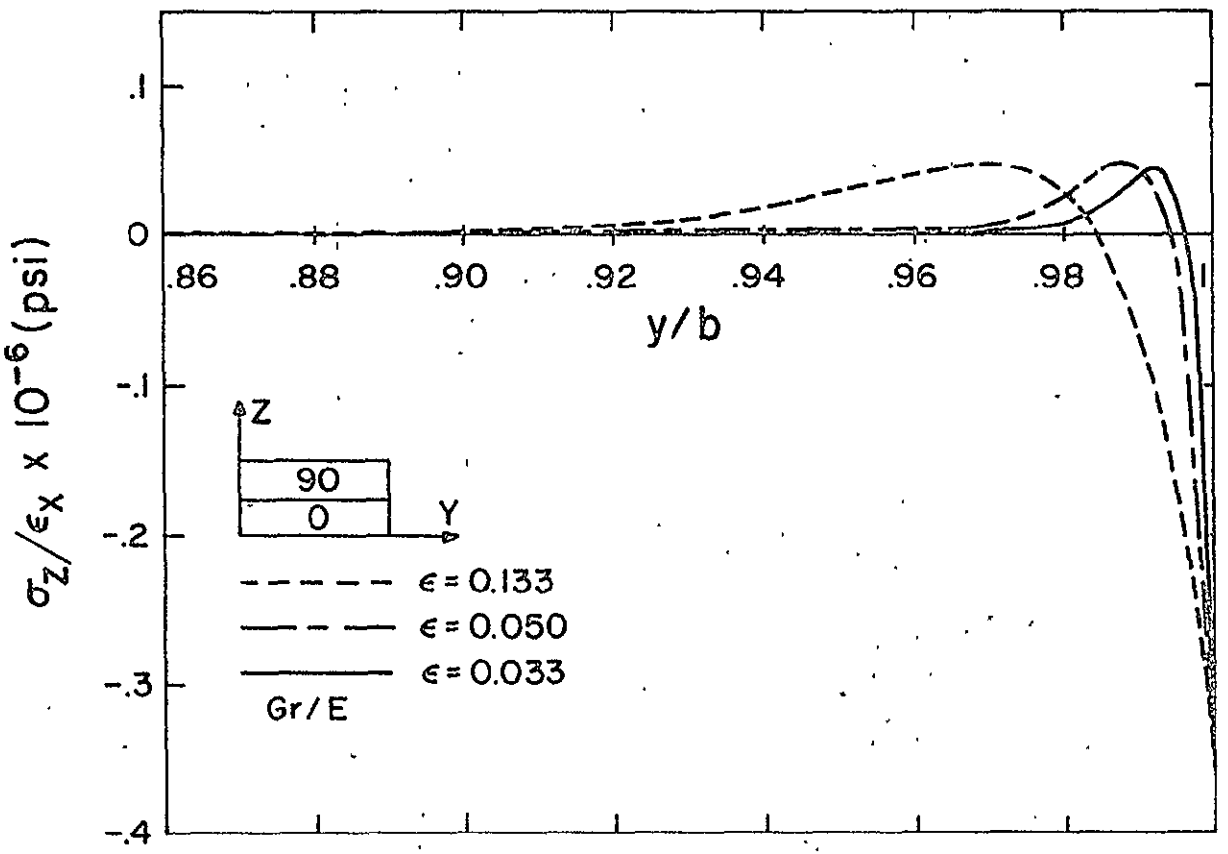

FIGURE 13. INTERLAMINAR NORMAL STRESS σ_z AS A FUNCTION OF ϵ FOR $[90/0]_s$.

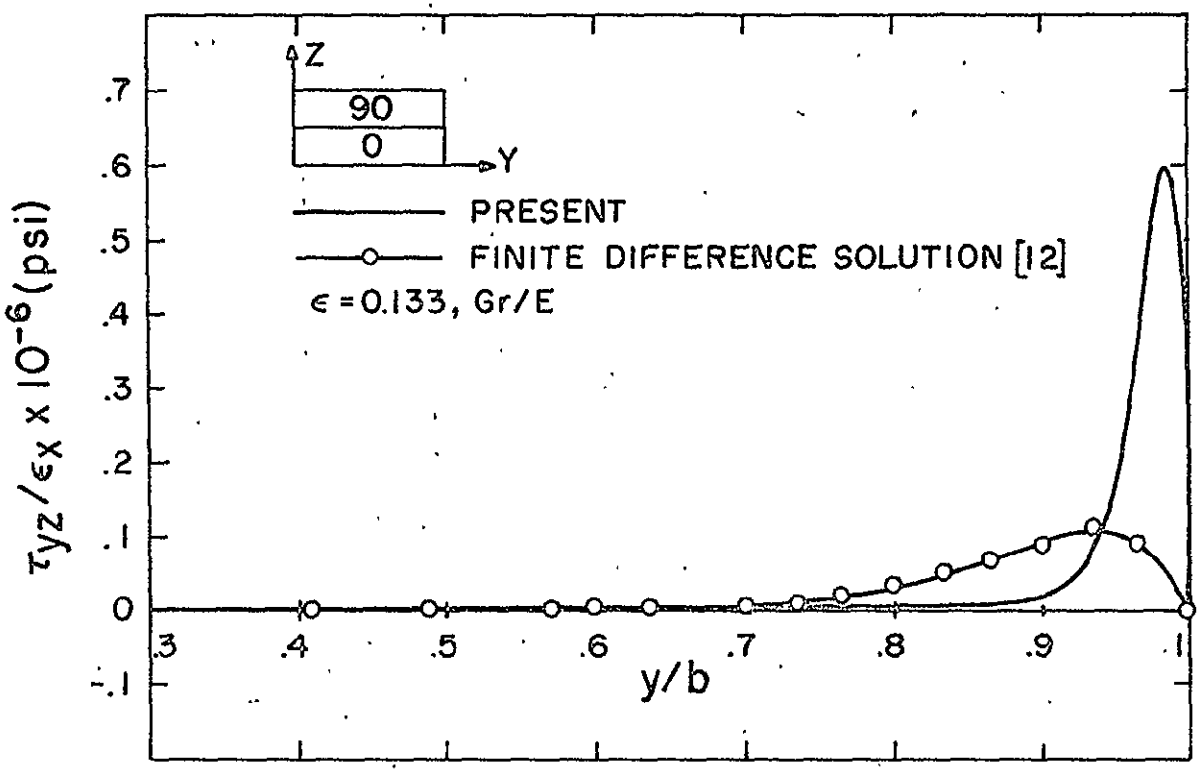

FIGURE 14. PRESENT THEORY AND FINITE DIFFERENCE RESULTS FOR τ_{yz} IN $[90/0]_s$

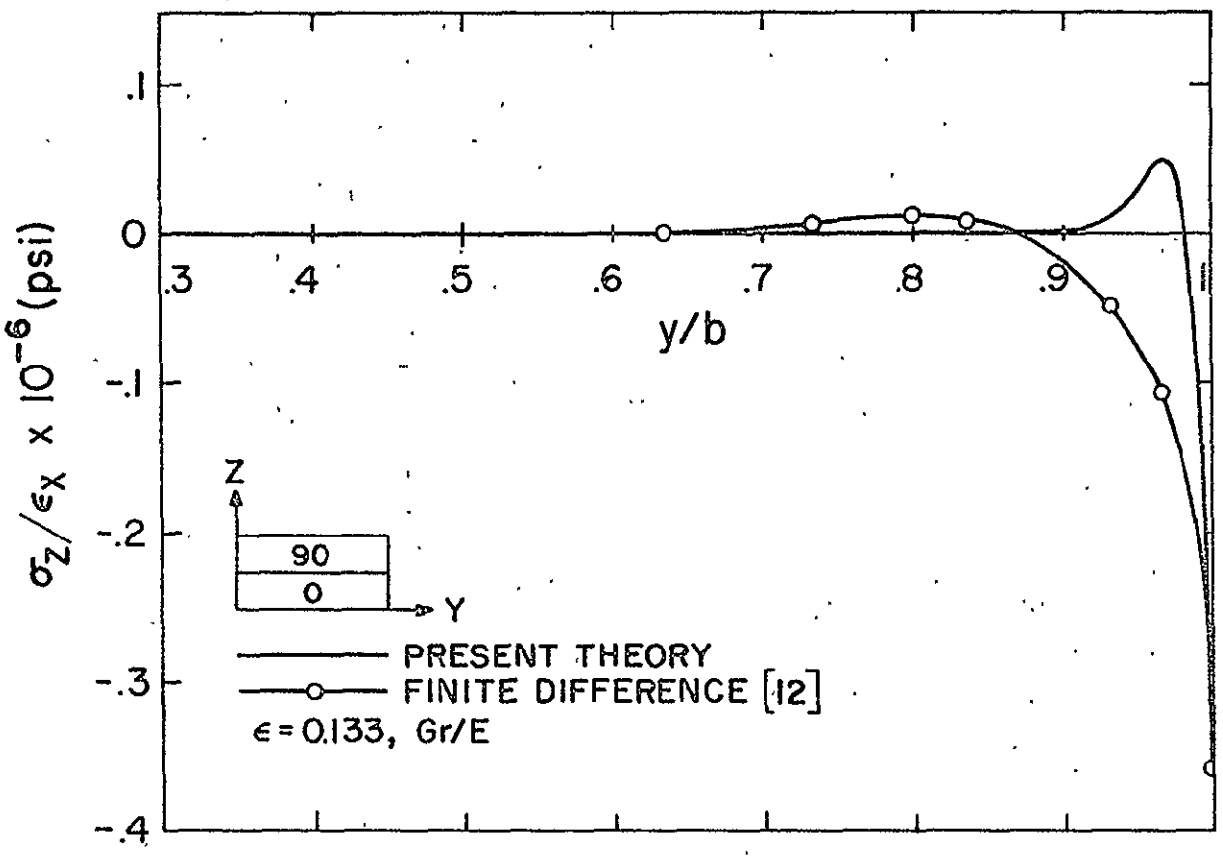

FIGURE 15. PRESENT THEORY AND FINITE DIFFERENCE RESULTS FOR σ_z IN $[90/0]_s$.

These stresses are plotted in Figs. 12 - 15.

3.2 ANGLE PLY LAMINATES WITH CONSTANT PLY THICKNESS

For contemporary fiber-reinforced composites having three mutually perpendicular planes of elastic symmetry, $C_{45}^{(k)}$ vanishes. If the laminate consists of one material with symmetric $[\theta/-\theta]_S$ or $[-\theta/\theta]_S$ orientations (Fig. 6b), it is called an angle ply laminate and the following relations between material constants are found,

$$\begin{aligned} C_{ij}^{(1)} &= C_{ij}^{(2)} \quad , \quad i = 1,2,3 \text{ and } j = 1,2,3 \\ C_{kk}^{(1)} &= C_{kk}^{(2)} \quad , \quad k = 4,5,6 \\ C_{n6}^{(1)} &= - C_{n6}^{(2)} \quad , \quad n = 1,2,3 \end{aligned} \tag{3.54}$$

The modified ZIR solution gives

$$\begin{aligned} U_o^{(1)} &= U_o^{(2)} = 0 \\ V_o^{(1)} &= V_o^{(2)} = - \frac{(C_{12}C_{33} - C_{13}C_{23})^{(1)} \varepsilon_x b}{(C_{22}C_{33} - C_{23}C_{23})^{(1)}} Y \\ W_o^{(1)} &= W_o^{(2)} = - \frac{(C_{13}C_{22} - C_{12}C_{23})^{(1)} \varepsilon_x h}{(C_{22}C_{33} - C_{23}C_{23})^{(1)}} Z \end{aligned} \tag{3.55}$$

On the central plane (Y = 0), the stresses are obtained from Equations (3.55), (2.2), and (3.1) as

$$\sigma_y^{(1)}(0,Z) = - \sigma_y^{(2)}(0,Z) = 0 \tag{3.56}$$

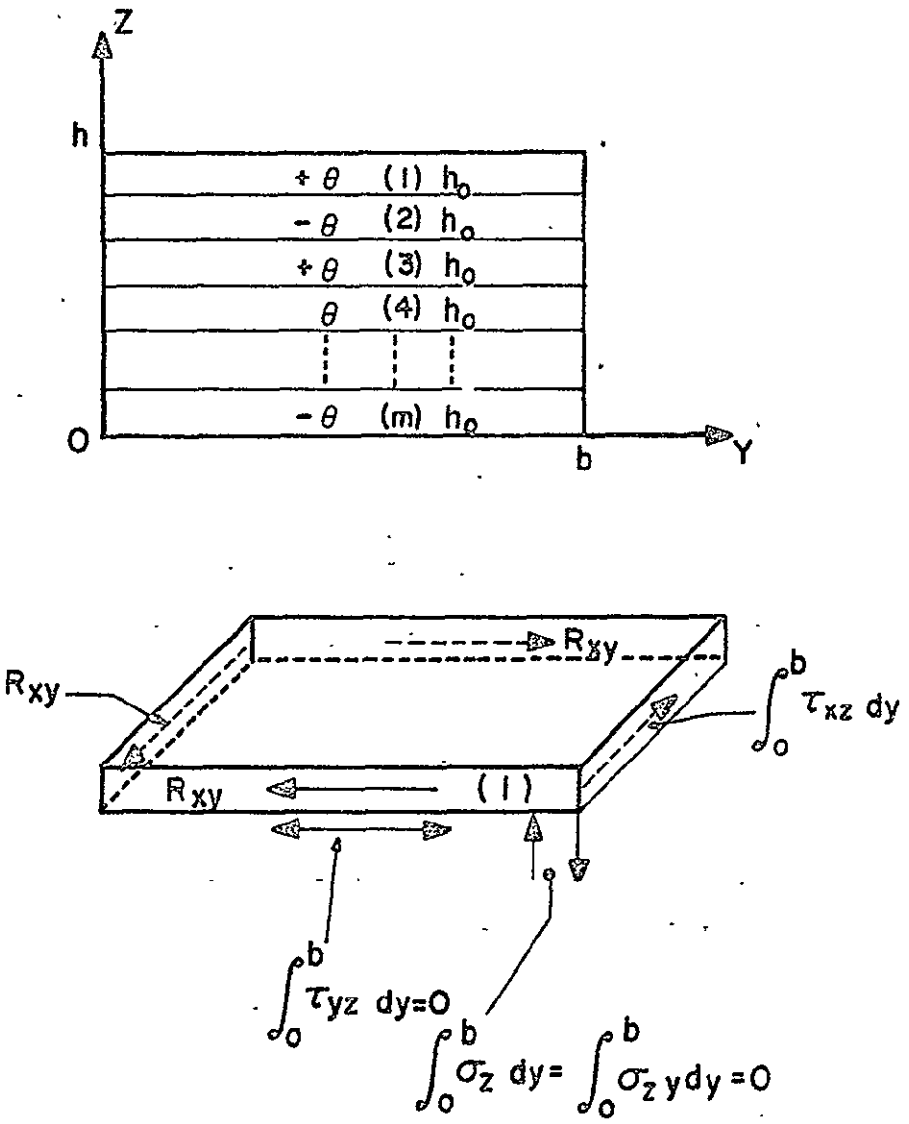

FIGURE 16. ANGLE-PLY LAMINATE OF 2m LAYERS

$$\tau_{xy}^{(1)}(0,Z) = -\tau_{xy}^{(2)}(0,Z)$$

$$= \left[C_{16} - \frac{C_{26}(C_{12}C_{33} - C_{13}C_{23})}{(C_{22}C_{33} - C_{23}C_{23})}\right] \varepsilon_x \qquad (3.57)$$

The first equation indicates that the zeroth order solution (3.55) contributes no transverse normal stress throughout the angle-ply laminate. For the laminate to be in equilibrium, two self-equilibrating conditions in addition to Equation (2.70) should be expected to hold (Fig. 16). Recalling Equations (3.38) through (3.41), the following equations may be established.

$$\int_{\infty}^{0} \tau_{yz}^{(k)}(\eta, \tfrac{1}{2} \pm \zeta)h\,d\eta = 0 \qquad k = 1,2 \qquad (3.58)$$

$$0 < \zeta \ll 1$$

$$-\int_{\infty}^{0} \sigma_z^{(k)}(\eta, \tfrac{1}{2} \pm \zeta)bh(1 - \varepsilon\eta)d\eta = 0 \qquad k = 1,2 \qquad (3.59)$$

Furthermore, the shear stress resultants $R_{xy}^{(1)}$ and $R_{xy}^{(2)}$ must also be in equilibrium (Fig. 3 with m = 2) as indicated in the following equations.

$$-\int_{\infty}^{0} \tau_{xz}^{(1)}(\eta, \tfrac{1}{2})h\,d\eta + R_{xy}^{(1)} = 0 \text{ where } R_{xy}^{(1)} = \int_{\frac{1}{2}}^{1} \tau_{xy}^{(1)}(0,Z)h\,dZ \qquad (3.60)$$

$$-\int_{\infty}^{0} \tau_{xz}^{(2)}(\eta, \tfrac{1}{2})h\,d\eta + R_{xy}^{(2)} = 0 \text{ where } R_{xy}^{(2)} = \int_{0}^{\frac{1}{2}} \tau_{xy}^{(2)}(0,Z)h\,dZ \qquad (3.61)$$

The characteristic equation (2.64) leads to two identical sixth order algebraic equations for both layers. Three positive roots to this equation must be dropped for matching considerations. The composite solution will be in the form of Equation (2.66) with $O(\varepsilon)$

truncated. A numerical example is presented in the following subsection.

3.2.1 $[45/-45]_s$ GRAPHITE-EPOXY LAMINATE

Consider the $[45/-45]_s$ graphite-epoxy laminate of constant ply thickness h/2 (Fig. 17a). The stiffness coefficients (after transformation) are

45(x 10^{-6} psi)	-45(x 10^{-6} psi)
$C_{11}^{(1)} = 6.745$	$C_{11}^{(2)} = 6.745$
$C_{12}^{(1)} = 5.045$	$C_{12}^{(2)} = 5.045$
$C_{13}^{(1)} = 0.521$	$C_{13}^{(2)} = 0.521$
$C_{22}^{(1)} = 6.745$	$C_{22}^{(2)} = 6.745$
$C_{23}^{(1)} = 0.521$	$C_{23}^{(2)} = 0.521$
$C_{33}^{(1)} = 2.213$	$C_{33}^{(2)} = 2.213$
$C_{16}^{(1)} = C_{26}^{(1)} = -4.506$	$C_{16}^{(2)} = C_{26}^{(2)} = 4.506$
$C_{36}^{(1)} = -0.04387$	$C_{36}^{(2)} = 0.04387$
$C_{44}^{(1)} = C_{55}^{(1)} = 0.85$	$C_{44}^{(2)} = C_{55}^{(2)} = 0.85$
$C_{66}^{(1)} = 5.33$	$C_{66}^{(2)} = 5.33$
$C_{45}^{(1)} = 0$	$C_{45}^{(2)} = 0$

The modified ZIR solution (3.55) gives

$$\begin{aligned} U_o^{(1)} &= U_o^{(2)} = 0 \\ V_o^{(1)} &= V_o^{(2)} = -0.7433\ \varepsilon_x bY \\ W_o^{(1)} &= W_o^{(2)} = -0.0604\ \varepsilon_x hZ \end{aligned} \tag{3.62}$$

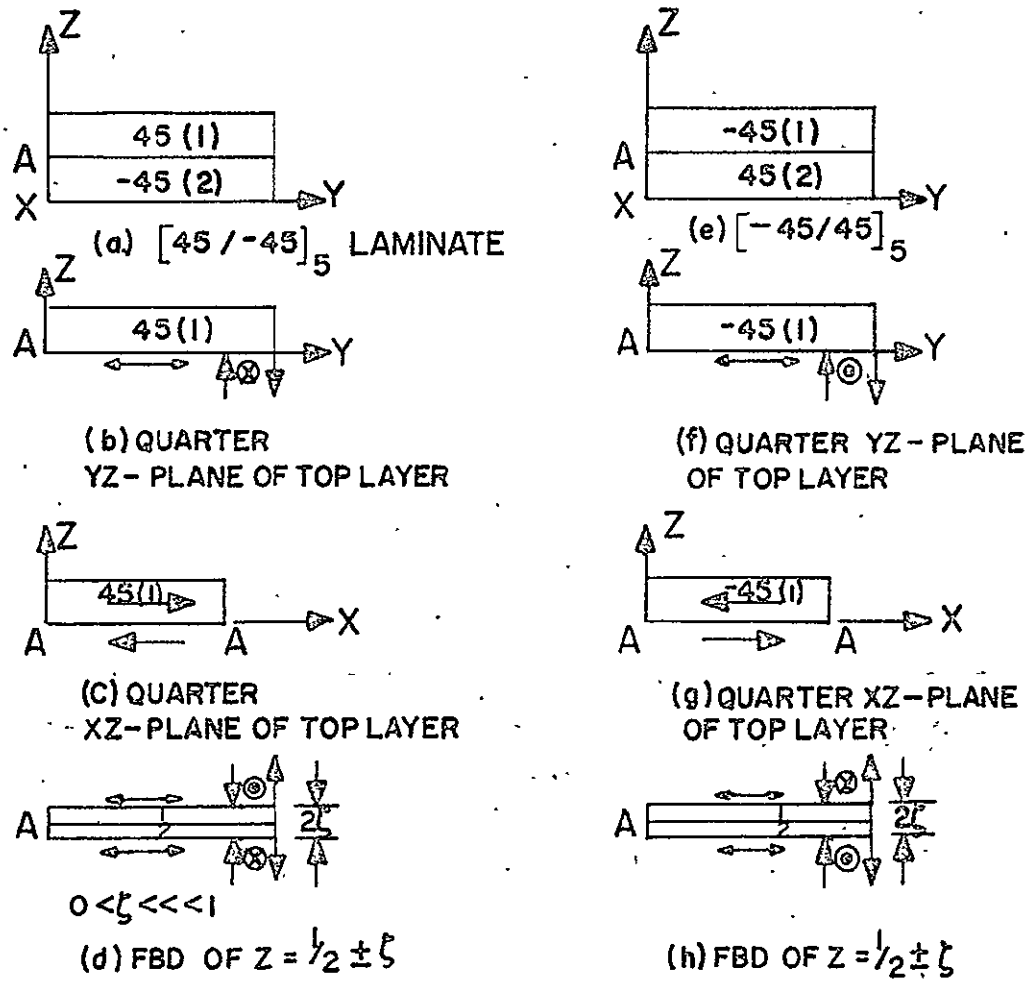

FIGURE 17. FOUR LAYER ANGLE-PLY LAMINATE

Equation (3.57) yields $\tau_{xy}^{(1)}(0,Z) = -\tau_{xy}^{(2)}(0,Z) = 1.154\varepsilon_x(10^6 \text{ psi})$.

The boundary layer equations (2.61) through (2.64) yield the algebraic equation for both layers

$$\lambda_o^6 - 2.5460\ \lambda_o^4\alpha_o^2 + 1.6337\ \lambda_o^2\alpha_o^4 - 0.1202\ \alpha_o^6 = 0 \qquad (3.63)$$

which is readily transformed to

$$\omega^3 - 2.5460\ \omega^2 + 1.6337\ \omega - 0.1202 = 0 \qquad (3.64)$$

by letting $$\lambda_o = \pm\ \alpha_o\omega^{1/2} \qquad (3.65)$$

Furthermore, setting $$\omega = \gamma - 1/3(-2.5460) = \gamma + 0.8487 \qquad (3.66)$$

results in $$\gamma^3 - 0.5269\ \gamma + 0.0438 = 0 \qquad (3.67)$$

Let $$\gamma = p_o + q_o \qquad (3.68)$$

and substitute it into Equation (3.67). The resulting set of algebraic equations are

$$\begin{aligned} p_o^3 + q_o^3 &= -0.0438 \\ p_o q_o &= 0.1756 \end{aligned} \qquad (3.69)$$

which give

$$\begin{aligned} p_o^3 &= (0.0736)\{\cos(2k\pi + 107.3°) + i\ \sin(2k\pi + 107.3°)\} \\ q_o^3 &= (0.0736)\{\cos(2k\pi + 252.7°) + i\ \sin(2k\pi + 252.7°)\} \\ k &= 0,1,2 \end{aligned} \qquad (3.70)$$

By applying DeMoivre's formula [26] and recalling Equation

(3.68), (3.66) and (3.65), the six roots for Equation (3.63) are found to be

$$\begin{aligned} \lambda_0(1,2) &= \pm\ 1.2364\ \alpha_0 \\ \lambda_0(3,4) &= \pm\ 0.2903\ \alpha_0 \\ \lambda_0(5,6) &= \pm\ 0.9659\ \alpha_0 \end{aligned} \tag{3.71}$$

Hence the zeroth order composite solution (Section 1.3) takes the form

$$\begin{aligned} U_c^{(k)} &= \{(P_1 e^{-\beta_1\alpha_0\eta} + P_2 e^{-\beta_2\alpha_0\eta} + P_3 e^{-\beta_3\alpha_0\eta})\cos\ \alpha_0 Z\}^{(k)} \\ V_c^{(k)} &= -\ 0.7433\ \epsilon_x bY + \{(R_1 e^{-\beta_1\alpha_0\eta} + R_2 e^{-\beta_2\alpha_0\eta} \\ &\qquad + R_3 e^{-\beta_3\alpha_0\eta})\cos\ \alpha_0 Z\}^{(k)} \\ W_c^{(k)} &= -\ 0.0604\ \epsilon_x hZ + \{(S_1 e^{-\beta_1\alpha_0\eta} + S_2 e^{-\beta_2\alpha_0\eta} \\ &\qquad + S_3 e^{-\beta_3\alpha_0\eta})\sin\ \alpha_0 Z\}^{(k)} \end{aligned} \tag{3.72}$$

where $\beta_1^{(k)} = 1.2364$

$\beta_2^{(k)} = 0.2903$

$\beta_3^{(k)} = 0.9659$

Satisfying the governing equations and the boundary conditions leads to the following equations:

$$
\begin{aligned}
P_1^{(1)} &= -0.5871\,\phi_1 \quad , \quad P_1^{(2)} = 0.5871\,\phi_2 \\
P_2^{(1)} &= 0.1707\,\phi_1 \quad , \quad P_2^{(2)} = -0.1707\,\phi_2 \\
P_3^{(1)} &= 1.2021\,\phi_1 \quad , \quad P_3^{(2)} = -1.2021\,\phi_2 \\
R_1^{(1)} &= -0.6309\,\phi_1 \quad , \quad R_1^{(2)} = -0.6309\,\phi_2 \\
R_2^{(1)} &= -0.1813\,\phi_1 \quad , \quad R_2^{(2)} = -0.1813\,\phi_2 \\
R_3^{(1)} &= 1.1897\,\phi_1 \quad , \quad R_3^{(2)} = 1.1897\,\phi_2 \\
S_1^{(1)} &= 1.1358\,\phi_1 \quad , \quad S_1^{(2)} = 1.1358\,\phi_2 \\
S_2^{(1)} &= 0.0347\,\phi_1 \quad , \quad S_2^{(2)} = 0.0347\,\phi_2 \\
S_3^{(1)} &= -1.0736\,\phi_1 \quad , \quad S_3^{(2)} = -1.0736\,\phi_2
\end{aligned}
\tag{3.73}
$$

where

$$
\begin{aligned}
\phi_1 &= \frac{\varepsilon_x h}{\alpha_0^{(1)} \cos\left(\alpha_0^{(1)}\left(\frac{1}{2} + \zeta\right)\right)} \\
\phi_2 &= \frac{\varepsilon_x h}{\alpha_0^{(2)} \cos\left(\alpha_0^{(2)}\left(\frac{1}{2} - \zeta\right)\right)}
\end{aligned}
\tag{3.74}
$$

$$0 < \zeta \lll 1$$

It can be shown that these coefficients lead to identical satisfaction of Equations (2.70), (3.54) and (3.55). Hence the correctness of these coefficients is confirmed.

Equation (3.61) then leads to

$$
\frac{\tan\left[\frac{\alpha_0^{(2)}}{2} - \zeta\,\alpha_0^{(2)}\right]}{\alpha_0^{(2)}} = 0.5 \tag{3.75}
$$

$$0 < \zeta \lll 1$$

which is identical to Equation (3.42).

Now consider Equations (3.69). It is clear that Layer 1 (+ 45°) and Layer 2 (- 45°) are antisymmetric in U and symmetric in V and W with respect to the infinitesimal thin slice (Fig. 17d). Upon enforcing exact continuity in displacements at $Z = \frac{1}{2}$, the following equation is obtained.

$$\lim_{\zeta \to 0} \cos\left[\frac{\alpha_0^{(1)}}{2} + \alpha_0^{(1)}\zeta\right] = \lim_{\zeta \to 0} \cos\left[\frac{\alpha_0^{(2)}}{2} - \alpha_0^{(2)}\zeta\right] = 0 \qquad (3.76)$$

which gives

$$\begin{aligned} \alpha_0^{(1)} &= (2n + 1)\pi \quad , \quad n = 0,1,2,.... \\ \alpha_0^{(2)} &= (2n + 1)\pi \quad , \quad n = 0,1,2,.... \end{aligned} \qquad (3.77)$$

Hence,

$$\cos\left[\frac{\alpha_0^{(1)}}{2} + \zeta\, \alpha_0^{(1)}\right] = \cos\left[\frac{\alpha_0^{(2)}}{2} - \zeta\, \alpha_0^{(2)}\right] \approx 0 \qquad (3.78)$$

$$\text{for } 0 < \zeta <<< 1$$

where $\alpha_0^{(1)}$ and $\alpha_0^{(2)}$ are given in Equations (3.77).

Thereby

$$\lim_{\zeta \to 0} \left| \tan\left[\frac{\alpha_0^{(k)}}{2} \pm \alpha_0^{(k)}\zeta\right] \right| = \infty \qquad (3.79)$$

and

$$\left| \tan\left[\frac{\alpha_0^{(k)}}{2} \pm \alpha_0^{(k)}\zeta\right] \right| = K \qquad (3.80)$$

$$0 < \zeta <<< 1$$

where K is a finite large positive value.

At this stage, assigning any large value for K determines the corresponding $\alpha_0^{(k)}$ and $\tan\left[\frac{\alpha_0^{(k)}}{2} \pm \alpha_0^{(k)}\zeta\right]$ and hence the interlaminar stresses. It may be shown that the only stresses related to $\tan\left[\frac{\alpha_0^{(k)}}{2} \pm \alpha_0^{(k)}\zeta\right]$ are $\tau_{xz}^{(k)}$ and $\tau_{yz}^{(k)}$. However, the latter vanishes identically at the free edge as required by the stress free boundary conditions (2.17). Hence the singular behavior is found in $\tau_{xz}^{(k)}$ at the intersection of the free edge and the interfacial plane $Z = \frac{1}{2}$. This provides a definite mathematical evidence for the predicted singularity in Reference [7] and will be further discussed in the following chapter.

The interlaminar stressea re plotted in Figures 18 - 20.

3.2.2 $[-45/45]_s$ GRAPHITE-EPOXY LAMINATE

Consider the laminate of Fig. 17e. Interchanging the superscripts 1 and 2 in Equations (3.62) through (3.73) gives a composite solution identical to (3.72). The corresponding interlaminar stresses are shown in Figures 21 - 23.

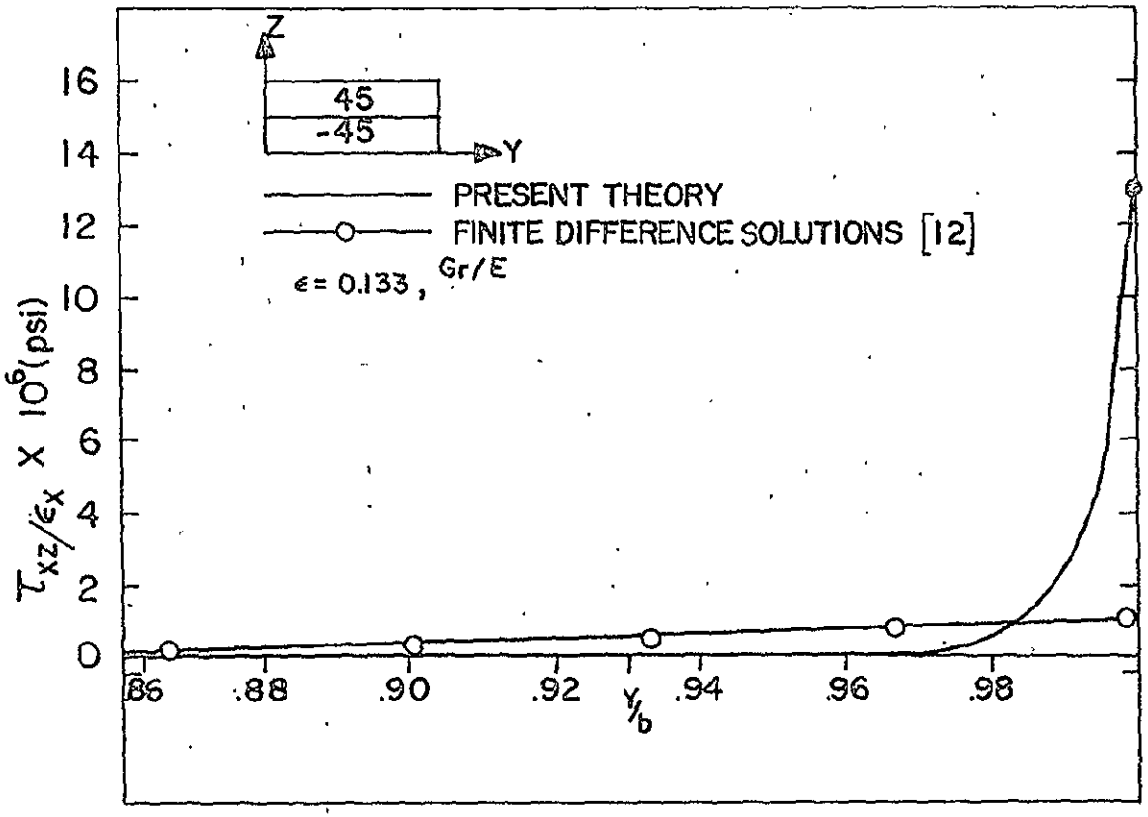

FIGURE 18. INTERLAMINAR SHEAR STRESS τ_{xz} IN $[45/-45]_S$

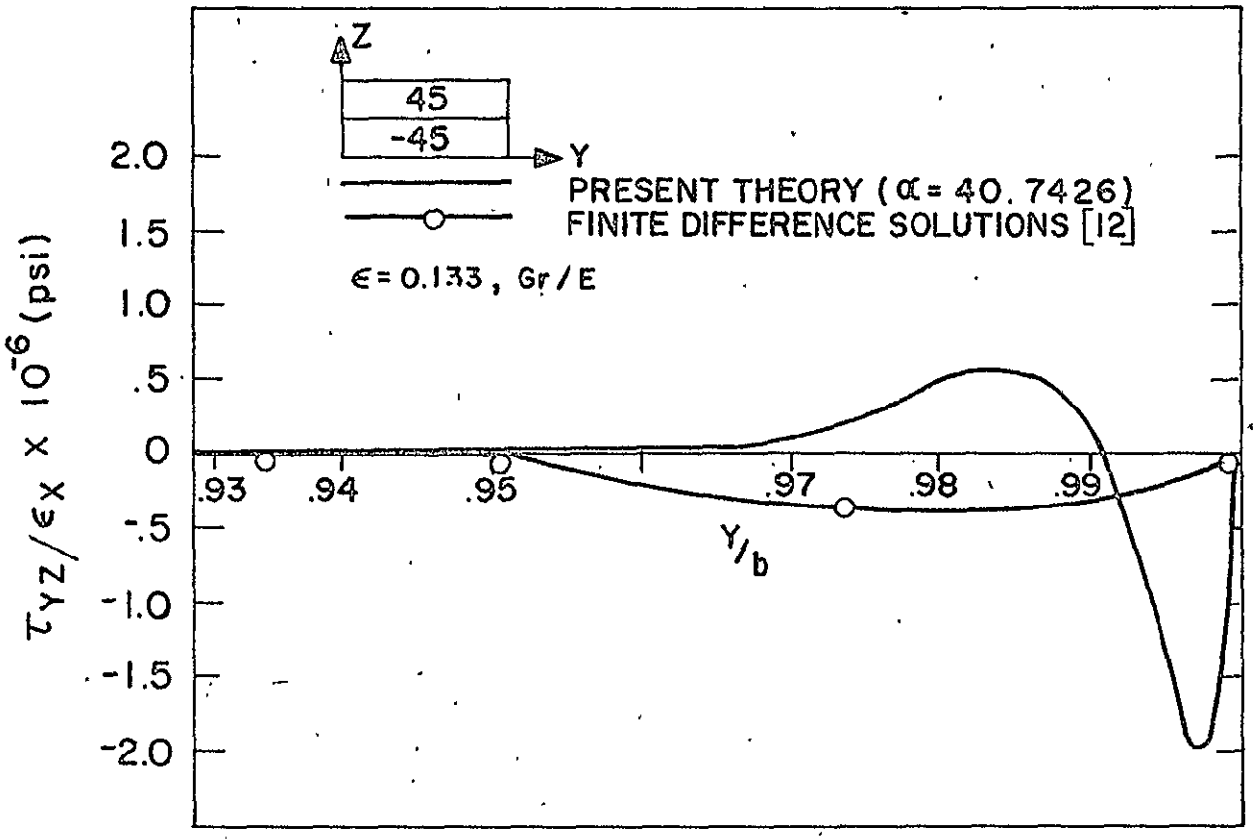

FIGURE 19. INTERLAMINAR SHEAR STRESS τ_{yz} IN $[45/-45]_c$

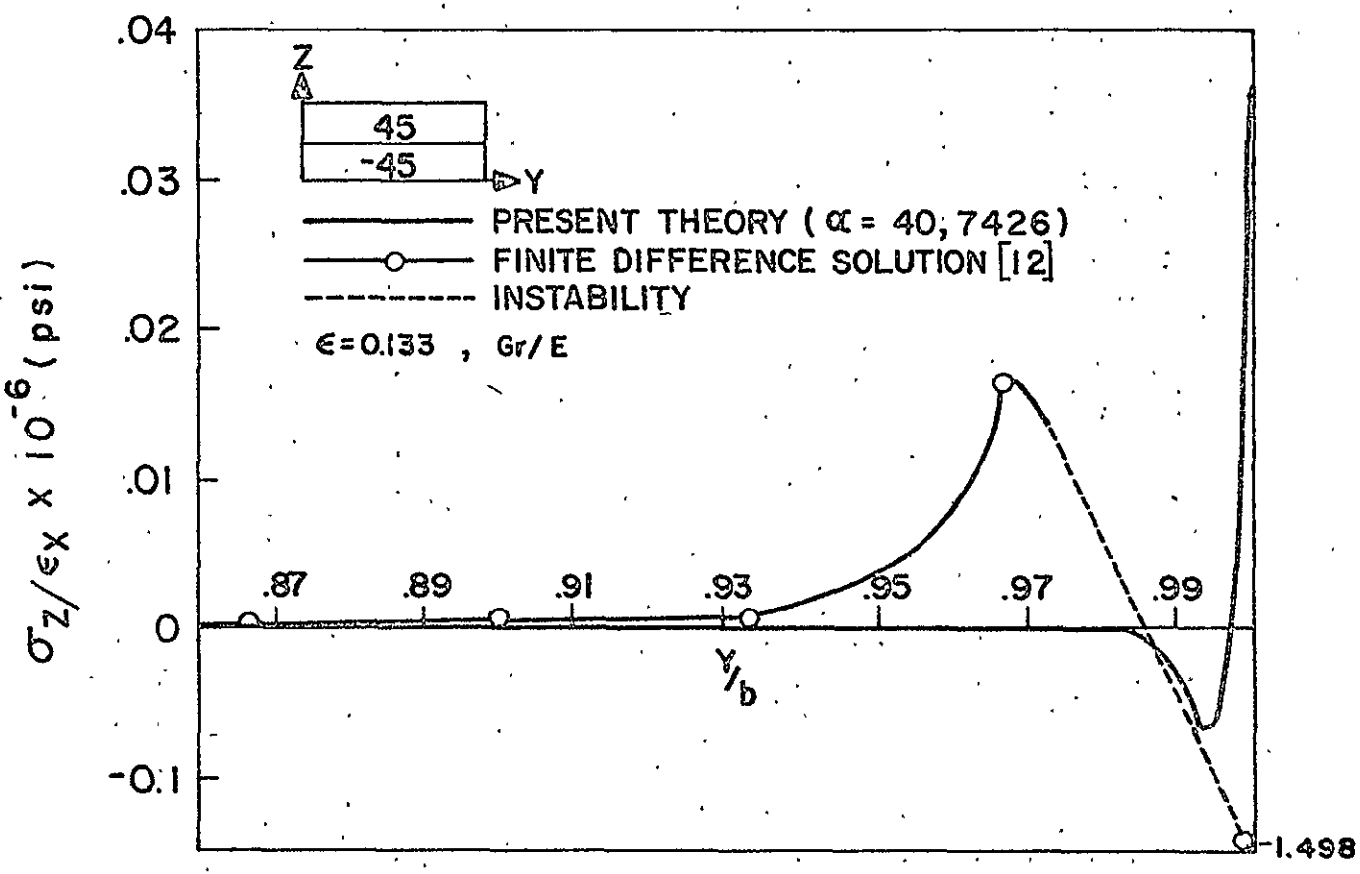

FIGURE 20. INTERLAMINAR NORMAL STRESS σ_z IN $[45/-45]_s$

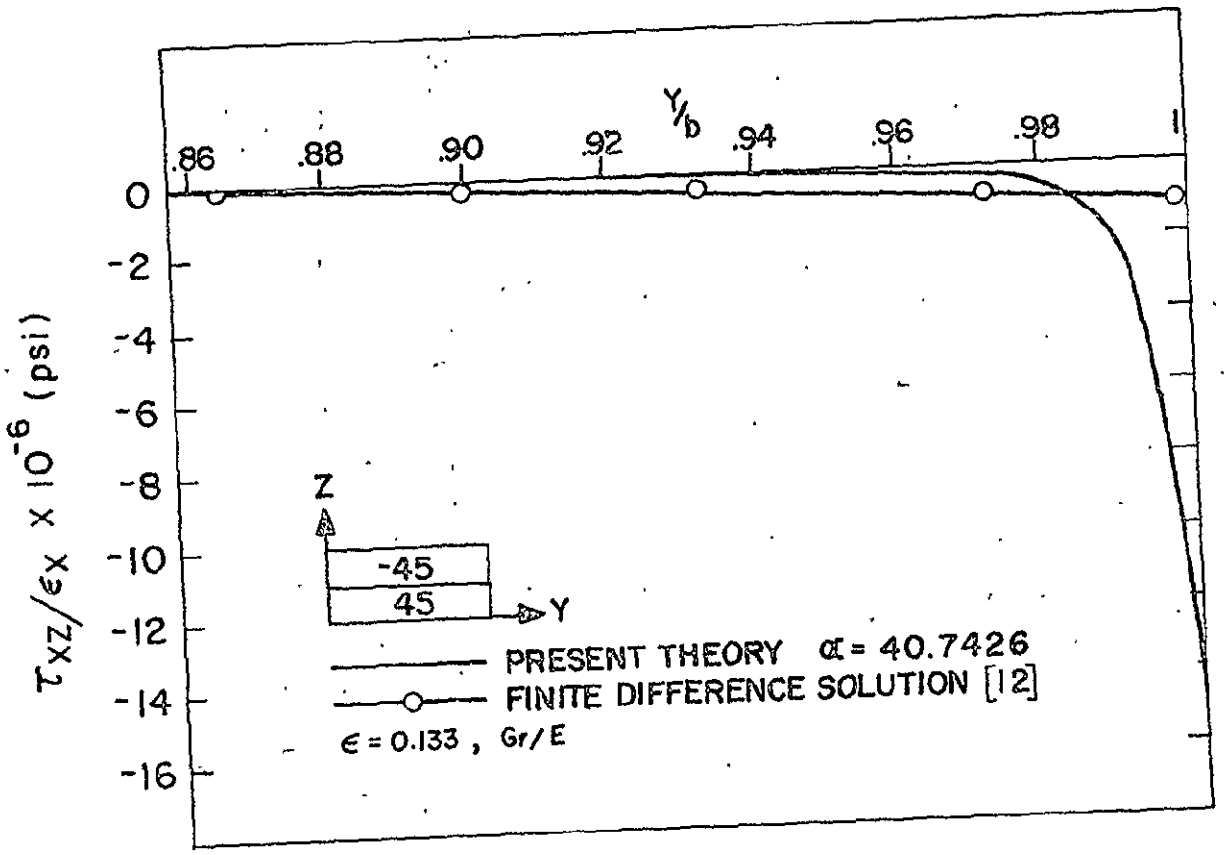

FIGURE 21. INTERLAMINAR SHEAR STRESS τ_{xz} IN $[-45/45]_S$

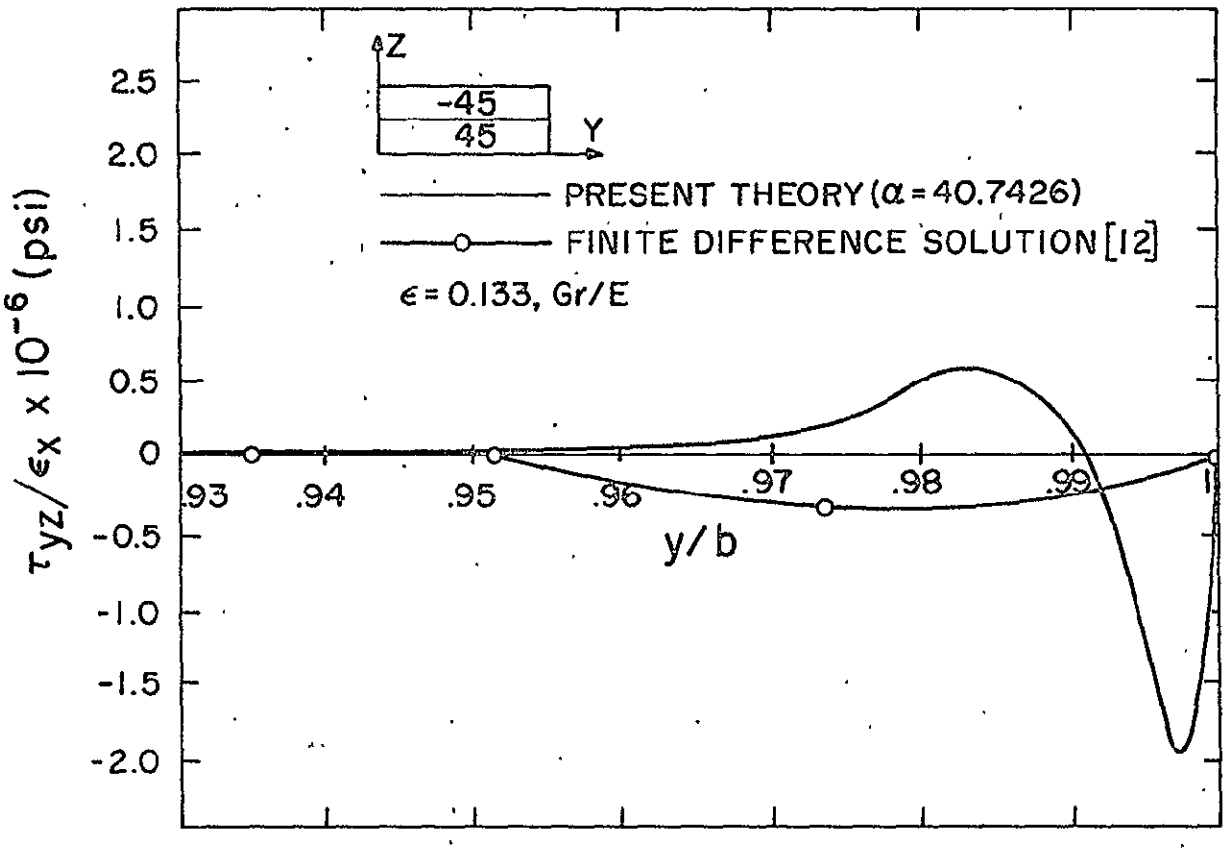

FIGURE 22. INTERLAMINAR SHEAR STRESS τ_{yz} IN $[-45/45]_s$.

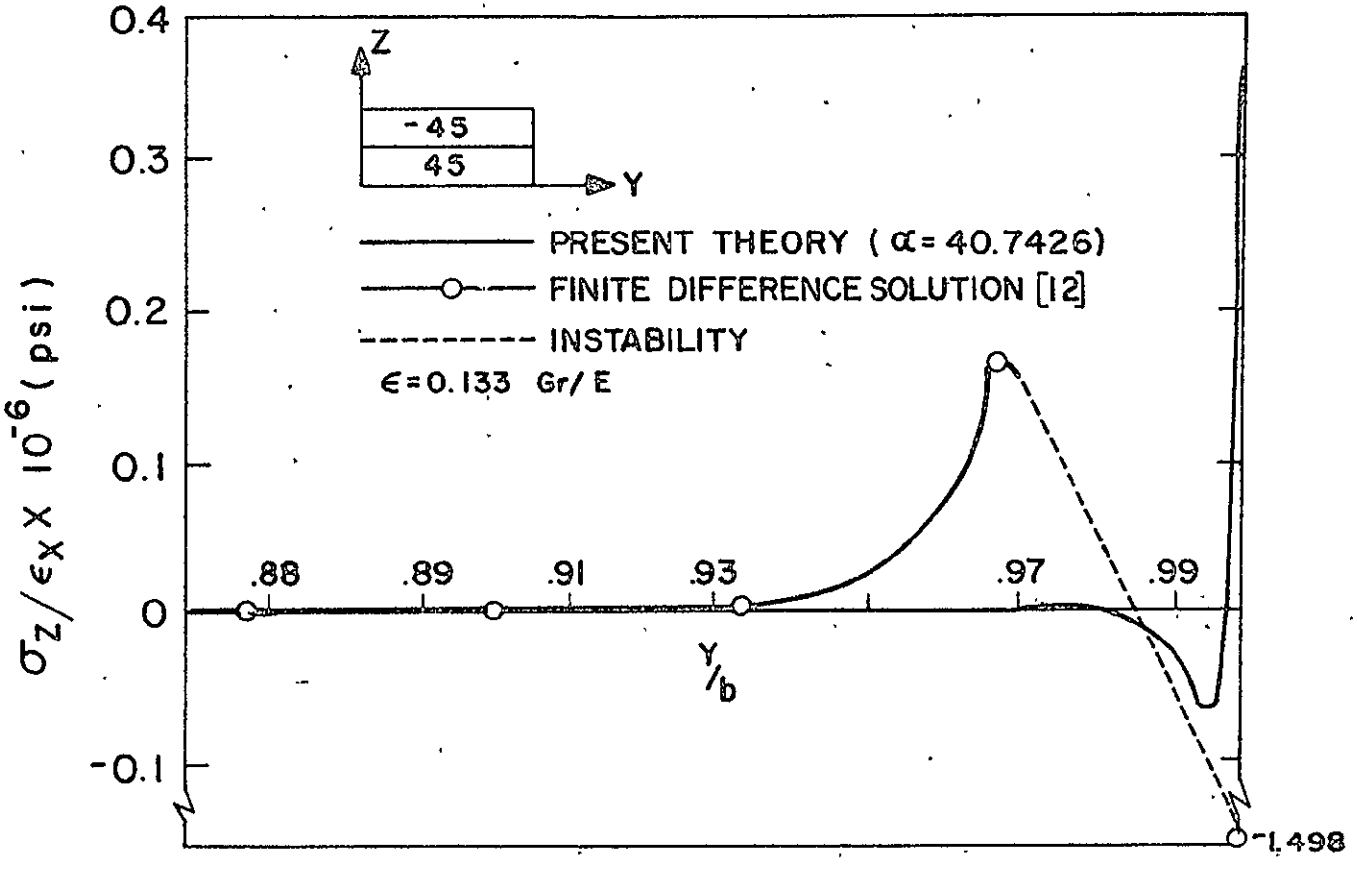

FIGURE 23. INTERLAMINAR NORMAL STRESS σ_z IN $[-45/45]_s$

Chapter IV

RESULTS AND DISCUSSION

In the preceding chapter, the general method of solution of Chapter II was applied to the special graphite-epoxy laminates $[0/90]_s$, $[90/0]_s$, $[45/-45]_s$ and $[-45/45]_s$. To demonstrate the capability of the solution the results for these laminates are presented and discussed in this chapter.

4.1 THE FOUR LAYER UNIDIRECTIONAL LAMINATES

It has been stated in Section 1.3 that the accuracy of the perturbation solution depends upon the perturbation parameter ε. That is, the smaller ε, the better the result. This will be demonstrated in what follows.

The interlaminar shear stress τ_{yz} and the interlaminar normal stress σ_z (the peel stress) as functions of the perturbation parameter ε are presented, respectively, in Figures 8 and 9 for the $[0/90]_s$ laminate. From the figures, it is clear that the boundary layer width becomes smaller as ε decreases in magnitude. (Asymptotic recovery of the lamination theory is implied by the incomplete domain of $\frac{y}{b}$.) It should be noted that the relative extreme values of the stresses are finite and remain unchanged as ε decreases. This indicates that the present theory is capable of approximating the maximum value of the interlaminar stress intensities for intermediate as well as small values of ε. Also, the difference between the cases $\varepsilon = 0.133$ and

$\varepsilon = 0.050$ is much more than that between $\varepsilon = 0.050$ and $\varepsilon = 0.033$. While the curve of $\varepsilon = 0.033$ serves as the most accurate of the three stress results for their corresponding ε, it lends confidence to say that for this $[0/90]_S$ graphite-epoxy laminate, a geometric ratio of 0.050 ($= \frac{1}{20}$) or smaller is sufficiently small to lead to good results using the present method of solution.

Numerical results obtained by this author using the finite difference program of Pipes [12] indicate that the smallest geometric ratio for which that program gives physically admissible result is $\varepsilon = 0.133$ ($\approx\frac{2}{15}$). Below this ratio, the instability in the solution does not yield satisfaction of the force equilibrium $\Sigma F_y = 0$ (Fig. 2 and Equation (2.26)). This may be attributed to the inherent sensitivity of the finite difference approximation to the ratio of the grid spacings for partial differential equations [27].

Comparisons between the results of the finite difference solution and the present theory are presented in Figures 10 and 11 for the case $\varepsilon = 0.133$. From Figure 10 it is clear that the present theory tends to predict a higher maximum intensity for the interlaminar shear stress τ_{yz}. The boundary layer width is approximately the same for both solutions. Figure 11 shows that the present theory predicts a smooth, continuous distribution for σ_z which identically satisfies the self-equilibrating condition $\Sigma F_z = 0$ (Equation (2.70)) whereas the finite difference solution yields unstable results near the free edge which obviously do not satisfy this equilibrium condition. In regions removed from the free edge, both solutions indicate asymptotic recovery

of the lamination theory.

Figures 12 and 13 show the interlaminar stresses for the $[90/0]_s$ laminate--the reversed stacking sequence from the previous example. From the figures, the physical validity of the present theory is confirmed by the sign reversals in both τ_{yz} and σ_z as a result of force and moment equilibrium (Fig. 7). Again, boundary layer shifts due to the reduction in ϵ are observed. The maximum stress intensities of τ_{yz} and σ_z in the $[90/0]_s$ laminate are found to be finite but higher than those in the $[0/90]_s$ laminate (Figs. 8 and 9). This is due to the fact that in the calculation for the $[90/0]_s$ laminate, the 0° layer was employed as the reference layer. On the other hand, in the calculation for the $[0/90]_s$ laminate, the 90° layer was employed as the reference layer.

Comparisons between the finite difference results and the present theory are presented in Figures 14 and 15. The present theory again predicts a higher τ_{yz} than the finite difference solution. Also, the present theory yields a more acceptable distribution for the interlaminar normal stress σ_z in view of the zero stress resultant requirement. In regions removed from the free edge, the lamination theory is recovered asymptotically in both solutions.

4.2 THE FOUR LAYER ANGLE-PLY LAMINATES

Pipes and Pagano [7] pointed out that the interlaminar shear stress τ_{xz} in a $[45/-45]_s$ laminate tends to grow without bound near the free edge (Section 1.1). Hence the calculated maximum intensity of τ_{xz} by the finite difference approximation, though higher than other

numerical investigations [6, 8, 11], is still very questionable. It was discussed in Section 1.2 that failure to satisfy some stress free boundary conditions were observed in the finite difference solution. Also, these results showed no sign reversals in σ_y, σ_z and τ_{yz} in consequence of reversing the stacking sequence.

In the present theory the mathematical evidence for the singularity in τ_{xz} can be shown (Subsection 3.2.1) to be in terms of the trignometric equation

$$\tan\left(\frac{\alpha^{(2)}}{2} - \alpha^{(2)}\zeta\right) = K \tag{4.1}$$

where $0 < \zeta <<< 1$ and K is a near-singular large number. The value of $\alpha^{(2)}$ must satisfy equation (3.75)

$$\frac{\tan\left(\frac{\alpha^{(2)}}{2} - \alpha^{(2)}\zeta\right)}{\alpha^{(2)}} = 0.5 \quad , \quad 0 < \zeta <<< 1 \tag{4.2}$$

Obviously, the limiting analysis of the present theory (Fig. 17d, h) provides no unique determination of the value of K. It is only through experimental investigation that this value may be realistically determined. Such an investigation should be considered as a future study. For the purpose of comparisons, K is taken to be 20.3713, a value that leads to a maximum stress intensity within the elastic limit.

Comparisons between the results of the finite difference solution and the present theory are presented in Figures 18 through 23. Figure 18 shows the variation of the interlaminar shear stress τ_{xz} along the

interface $Z = \frac{1}{2}$. The near-singular free edge intensity of the present theory is much higher than the finite difference result and the boundary layer width is much smaller. Figure 19 shows the variation of the interlaminar shear stress τ_{yz}. Both solutions satisfy the stress free boundary condition $\tau_{yz} = 0$ at the free edge. The negative-positive variation of the present theory confirms the additional self-equilibrating condition

$$\Sigma F_y = \int_0^b \tau_{yz}\, dy = 0 \tag{4.3}$$

(as a result of the zeroth order vanishing of σ_y in the interior region). The finite difference solution, on the other hand, cannot satisfy such a condition. The erroneous σ_y of the finite difference solution at the free edge (not shown in the figures), as described in Section 1.2, is believed to be caused by inherent errors. In Figure 20 the interlaminar normal stress σ_z of the finite difference solution indicates instability near the free edge; hence, no comparison can be made between the two solutions in this region. Since the automatic satisfaction of the self-equilibrating condition

$$\Sigma F_z = \int_0^b \sigma_z\, dy = 0 \tag{4.4}$$

has been demonstrated by the present theory (Chapter III) and can be observed from the figure, and since σ_z is not proportional* to the

---

*As shown in Equations (3.46) - (3.53).

near-singular value of K, the present theory is believed to have predicted a more accurate maximum finite intensity of the interlaminar normal stress. Such a determination is most important in the delamination failure mode [21, 28] of composites. Although the moment self-equilibrating condition (Fig. 16) is not directly observable from Figure 20, the magnitude of this couple moment can be determined as

$$\Sigma M = \int_0^b \sigma_z \, y \, dy = 0.0027 \, \frac{h\varepsilon_x 10^6}{(\alpha^{(2)})^2} \left(\frac{\text{in - lb}}{\text{length}}\right) \tag{4.5}$$

where $\alpha^{(2)}$ equals 2K, a near-singular value from Equations (4.1) and (4.2). Hence the self-equilibrating condition of the couple moment is confirmed immediately.

When the stacking sequence is reversed to $[-45/45]_s$ (Figs. 21, 22, 23), the interlaminar shear stress τ_{xz} experiences a sign change in order to balance the central plane shear resultant $\int_{\frac{1}{2}}^{1} \tau_{\overline{xy}}^{(1)}(0,Z)hdZ$ which also experiences a sign reversal. The sign of both τ_{yz} and σ_z remain unchanged. This is in agreement with the finite difference results (Figs. 19 and 22, 20 and 23). For $\varepsilon = 0.133$, the finite difference solution predicts a small uniform σ_y along the central plane (not shown in the figures) which does not change its sign and magnitude for the reversed stacking sequence. For $\varepsilon \leq 0.0133$ the finite difference solution yields erroneous results for σ_y due to the instability of the solution. The present theory exhibits no such instabilities.

It is important to note that the interlaminar normal stress σ_z is independent of the stacking sequence and always tensile near the

free edge. For both the $[45/-45]_S$ and the $[-45/45]_S$ laminates, a finite maximum intensity is predicted at the exact free edge (Figs. 20, 23). This indicates that the delamination failure mode [21, 28] should always be considered for reliable design of such laminate configurations.

It is clear that the present study has obtained improved results for the interlaminar behavior of the $[45/-45]_S$ and $[-45/45]_S$ graphite-epoxy laminates. Since the aforementioned self-equilibrating conditions were originally considered for the 2m layer angle-ply laminate (Fig. 16), the interlaminar stress variations in any angle-ply laminate may be expected to be similar to those in Figures 18 through 23.

4.3 ACCURACY AND LIMITATIONS

As discussed earlier, the accuracy of the present theory depends upon the geometric ratio $\varepsilon = \frac{h}{b}$. Hence, the relative order of magnitude of the individual terms in the governing equations, in relation to $\frac{h}{b}$, should be further discussed.

4.3.1 BIDIRECTIONAL LAMINATES

The coupled governing differential equations for bidirectional laminates (Equations (3.2)) are

$$\begin{aligned} &\{Q_{22}(\tfrac{h}{b})^2 V_{,YY} + Q_{44} V_{,ZZ} + (Q_{44} + Q_{23})(\tfrac{h}{b}) W_{,YZ} = 0\}^{(k)} \\ &\{(Q_{44} + Q_{23})(\tfrac{h}{b}) V_{,YZ} + Q_{44}(\tfrac{h}{b})^2 W_{,YY} + Q_{33} W_{,ZZ} = 0\}^{(k)} \end{aligned} \tag{4.6}$$

From these dimensionless equations, it is essential that the order of magnitude of the coefficients of $V_{,YY}$ and $W_{,YY}$, $V_{,YZ}$ and

$W_{,YZ}$, $V_{,ZZ}$ and $W_{,ZZ}$ be $O(\bar{\varepsilon}^2) < O(\bar{\varepsilon}) < O(1)$*, respectively, in order to properly stretch the boundary layer region with a transformation in the form

$$\eta = \frac{(1 - Y)}{\bar{\varepsilon}} \tag{4.7}$$

Hence, if the material properties are fixed, the geometric ratio $\frac{h}{b}$ obviously plays the dominant role. For the graphite-epoxy laminate with $\frac{h}{b} = 0.133$ (Chapter III), Equations (4.6) may be transformed to

$$(0°) \begin{cases} 0.046\ V_{,YY} + V_{,ZZ} + 0.208\ W_{,YZ} = 0 \\ 0.080\ V_{,YZ} + 0.007\ W_{,YY} + W_{,ZZ} = 0 \end{cases} \tag{4.8}$$

$$(90°) \begin{cases} 0.42\ V_{,YY} + V_{,ZZ} + 0.22\ W_{,YZ} = 0 \\ 0.085\ V_{,YZ} + 0.007\ W_{,YY} + W_{,ZZ} = 0 \end{cases} \tag{4.9}$$

It may be observed that, for this geometric ratio, a perturbation solution using the 0° layer as the reference layer should lead to more accurate results.

If the geometric ratio is now reduced to 0.050 for the same laminate material, Equations (4.6) become

$$(0°) \begin{cases} 0.0065\ V_{,YY} + V_{,ZZ} + 0.0782\ W_{,YZ} = 0 \\ 0.030\ V_{,YZ} + 0.001\ W_{,YY} + W_{,ZZ} = 0 \end{cases} \tag{4.10}$$

$$(90°) \begin{cases} 0.05\ V_{,YY} + V_{,ZZ} + 0.083\ W_{,YZ} = 0 \\ 0.032\ V_{,YZ} + 0.001\ W_{,YY} + W_{,ZZ} = 0 \end{cases} \tag{4.11}$$

---

* $\bar{\varepsilon}$ represents the approximate order of the products of Q_{ij} and ε.

It is clear that the order of each term relative to $V_{,ZZ}$ or $W_{,ZZ}$ shrinks as ε diminishes. This means that the degree of accuracy of the zeroth order perturbation solution is improved by the diminishing geometric ratio. Obviously, these equations provide mathematical evidence to support the judicious statement made in Section 4.1--"A geometric ratio of 0.050 or smaller leads to sufficiently accurate results."

4.3.2 ANGLE-PLY LAMINATES

The governing differential equations for the ± 45° graphite-epoxy laminate with $\frac{h}{b} = 0.133$ are

$$(45°)\begin{cases} 0.111\,U_{,YY} + U_{,ZZ} - 0.094\,V_{,YY} - 0.007\,W_{,YZ} = 0 \\ -0.094\,U_{,YY} + 0.140\,V_{,YY} + V_{,ZZ} + 0.215\,W_{,YZ} = 0 \\ -0.003\,U_{,YZ} + 0.083\,V_{,YZ} + 0.007\,W_{,YY} + W_{,ZZ} = 0 \end{cases} \tag{4.12}$$

$$(-45°)\begin{cases} 0.111\,U_{,YY} + U_{,ZZ} + 0.094\,V_{,YY} + 0.007\,W_{,YZ} = 0 \\ 0.094\,U_{,YY} + 0.140\,V_{,YY} + V_{,ZZ} + 0.215\,W_{,YZ} = 0 \\ 0.003\,U_{,YZ} + 0.083\,V_{,YZ} + 0.007\,W_{,YY} + W_{,ZZ} = 0 \end{cases} \tag{4.13}$$

Again, the order of magnitude of each coefficient relative to $U_{,ZZ}$, $V_{,ZZ}$ and $W_{,ZZ}$ can be observed. From Equations (4.12) and (4.13), it can be safely stated that the present theory should lead to sufficiently accurate results for $\frac{h}{b} = 0.133$ or below. Hence no further reduction of the geometric ratio needs be elaborated upon.

From the above discussion, the fact that the boundary layer penetration becomes weaker as $\frac{h}{b}$ decreases can be detected simply by

examining the relative orders of various terms in the governing differential equations. The smaller the coefficients relative to the coefficient one of $U_{,ZZ}$, $V_{,ZZ}$ and $W_{,ZZ}$, the weaker the boundary layer effect. Hence the uniform stress distribution in the central plane (Section 2.2) is justified by the more rapid recovery of the lamination solution.

It must be recalled that in the interior region of the present theory the exact satisfaction of the vanishing stress boundary conditions on the top and bottom surfaces, the continuities in the interlaminar stresses, and the force equilibrium in the central plane were inforced. Also in the interior region the exact displacement continuii in U and V were satisfied by the modified zeroth order interior region (Subsection 2.3.2). For bidirectional laminates, the slight dif ference found in the displacement W (Table 1) for the two layers may be reduced or eliminated by higher order considerations. This is mainly due to the differences in material properties that constitute the governing differential equations. For the angle-ply laminates, the exact continuity in this displacement was found to be satisfied automatically (Table 2).

In the boundary layer region, the bidirectional laminates again reveal differences in the exponential functions (Equations (3.33)) owing to the intractable material dissimilarities. Hence no exact displacement continuity in this region may be inforced for the limiting free body considered in Figure 7. Nevertheless, the satisfaction of the symmetry conditions, the stress boundary conditions at the free

edge, the force and moment equilibrium about this free body, and the continuity in interlaminar tractions, is believed to have attained a solution which is an improvement over previously available solutions.

On the other hand, the boundary layer region solution for the angle-ply laminate exactly satisfies the symmetry conditions, the stress boundary conditions at the free edge, the displacement and stress continuity conditions, and the force and moment equilibrium requirements (Figs. 16, 17). This exactness of the present theory is entirely due to the favorable parametric relations

$$\begin{aligned} C_{ij}^{(1)} &= C_{ij}^{(2)} \quad , \quad i = 1, 2, 3 \text{ and } j = 1, 2, 3 \\ C_{kk}^{(1)} &= C_{kk}^{(2)} \quad , \quad k = 4, 5, 6 \\ C_{n6}^{(1)} &= -C_{n6}^{(2)} \quad , \quad n = 1, 2, 3 \end{aligned} \tag{4.14}$$

Moreover, it is this exactness that leads to the mathematical evidence for the stress singularity in the interlaminar shear stress τ_{xz}.

4.4 GENERALITY AND APPLICABILITY

From the solution method developed in Chapters II and III, it is clear that the detailed solution procedures of the present theory can be readily programmed for a computer. The simple calculation steps require no approximate or iterative techniques. The generality of the theory can be directly applied to variable laminate configurations (Fig. 1) with more layers than any existing computer program can possibly handle. Thermal strains can be readily included through the constitutive equations (2.1) to determine the induced thermal stresses

due to the temperature drop from the curing temperature of the laminate or for laminates in a high temperature environment. The computer program thus developed would be capable of predicting the interlaminar stress intensities between any two layers including the midplane $Z = 0$. Failure hypotheses can then be established based on the interfacial plane where the stress intensity reaches a relative maximum.

Finally the generality of the solution procedures in the present theory can be directly applied to explore related problems such as a laminate with internal free edge in the form of center holes, cracks, etc., a laminate subject to pure bending at the ends $x = \pm L$, time-dependent boundary layer effects due to cyclic loadings, and so forth. The important experimental determination of the material parameter K may also be pursued as a future research topic.

Chapter V

CONCLUSIONS

In the present thesis a general method of solution for a balanced symmetric composite laminate subject to a uniaxial extension has been developed based upon a perturbation analysis of an elastic limiting free body containing an interfacial plane.

In summary of the theoretical achievements of the present study, the following conclusions can be made.

(1) The solution satisfies the symmetry conditions, the stress free boundary conditions, most continuity conditions, and the force and moment equilibrium of the limiting free body.

(2) The solution predicts smooth continuous interlaminar stresses with no instabilities.

(3) The solution provides the finite maximum magnitude of the interlaminar normal stress σ_z for all laminate configurations.

(4) For given material properties, the solution accuracy depends upon the geometric ratio $\varepsilon = \frac{h}{b}$. For $[0/90]_s$ Gr/E laminate, $\varepsilon \leq \frac{1}{20}$ leads to satisfactory results while for $[\pm 45]_s$ Gr/E laminate, $\varepsilon \leq \frac{2}{15}$ predicts satisfactory results.

(5) For all laminates with geometric ratio, $0 < \frac{h}{b} << 1$, high gradient displacement, strain and stress fields are shown to exist near the free edge.

(6) The above boundary layer effect decays exponentially to recover the lamination solution in the interior regions.

(7) For bidirectional laminates the axial displacement function U is identically zero. Hence no τ_{xy} or τ_{xz} exist in the laminate.

(8) For bidirectional laminates, the interlaminar normal stress σ_z is finite with the sign depending upon the stacking sequence. For example, for a $[0/90]_s$ Gr/E laminate, a maximum tensile σ_z exists at the free edge while for a $[90/0]_s$ Gr/E laminate, a maximum compressive σ_z is predicted.

(9) For angle-ply laminates, the exactness of the solution leads to the mathematical evidence of singular interlaminar shear stresses τ_{xz} and τ_{yz} at or near the free edge.

(10) For angle-ply laminates, the interlaminar normal stress σ_z takes on a finite maximum tensile value at the free edge, and is independent of the stacking sequence.

(11) The solution procedure can be readily programmed for a computer. Such a generalized computer program would be capable of predicting interlaminar stresses between any two layers of a general multi-layered laminate.

(12) The present theory suggests vaiable means for solving important related problems of practical interest.

REFERENCES

1. J. E. Ashton, J. C. Halpin and P. H. Petit, "Primer on Composite Materials: Analysis, Technomic Publishing Co. (1969).

2. A. H. Nayfeh, "Perturbation Methods," Wiley-Interscience, New York (1973).

3. D. B. Bogy, "Edge-Bonded Dissimilar Orthogonal Elastic Wedges Under Normal and Shear Loading," J. Applied Mechanics, Vol. 35 (1968), p. 460.

4. V. L. Hein, "Residual Stresses in a Two-Material Wedge and a Finite Cylinder," Ph.D. Thesis, Lehigh University (1968).

5. M. S. Hess, "The End Problem for a Laminated Elastic Strip--II. Differential Expansion Stresses," J. Composite Materials, Vol. 3 (1969), p. 630.

6. A. H. Puppo and H. A. Evensen, "Interlaminar Shear in Laminated Composites Under Plane Stress," J. Composite Materials, Vol. 4, (1970), p. 204.

7. R. B. Pipes and N. J. Pagano, "Interlaminar Stresses in Composite Laminates Under Uniform Axial Extension," J. Composite Materials, Vol. 4 (1970), p. 538.

8. G. Isakson and A. Levy, "Finite-Element Analysis of Interlaminar Shear in Fibrous Composites," J. Composite Materials, Vol. 5 (1971), p. 273.

9. O. C. Zienkiewicz, "The Finite Element Method in Structural and Continuum Mechanics," McGraw-Hill, (1967).

10. A. Levy, H. Armen, Jr., and J. Whiteside, "Elastic and Plastic Interlaminar Shear Deformation in Laminated Composites Under Generalized Plane Stress," Proc. of 3rd conference on Matrix Methods in Structural Mechanics, Wright-Patterson Air Force Base, Ohio, (1969).

11. E. F. Rybicki, "Approximate Three-Dimensional Solutions for Symmetric Laminates Under Inplane Loading," J. Composite Materials, Vol. 5 (1971), p. 354.

12. R. B. Pipes, "Interlaminar Stresses in Composite Laminates," AFML-TR-72-18, 1972.

13. R. B. Pipes and I. M. Daniel, "Moire' Analysis of the Interlaminar Shear Edge Effect in Laminated Composites," J. Composite Materials, Vol. 5 (1971), p. 255.

14. C. T. Herakovich, "Tensile Strength Behavior of Composite Reinforced Metals," VPI-E-72-11, (1972), p. 54.

15. D. W. Oplinger, B. S. Parker, and F. P. Chiang, "Edge Effect Studies in Fiber-Reinforced Laminates," AMMRC-TR-73-41, Army Materials and Mechanics Research Center, Watertown, Massachusetts.

16. R. B. Pipes and N. J. Pagano, "Interlaminar Stresses in Composite Laminates--An Approximate Elasticity Solution," Mechanics and Structures Research Report No. 73-1, Drexel University, (1973).

17. N. J. Pagano, "On the Calculation of Interlaminar Normal Stress in Composite Laminate," J. Composite Materials, Vol. 8 (1974), p. 65.

18. J. M. Whitney and C. T. Sun, "A Higher Order Theory for Extensional Motion of Laminated Composites," J. Sound and Vibration, Vol. 30 (1973), p. 85.

19. S. Tang, "A Boundary Layer Theory for Laminated Composite in Plane Stress--Part I," J. Composite Materials, Vol. 9 (1975), p. 33.

20. E. L. Reiss and S. Locke, "On the Theory of Plane Stress," Quar. Appl. Math., Vol. 19 (1961), p. 195.

21. N. J. Pagano and R. B. Pipes, "Some Observations on the Interlaminar Strength of Composite Laminates," Int. J. Mech. Sci., Vol. 15 (1973), pp. 679-688.

22. M. Van Dyke, "Perturbation Methods in Fluid Mechanics," Academic Press, New York and London, (1964).

23. S. P. Timoshenko and J. N. Goodier, "Theory of Elasticity," 3rd edition, McGraw-Hill (1970).

24. N. J. Pagano and R. B. Pipes, "The Influence of Stacking Sequence on Laminate Strength," J. Composite Materials, Vol. 5 (1971), p. 50.

25. J. W. Archbold, "Algebra," Sir Isaac Pitman & Sons, London (1964), p. 174.

26. I. S. Sokolnikoff and R. M. Redheffer, "Mathematics of Physics and Modern Engineering," McGraw-Hill, (1966), p. 528.

27. D. U. Von Rosenberg, "Methods for the Numerical Solution of Partial Differential Equations," Elsevier, New York (1969).

28. S. W. Tsai and H. T. Hahn, "Failure Analysis of Composite Materials," presented at 1975 ASME Winter Annual Meeting, Houston, Texas (Nov. 30 - Dec. 5, 1975).

SECURITY CLASSIFICATION OF THIS PAGE (When Data Entered)

REPORT DOCUMENTATION PAGE

READ INSTRUCTIONS BEFORE COMPLETING FORM

1. REPORT NUMBER: VPI-E-76-1	2. GOVT ACCESSION NO.
3. RECIPIENT'S CATALOG NUMBER	
4. TITLE (and Subtitle): INTERLAMINATE STRESSES IN COMPOSITE LAMINATES -- A PERTURBATION ANALYSIS	5. TYPE OF REPORT & PERIOD COVERED
6. PERFORMING ORG. REPORT NUMBER: VPI-E-76-1	
7. AUTHOR(s): Peter W. Hsu and Carl T. Herakovich	8. CONTRACT OR GRANT NUMBER(s): NGR 47-004-090
9. PERFORMING ORGANIZATION NAME AND ADDRESS: Virginia Polytechnic Institute and State University, Engineering Science & Mechanics, Blacksburg, Virginia 24061	10. PROGRAM ELEMENT, PROJECT, TASK AREA & WORK UNIT NUMBERS
11. CONTROLLING OFFICE NAME AND ADDRESS: National Aeronautics & Space Administration, Langley Research Center, Hampton, Virginia 23665	12. REPORT DATE: January, 1976
	13. NUMBER OF PAGES: 97
14. MONITORING AGENCY NAME & ADDRESS (if different from Controlling Office): Virginia Polytechnic Insitute & State University, Engineering Science & Mechanics, Blacksburg, Virginia 24061	15. SECURITY CLASS. (of this report): Unclassified
	15a. DECLASSIFICATION/DOWNGRADING SCHEDULE

16. DISTRIBUTION STATEMENT (of this Report)

Approved for public release; distribution unlimited.

17. DISTRIBUTION STATEMENT (of the abstract entered in Block 20, if different from Report)

Approved for public release; distribution unlimited.

18. SUPPLEMENTARY NOTES

19. KEY WORDS (Continue on reverse side if necessary and identify by block number)

Interlaminar Stresses, Edge Effects, Perturbation Analysis, Composites, Bi-directional Laminates, Angle-ply Laminates, Graphite/Epoxy, Singularity

20. ABSTRACT (Continue on reverse side if necessary and identify by block number)

See page ii.

DD FORM 1 JAN 73 1473 EDITION OF 1 NOV 65 IS OBSOLETE

SECURITY CLASSIFICATION OF THIS PAGE (When Data Entered)

DISTRIBUTION LIST

Dr. Longin B. Greszczuk
McDonnell Douglass Astronautics Co.
5301 Bolsa Avenue
Huntington Beach, CA 92647

Dr. Nicholas J. Pagano
WPAFB/MBM
Wright-Patterson Air Force Base
OH 45433

Dr. R. Byron Pipes
Dept. of Mechanical and Aerospace Engr.
107 Evans Hall
University of Delaware
Newark, DE 19711

Dr. Edmund F. Rybicki
Batelle
Columbus Laboratories
505 King Avenue
Columbus, OH 43201

Dr. Michael J. Salkind
Sikorsky Aircraft
United Aircraft Corporation
Stratford, CT 06602

Dr. George P. Sendeckyj
Structures Division
Air Force Flight Dynamics Lab.
Wright-Patterson Air Force Base
OH 45433

Dr. Carl H. Zweben
Textile Fibers Dept.
E.I. DuPont de Nemours & Company, Inc.
Experimental Station/B262
Wilmington, DE 19898

Dr. B. W. Rosen
Materials Science Corporation
Blue Bell Office Campus
Blue Bell, PA 19422

Dr. S. W. Tsai
Nonmetallic Materials Division
Air Force Materials Laboratory
Wright-Patterson Air Force Base, OH

Dr. J. M. Whitney
Nonmetallic Materials Division
Air Force Materials Laboratory
Wright-Patterson Air Force Base, OH

Prof. R. E. Rowlands
Dept. of Engineering Mechanics
University of Wisconsin
Madison, WI 53706

Prof. R. A. Schapery
Civil and Aerospace Engineering Dept.
Texas A & M University
College Station, TX 77840

Dr. R. L. Foye
U.S. Army Mobility Res. & Dev. Laboratory
Langley Research Center
Hampton, VA 22065

Dr. John G. Davis, Jr.
Mail Code No. 188A, Bldg. No. 1148
Langley Research Center
Hampton, VA 23665

Dr. John R. Davidson
Mail Code - 188E, Bldg. 1205
MD-Structural Integrity Branch
Langley Research Center
Hampton, VA 23665

Herbert F. Hardrath
Mail Code 188M, Bldg. 1205
Materials Division
Langley Research Center
Hampton, VA 22065

Dr. Darrell R. Tenney
Mail Code 188M, Bldg. No. 1148
MD-Materials Research Branch
Langley Research Center
Hampton, VA 22065

Dr. I. M. Daniel, Manager
IIT Research Institute
10 West 35 Street
Chicago, IL 60616

Mr. Dave Purdy
Douglas Aircraft Co.
Longbeach, CA 90801

Dr. R. A. Cruse
Scientific Analysis Group
Draft & Whitney Aircraft
Division of United Aircraft Corp.
East Hartford, CT 06118

Prof. Donald F. Adams
Dept. of Mechanical Engineering
University of Wyoming
Larmie, WY 82070

Prof. Phil Hodge
107 Aeronautical Engineering Bldg.
University of Minnesota
Minneapolis, Minnesota 55455
(612)373-2174

Glenn C. Grimes, Engr. Specialist
Structures R & T, Dept. 3780/62
Northrop Corp., Aircraft Div.
3901 W. Broadway
Hawthorne, CA 90250

Dr. Martin M. Mikulas
Mail Stop 190
NASA-Langley
Hampton, VA 23665

Dr. Paul A. Cooper
Mail Stop 208
NASA-Langley
Hampton, VA 23665

Prof. J. Tinsley Oden
Texas Inst. for Computational Mechanics
Engineering Mechanics Division, ASE-EM Dept.
The University of Texas at Austin
Austin, Texas 78712